Function of interneuronal gap junctions in hippocampal sharp wave-ripples

D I S S E R T A T I O N

zur Erlangung des akademischen Grades

Dr. rer. nat.
im Fach Biologie

eingereicht an der
Lebenswissenschaftlichen Fakultät
Humboldt-Universität zu Berlin

von
M.Sc. André Jörg Holzbecher

Präsidentin der Humboldt-Universität zu Berlin:
Prof. Dr.-Ing. Dr. Sabine Kunst

Dekan der Lebenswissenschaftlichen Fakultät:
Prof. Dr. Bernhard Grimm

Gutachter:
1. Prof. Dr. Richard Kempter
2. Prof. Dr. Benjamin Lindner
3. Prof. Dr. med. Imre Vida

eingereicht am: 02.05.2018
Tag der mündlichen Prüfung: 20.07.2018

Ich widme diese Arbeit meinen Eltern.
Danke für alles.

Abstract

A self-determined life in our society is unthinkable without memory. To develop holistic, bottom-up theories for such complex cognitive functions poses a major challenge for neuroscience as it requires linking neuronal dynamics to cognitive function. A unique experimental observation that opens ways for such a theory are sharp-wave ripples (SWRs). SWRs are generated in local neuronal networks and are important for memory consolidation, putatively supported by fast replays of previous experiences occurring during SWRs.

SWRs are prominent features of the extracellular field potentials in the mammalian hippocampus that occur during rest and sleep; they are characterized by sharp waves, $\approx 100\,\mathrm{ms}$ long voltage deflections, that are accompanied by ripples, i.e., 110–250 Hz oscillations. The mechanisms underlying sharp waves and ripples are not understood but this knowledge is crucial to comprehend their function. In this thesis, I worked on advancing the understanding of ripple generation.

While many origins for ripples have been proposed, recent experiments support the view that ripples are clocked by recurrent networks of inhibitory interneurons (INT-INT), which are likely constituted by networks of parvalbumin-positive basket cells (PV+BCs). PV+BCs are not only recurrently coupled by inhibition but also by gap junctions (GJs). GJs directly connect the neuronal cytoplasms and hence act as (fast) electrical synapses, which have been shown to increase synchrony in neuronal networks. The function of GJs for ripple oscillations, however, is not well understood. Therefore, in this thesis, I investigate the specific function of interneuronal GJs in hippocampal ripples.

For this, I review the discovery, the morphology, the function, and the abundance of gap junctions in the brain. Specifically, I discuss experiments that showed GJ coupling between PV+BCs – the putative generator of ripple oscillations. Furthermore, I discuss experimental studies that probed the function of gap junctions in SWRs, whose outcomes are ambiguous and hence inconclusive.

Consequently, I simulate INT-INT networks and demonstrate that gap junctions increase the neuronal synchrony and firing rates during ripple oscillations, while the ripple frequency is only affected mildly. I further show that GJs only have these supporting effects on ripples when they are sufficiently fast ($\lesssim 0.5\,\mathrm{ms}$), which requires proximal GJ coupling ($\lesssim 100\,\mu\mathrm{m}$). Additionally, I find that gap junctions increase the oscillatory power of ripple oscillations and by this means reduce the minimal network size required for INT-INT networks to generate ripple oscillations.

Finally, I analyze whether INT-INT networks that are exclusively coupled by GJs can generate ripple-like oscillations. Therefore, I reassess experimental data in which ripple-like oscillations were triggered in the absence of chemical synaptic transmission by the application of potassium chloride, and compare this data to my simulations of exclusively GJ-coupled INT-INT networks. This analysis demonstrates that exclusively GJ-coupled INT-INT networks can oscillate at ripple frequency, however, are unlikely the generator of the experimentally observed ripple-like oscillations because experimental observed and theoretical predicted network properties mismatch.

In sum, my results show that fast interneuronal gap junction coupling promotes the emergence of ripples and hereby supports SWRs, which are important for the formation of memory.

Zusammenfassung

Ein selbstbestimmtes Leben in unserer Gesellschaft ist nicht möglich ohne Gedächtnis. Ganzheitliche Theorien für solch komplexe Funktionen zu entwickeln ist eine der größten Herausforderungen für die Neurowissenschaft, da hierfür eine Verbindung zwischen neuronaler Dynamik und kognitiver Funktion benötigt wird. Eine einzigartige experimentelle Beobachtung könnte die Basis für eine solche Theorie sein: sharp wave-ripples (SWRs). SWRs werden in lokalen Neuronennetzwerken erzeugt und sind wichtig für Gedächtniskonsolidierung, die nach vorherrschender Theorie von schnellen Wiederholungen vorheriger neuronaler Aktivität, welche während SWRs auftreten, unterstützt wird.

SWRs sind charakteristische Ereignisse der lokalen Feldpotentiale im Hippocampus des Säugetiers, die in Phasen von Schlaf und Ruhe vorkommen. Eine SWR besteht aus einer sharp wave, einer $\approx 100\,\mathrm{ms}$ langen Auslenkung des Feldpotentials, welche mit ripples, 110–250 Hz Oszillationen, überlagert ist. Wie sharp waves und ripples genau erzeugt werden ist unklar, dieses Wissen ist jedoch unersetzlich für das Verständnis ihrer Funktion. In dieser Arbeit untersuche ich die Erzeugung von ripple-Oszillationen.

Es existieren unterschiedliche Modelle um ripples zu erklären, jedoch bekräftigen jüngste Experimente die Theorie, dass sie von rekurrenten Netzwerken inhibitorischer Interneurone (INT-INT) erzeugt werden, die höchstwahrscheinlich aus parvalbumin-positive basket cells (PV+BCs) bestehen. PV+BCs sind untereinander über rekurrente inhibitorische Synapsen und Gap Junctions (GJs) gekoppelt. GJs wirken als (schnelle) elektrische Synapsen, indem sie die neuronalen Zytoplasmen verbinden, und sie sind bekannt dafür die Synchronität in Neuronennetzen zu erhöhen. Die Funktion von GJs für ripple Oszillationen ist jedoch nicht gut verstanden. Daher untersuche ich in dieser Arbeit die spezifische Funktion von interneuronalen Gap Junctions in hippocampalen ripples.

Dafür fasse ich die Literatur über die Entdeckung, die Morphologie, die Funktion und die Verbreitung von GJs im Gehirn zusammen. Den Schwerpunkt lege ich hierbei auf Experimente, welche GJ Kopplungen von PV+BCs zeigen, den potentiellen ripple-Erzeugern. Des Weiteren diskutiere ich Experimente, in denen die Funktion von GJs für SWRs untersucht wurde. Diese Experimente liefern jedoch zweideutige und nicht beweiskräftige Ergebnisse.

Im Hauptteil dieser Arbeit demonstriere ich, dass GJs in INT-INT Netzwerken die neuronale Synchronität und die Feuerrate während ripples erhöhen, die ripple-Frequenz sich hingegen nur leicht verändert. Zusätzlich zeige ich, dass diese ripple-unterstützenden Effekte nur dann auftreten, wenn die GJ-Transmission schnell genug ist ($\lesssim 0.5\,\mathrm{ms}$), was wiederum somanahe Kopplung voraussetzt ($\lesssim 100\,\mu\mathrm{m}$). Darüber hinaus zeige ich, dass GJs die oszillatorische Stärke der ripples erhöhen und so die minimale für ripples notwendige Netzwerkgröße verringern.

Abschließend analysiere ich, ob INT-INT Netzwerke, welche ausschließlich mit Gap Junctions gekoppelt sind, ripple-artige Oszillationen generieren können. Dafür werte ich experimentelle Daten aus, in denen in Abwesenheit von chemischer synaptischer Transmission ripple-artige Oszillationen durch Kaliumchloridinjektionen ausgelöst wurden, und vergleiche diese Daten mit Simulationen von ausschließlich mit GJ gekoppelt INT-INT Netzwerken. Ich lege dar, dass die ausschließlich mit Gap Junctions gekoppelten INT-INT Netzwerke zwar mit ripple Frequenz oszillieren können,

aber wahrscheinlich nicht der Erzeuger der experimentell beobachteten ripple-artigen Oszillationen sind, da sich experimentell beobachtete und theoretische vorgesagte Netzwerkeigenschaften unterscheiden.

Zusammengenommen zeigen meine Resultate, dass schnelle Gap Junction-Kopplung von Interneuronen die Enstehung von ripples begünstigt und somit SWRs unterstützt, welche einen wichtigen Beitrag zur Bildung unserers Gedächtnisses leisten.

Contents

1 Introduction: hippocampal ripple oscillations can be generated by interneuronal networks

> You have to begin to lose your memory, if only in bits and pieces, to realize that memory is what makes our lives. Life without memory is no life at all, just as an intelligence without the possibility of expression is not really an intelligence. Our memory is our coherence, our reason, our feeling, even our action. Without it, we are nothing.
>
> Luis Buñuel

The brain is an incredible organ. It defines who we are, as a species and an individual, and it is the target of many unanswered questions that have been passionately debated in academia and in society, our generous funding source: Who are we? How do we think? And what is a thought? What is memory? How do we interact with the world? Despite the research and successes of the last decades, we are still far away from being able to give satisfying answers to any of these fundamental questions.

From the evolutionary perspective, the brain was developed to coordinate motion in an environment. However, supralinear growth over the past millions of years has enabled our brains to be capable of much more, such as complex problem solving, social interactions, planning, and long-term storage of memory. The value of our brain is reflected in the fact that it makes up $\approx 20\,\%$ of our energy consumption, while it only contributes $\approx 2\,\%$ to our average body weight.

The challenge of understanding the brain has united a potpourri of researchers from different backgrounds who are all working on the same questions. This symbiosis of medicine, biology, chemistry, mathematics, physics, computer science, and psychology creates an intriguing research environment.

In the recent years, theoretical neuroscience has gained more importance acknowledging that verifiable mathematical models are necessary to generate testable pre- and postdictions, which allow to identify the abstract rules that organize neuronal activity (Abbott, 2008) and bring order into the vast amounts of experimental data. One particular challenge of (theoretical) neuroscience is to bridge the temporal and spatial scales of neuronal computation (Dayan and Abbott, 2005, preface): How do we get from activity of a single neuron to cognitive function?

A strong example in which shared experimental and theoretical efforts succeeded to create a link from the neuronal to the cognitive level is long-term memory. Here, a "definite biomarker for cognitive function" has been identified on the level of neuronal

networks (Buzsáki, 2015). These biomarkers are sharp wave-ripples (SWRs), i.e., characteristic events recorded in extracellular field potentials (EFPs) of an inner structure of the mammalian brain, the hippocampus. SWRs are 40–100 ms lasting voltage deflections, the sharp wave, overlayed by ≈ 110–250 Hz oscillations, ripples (Buzsáki, 2015; Maier and Kempter, 2017). At the cognitive level, it has been shown in rodent models that SWRs are necessary to memorize spatial information (Girardeau et al., 2009). At the level of neurons and neuronal networks, it has been found that previous experiences are replayed during SWRs in rest and sleep, which proposes a mechanism for how we might establish long-term memory (Wilson and McNaughton, 1994; Diba and Buzsáki, 2007) and underlines the importances of a good night's sleep (Rasch and Born, 2013).

It is an ongoing debate how SWRs and their components, sharp waves and ripples, are generated. A detailed knowledge of the mechanism(s) underlying SWRs, however, is required to understand their function in cognition. Ripple oscillations are likely generated by recurrent networks of inhibitory interneurons (Ylinen et al., 1995) that have been shown to be coupled by gap junctions (Katsumaru et al., 1988a). Gap junctions are small channels that directly connect the cytoplasms of two neurons, and hence act as electrical synapses. How gap junctions affect ripple oscillations in interneuronal networks has not been investigated thoroughly, yet.

In this thesis, I aim to understand the function of interneuronal gap junctions in hippocampal ripple oscillations to advance our understanding of ripple and SWR genesis.

In the next section, I give a broader introduction to SWRs, starting off with the hippocampus, the remarkable brain structure that gives rise to SWRs[1].

1.1 Hippocampus

In The Hippocampus Book, the authors named the hippocampus (HC) the *neuronal Rosetta Stone* (chapter 1, p. 3, Andersen et al., 2006). I think this is a good analogy because research on the HC has not only given insights in its function but has also stimulated the development of a paramount variety of experimental methods. Some of these are in vivo tetrode recordings in behaving animals, in vitro slice preparations, and intracellular recordings. This advance of methodology has allowed to reveal general mechanisms of neuronal computations, e.g., the nature of excitatory and inhibitory neurons, long-term potentiation and depression, the representation of space, memory consolidation, and has bolstered the idea of "brain systems", which associates spatially confined brain areas with specific functions. These tools and concepts have been successfully used to record, decipher, describe, and analyze data from other brain regions (chapter 1, Andersen et al., 2006).

In the end of 19th century, Santiago Ramón y Cajal, a neuroscientist, artist, and Nobel laureate for Medicine, was already amazed by the regular anatomy of the HC, and devoted many hours of his life to abstract his observation and draw detailed maps of stained brain slices (Ramón y Cajal, 1911; for a beautiful reprint of his drawings see Swanson et al.,

[1] For all abbreviations used in the text see the List of abbreviations, which can be found at the end of this thesis.

2017). In these drawings, the hippocampal structures are depicted so clearly that Cajal deduced the signal flow in the HC solely based on his structural observations (Fig. 1.1A). In the following century, his theories about the connectivity have been widely confirmed (chapter 2.4.1, Andersen et al., 2006).

The importance of the hippocampus is underlined by the fact that it is present in all mammals, and shows a high morphological resemblance across species. Buried below the neocortex, the hippocampus is considered as a sensory hub for the rest of the brain because it receives processed inputs from all senses (e.g., Rolls, 2004).

The ultimate goal of neuroscience research is to understand the human brain. For practical reasons, however, the most researched brains are those from mice and rats. In the hope that most of the findings are transferable across species – a debate for itself – most of the neuroscience research uses rodents as the standard animal model (next to mice, monkeys, cats and bats). In the remainder of this thesis, I restrict myself to data from rodents and mention explicitly when I refer to other animals.

In the following, I first introduce the basic morphology of the hippocampus, and subsequently review the most important functions that are associate with the hippocampus.

1.1.1 Hippocampal morphology and physiology

The morphology of the hippocampus has been described in great detail. Here, I only give a brief overview. To satisfy more detailed interests, I refer the reader to Chapter 3 of The Hippocampus Book (Andersen et al., 2006).

The hippocampal formation

The hippocampal formation is located in the temporal lobe of the brain and includes the hippocampal proper, dentate gyrus (DG), subiculum, pre- and parasubiculum, and entorhinal cortex (EC; Andersen et al., 2006, Chapter 3). What exactly is meant by the term *hippocampus* depends on the definition. Throughout this thesis, I use the term hippocampus as a synonym for the hippocampus proper that consists of the cornu ammonis (CA) areas CA1, CA2 and CA3 (Chapter 3, Andersen et al., 2006). The morphology and location of the hippocampus is described nicely in the Hippocampus Book:

> "The rat hippocampal formation is an elongated, banana-shaped structure with its long axis extending in a C-shaped manner from the midline of the brain near the septal nuclei (rostrodorsally) over and behind the thalamus into the incipient temporal lobe (caudoventrally). The long axis of the hippocampal formation is referred to as the septotemporal axis and the orthogonal axis as the transverse axis."
>
> The Hippocampus Book, p. 44, chapter 3 (Andersen et al., 2006)

The gate to the hippocampus is the entorhinal cortex, which gives input to the HC via the perforant path, and also receives the main hippocampal outputs. The entorhinal cortex

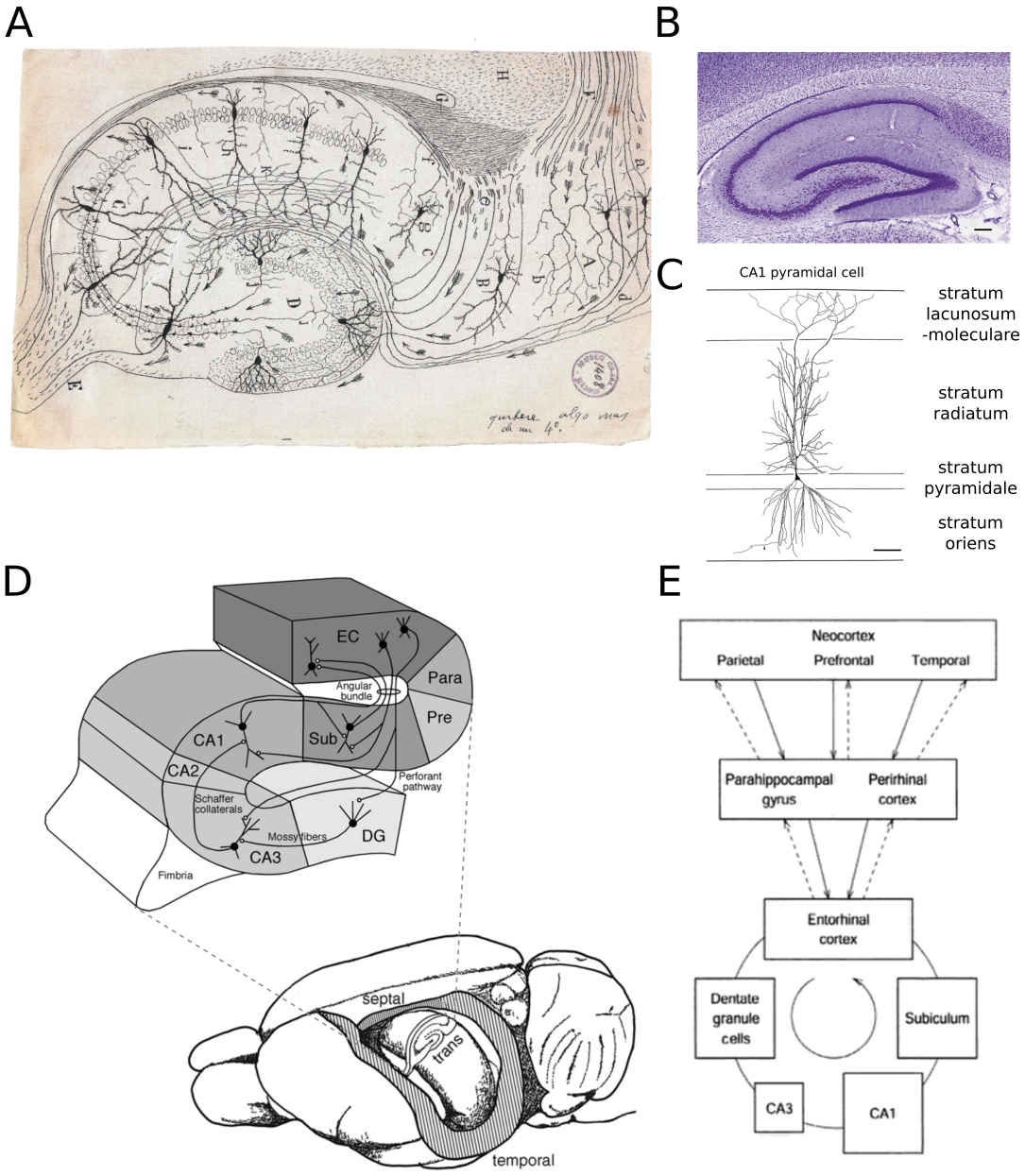

Figure 1.1: The hippocampus. **A**, Drawing from Ramón y Cajal (1911) of the hippocampal formation from a rat including entorhinal cortex (EC), subiculum (Sub), denate gyrus (DG), and the cornu ammonis areas. **B**, Nissl stained hippocampal slice of the rat. Principle cells form bands that remind of two interlocked C's. Scale bar: 200 µm. (Taken from brainmaps.org; Mikula et al., 2007; reproduced with permission). **C**, Camera lucida drawing of a typical CA1 pyramidal cell including the strata of the hippocampus cornu ammonis regions. Scale bar: 100 µm (Chapter 3, Andersen et al., 2006; reproduced with permission). **D**, Three dimensional structure of the hippocampus and its position in the rat brain (Chapter 3, Andersen et al., 2006; adapted with permission). **E**, Main pathways into, within, and out of the hippocampal formation (Rolls, 2004; reproduced with permission). The hippocampus receives input from and sends output to the entire neocortex.

maintains bidirectional synaptic contacts to the neocortex, i.e., signals are projected back to the neocortex after they have been processed in the hippocampus (Fig. 1.1E; Rolls, 2004). This high convergence of the sensory inputs mediated by the entorhinal cortex makes the hippocampus an ideal candidate for forming associations between multiple sensory inputs.

The main fibers within the hippocampus are unidirectional excitatory pathways along the transverse axis: The perforant pathways projecting from superficial layers of entorhinal cortex to DG, the mossy fibers projecting from DG to CA3, and the Schaffer collaterals projecting from CA3 to CA1 (Fig. 1.1A, D, E). This pathway has been already identified by Cajal (Ramón y Cajal, 1911) and it is named the "trisynaptic loop" (Fig. 1.1A). The loop is closed by projections back from CA1 to deeper layers of the entorhinal cortex, including a possible intermediate synapse in the subiculum. Next to these excitatory pathways, there are also direct projection from the EC to CA3 and CA1.

CA1

From the CA areas, CA1 and CA3 have received most of the attention of hippocampal research because they are part of the main projections in HC and spatially more extended (Fig. 1.1D). The work in this thesis concerns the area CA1, and hence I restrict myself here to this area.

The defining structure of the hippocampal formation, including CA1, is the dense band of excitatory neurons that is called stratum (st.) pyramidale, which is recognizable by the unaided eye (Fig. 1.1B). The pyramidal-shaped somata, which gave the name to the pyramidal cells (PCs), and their dendritic trees are oriented orthogonal to this band (Fig. 1.1A, C). The dendrites extend into the st. oriens on the one side (basal dendrites), and into the st. radiatum up to the st. lacunosum-moleculare on the other side (apical dendrites; Fig. 1.1A–C).

For the last decades, pyramidal cells have been the main target of investigations in CA1, resulting in detailed knowledge about place cells (O'Keefe and Dostrovsky, 1971; O'Keefe and Nadel, 1978) and long-term potentiation of Schaffer collateral synapses (LTP; recent review by Kumar, 2011), which made pyramidal cells the probably best described cell type in the mammalian brain.

Excitatory PCs make up around 90 % of the neurons in the CA1 region, i.e., around 300 000 (Bezaire and Soltesz, 2013). Given the great morphological similarity of PCs, it was assumed for a long time that they are a homogeneous population; however, this view was recently challenged (for review see Soltesz and Losonczy, 2018), showing that PCs in CA1 express different genes across the dorsal-ventral axis (Cembrowski et al., 2016), and differ in their biophysical properties (McKiernan and Marrone, 2017). Furthermore, it was shown that PCs close to the border of st. pyramidale and st. oriens, i.e., superficial PCs, and PCs close to the border of st. pyramidale and st. radiatum, i.e., deep PCs, express distinct synaptic connectivity patterns (Lee et al., 2014).

The residual 10 % of neurons, i.e., $\approx$ 40 000, are inhibitory interneurons. In contrast to the PCs, there is no debate about interneuronal diversity: there is a whole zoo of interneurons in CA1, featuring at least 21 different subtypes (McBain and Fisahn, 2001;

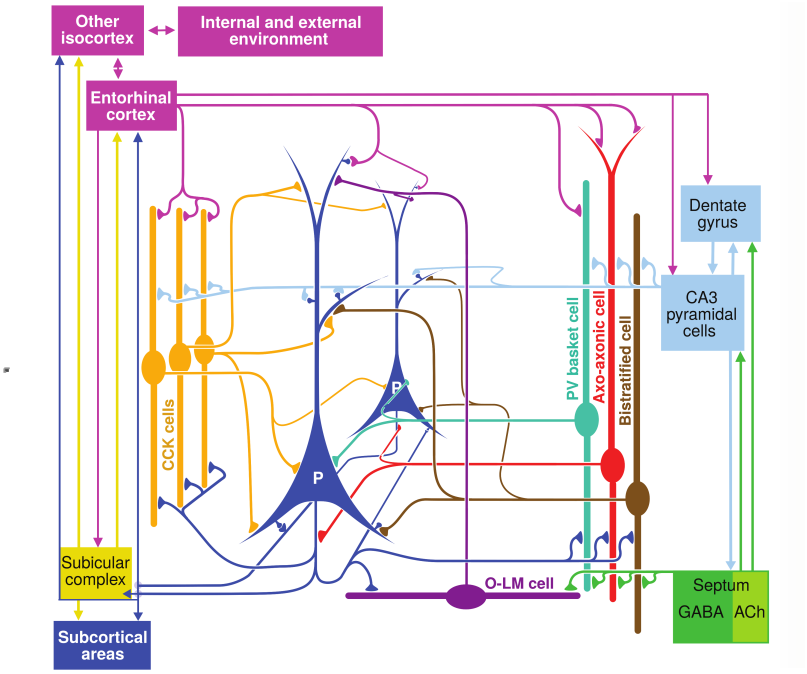

Figure 1.2: Overview of interneuronal diversity in hippocampal area CA1. Connectivity between interneuron types and pyramidal cells (P). The interneuron types are parvalbumin (PV)-positive basket cells, axo-axonic cells, bistratified cells, oriens lacunosum-moleculares (O-LM) cells, and cholecystokinin (CCK)-expressing interneurons. Klausberger and Somogyi, 2008; reprinted with permission from AAAS.

Klausberger and Somogyi, 2008; Chamberland and Topolnik, 2012; Bezaire and Soltesz, 2013). I provide a brief tour through the main interneuronal types of CA1 that are relevant for my research in the next section.

Interneurons in CA1

Inhibitory interneurons have been assumed to maintain and clock local excitatory activity (Klausberger and Somogyi, 2008). In general, the vast amount of interneurons is mostly classified by firing patterns, morphology, molecular markers, and postsynaptic targets. However, the best classification categories and the functional relevance of these categories are still debated (Defelipe et al., 2013).

Here, I just briefly mention the main types of interneurons occurring in CA1 (Fig. 1.2), putting emphasis on the interneuron types that are putatively involved in SWRs.

Parvalbumin-positive basket cells (PV+BCs) are one of the most common interneuron types in CA1, mostly found within st. pyramidale (Fig. 1.2, also Fig. 1.6B). PV+BCs have been first identified by Katsumaru et al. (1988b) in CA1, and they belong to the class of fast-spiking interneurons. PV+BCs express the calcium binding protein paravalbumin that can be stained by antibodies. The name *basket*

cells stems from their multiple branching axonal arborizations that form a dense basket around the somata of PCs (Fig. 1.6B). They innervate PCs at their basal dendrites and somata, hence have a strong control over somatic APs of excitatory neurons (Klausberger and Somogyi, 2008). Its high divergence allows a average single PV+BC to inhibit more than 1000 PCs (Chapter 3.4.2, Andersen et al., 2006). They are also strongly recurrently connected amongst each other by inhibitory synapses and gap junctions, which act as electrical synapses (Chapter 3.2 and 2; Sik et al. 1995; Katsumaru et al. 1988a; Galarreta and Hestrin 2001a). In this thesis, PV+BCs play a crucial role because they are critical for models of ripple oscillations in CA1 (Section 1.3.1; Klausberger et al., 2003; Donoso et al., 2018).

Bistratified cells inhibit pyramidal cells at their basal dendrites, where the majority of the Schaffer Collaterals arrive from CA3 (Fig. 1.2). They are also located in st. pyramidale, and also express PV and additionally somatostatin.

Axo-axonic cells or chandelier cells target exclusively axons of PCs and are located close to st. pyramidale (Fig. 1.2). They also express PV.

Oriens lacunosum-moleclares cells are projecting on the apical dendrites and are located in the st. oriens. They express somatostatin.

This list is far from being complete, and for more details on the different interneuron types, the reader is referred to the steadily growing literature (e.g., McBain and Fisahn, 2001; Klausberger and Somogyi, 2008; Chamberland and Topolnik, 2012; Bezaire and Soltesz, 2013). The firing statistics of the different interneuron types during SWRs are discussed in Section 1.2.2.

After giving an overview of the hippocampal anatomy, more specifically of the area CA1 and the neurons therein, I summarize the functions that the hippocampus has been related to.

1.1.2 Hippocampal function

The most essential functions associated with the hippocampus are the representation of space, the consolidation of long-term memory, and their combination, i.e., spatial memory. First, I introduce the relation between the hippocampus and spatial representation (Section 1.1.2). Thereafter, I give a general introduction to different types of memory (Section 1.1.2), then narrow down the focus to hippocampus-related memories, and elucidate the concept of memory consolidation and spatial memory (Section 1.1.2).

Many functions have been associated with the hippocampus, and I can only account for a few in this Introduction. For further information on the hippocampus function please see Chapters 12 and 13 of The Hippocampus Book and references therein (Andersen et al., 2006).

Place cells, time cells, and conceptual cells

How does the brain represent an environment?

In 1971, O'Keefe and Dostrovsky moved one step closer to answer this question by identifying cells in the CA1 area of the rat hippocampus that are always active at a certain place, and hence code for an allocentric location of the animals: a cognitive map (O'Keefe and Nadel, 1978). These cells were identified as pyramidal cells in CA1 (Section 1.1.1) and named place cells (O'Keefe and Dostrovsky, 1971; O'Keefe and Nadel, 1978). While a single place cell represents a location in the environment, the sequential activation of several place cells encodes a trajectory in space (Wilson and McNaughton, 1994). The discovery of place cells was awarded with the Nobel Prize in 2014 (O'Keefe et al., 2014). These honors given for "their discoveries of cells that constitute a positioning system in the brain" (The Nobel Prize, 2014) were shared with May-Britt Moser and Edvard I. Moser, who first described grid cells, which also represent space (Hafting et al., 2005). In contrast to place cells, grid cells are not activated at one specific place but at multiple locations that form a grid pattern in real space.

Encouraged by the finding of grid and place cells, spatial representations have been the focus of many experimental studies. Admittedly, space has an important role in our, and a probably even more important role in a rodent's life. However, it is an interesting question whether the HC exclusively represents space, or whether the HC also encodes other environmental dimensions. Evidence for the latter hypothesis is provided by the discovery of neurons that "represent the flow of time" (Eichenbaum, 2014). These "time cells" could be explicitly relevant for generation of episodic memory and are the topic of a recent review by Eichenbaum (2014).

Further evidence that the HC represents environmental dimensions beyond space was provided by Quian Quiroga et al. (2005). They identified cells in the human hippocampus that responded to pictures of celebrities, for example, Jennifer Aniston. Interestingly, the authors found that some cells did not only respond to the picture of person but also to their written names. This hints in the direction that the activation of such cells does not depend on a particular visual input, but represents the abstract information of recognizing the person. These cells have been called conceptual cells (Quian Quiroga, 2012). For a recent view on this topic see Moscovitch et al. (2016).

Consolidation of long-term memory

What is a memory? What different classes of memory are there?

There are two classes of long-term memory: explicit memory/declarative memory, and implicit memory. Explicit memory, which can be subdivided into the memories of personal events (episodic memory), and facts (semantic memory), includes all the memories that can be accessed explicitly: What did I do yesterday? What is my favorite artist? What is your name? All these questions do have an explicit answer. Implicit memories are procedural memories like motor skills: How to keep upright? How to ride a bike? How to write a mirror inverted text? While many people express these skills, they will not be able to give an explicit answer to these questions. Fig. 1.3 shows a diagrammatic overview of the two classes of memory and the brain regions associated with them.

From our daily experience, we know that explicit and implicit memories are generated

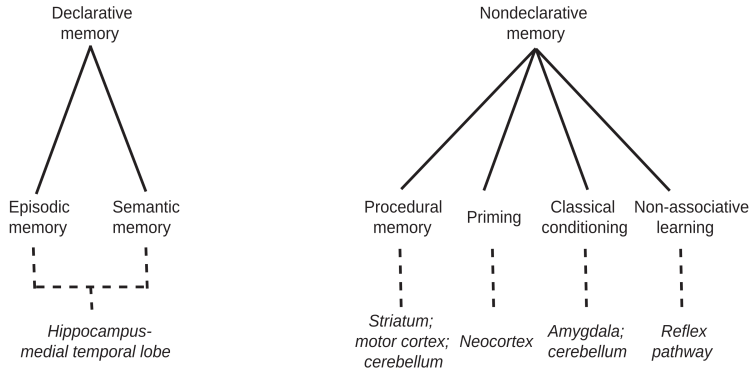

Figure 1.3: Categories of memory. The two main classes of memories: declarative/explicit and non-declarative/implicit memories, including their subdivisions and associated brain areas (Chapter 13, Andersen et al., 2006, reproduced with permission).

differently. While we do remember facts, more or less, and places that we visited after one occasion, so called one-shot learning, it can take us a lifetime and many repetitions to master certain motor skills, e.g., how to stand backwards on a skateboard juggling balls. It may hence not be a surprise that explicit and implicit memories rely on different neuronal systems (Fig. 1.3; Chapter 12 and 13, Andersen et al., 2006).

Hippocampus-related memories. Explicit memories depend on the hippocampus. This was demonstrated impressively by the studies of the probably best known patient of the recent history: HM (Scoville, 1954). During adolescence, HM developed a severe bilateral epilepsy originating from the hippocampal formation. As a result, his doctors performed a bilateral hippocampi lobectomy. After the removal of both hippocampi the epilepsy was cured, however, HM was suffering from a complete anterograde amnesia, i.e., he could not form new explicit memories any longer, and also lost the memory of his recent past. Nevertheless, he was still able to form implicit memories, could still recall episodic memories that dated back to a more distant past, and perform tasks that required normal cognitive function.

The consequences of a full hippocampal lobectomy for cognition were documented by multiple studies from Scoville and Milner (Scoville, 1954; Scoville and Milner, 1957; Milner et al., 1998), and triggered the hippocampal research as we know it today.

Building on these findings, Squire and Zola-Morgan (1991) synthesized studies from humans, most famously HM, and from several animals models to conclude that the mammalian hippocampus is responsible for storing and consolidating explicit memories. Further, they deduced that the hippocampus serves as a memory storage for recent memories and is not responsible for working and implicit memory, and general cognitive function. This research gave rise to the definition of the medial temporal lobe memory system (Squire and Zola-Morgan, 1991).

Memory consolidation. How do we store explicit memories?

In every moment of our lives, we are subject to a constant stream of sensory inputs. Most of this sensory information we never notice, however, of some we become aware and store them for a longer time, maybe lifetime. Recent experiences are converted into memory traces via synaptic plasticity that alters the neuronal circuits of the brain (e.g., Chapter 24 and 25 in Bear et al., 2007). Memory consolidation is the process in which these fresh memory traces are strengthened and stabilized, and ultimately, are transformed into long-term memories (for recent review see Dudai et al., 2015). Memory consolidation includes molecular, synaptic, and neuronal processes, which act locally, as well as the redistribution and integration of new memories into existing memories, which takes place on the system level (Dudai et al., 2015).

The hippocampus has been shown to be crucial for memory consolidation of explicit memories as stated in the medial temporal lobe memory system theory (Squire and Zola-Morgan, 1991). The hippocampus is a very plastic region (review by Leuner and Gould, 2010), and hence new information is rapidly stored but is under constant thread to be overwritten: a stability-plasticity dilemma. In line with these facts, the hippocampus is critically involved in storage of recent memories. More distant memories, however, tend to be dependent on the reactivation of the neocortex and can become independent of the hippocampus (Wiltgen et al., 2004).

Two-stage model of memory consolidation. In 1989, Buzsáki proposed that there are two stages of memory consolidation in the hippocampus: an exploration stage and a consolidation stage. These two behavioral stages are associated with distinct oscillatory patterns of the hippocampal extracellular field potentials (EFPs).

The first stage is exploration. Here, new experience are encoded into memory traces via synaptic plasticity in the neuronal circuits of the hippocampus. During the exploration stage, prominent theta oscillations (8–12 Hz) paired with gamma oscillations (30–90 Hz) are present within the EFP of the hippocampal formation.

The second phase is consolidation, which occurs during periods of rest and sleep. Here, previous experiences are consolidated, and sharp wave-ripples (SWRs, Section 1.2) are present in the hippocampal EFPs, most prominently in CA1. Consolidation of memory is achieved by replaying the previous experienced neuronal activity during SWRs. After many replays, strong and stable associations are formed that are hypothesized to build the basis for episodic memory (Buzsáki, 1989).

Synopsis. In the last two sections, two different aspects of hippocampal function are presented. The HC as substrate for place cells that are observed on the single-cell level, and the role of the hippocampus in memory consolidation on the systems level. These two findings are mutually dependent, and a cognitive biomarker linking these two different scales are SWRs. SWRs are the topic of the next section, and their contribution to memory consolidation is discussed in Section 1.2.1.

1.2 Sharp wave-ripples (SWRs)

Sharp wave-ripples (SWRs) are observed throughout the hippocampus and dentate gyrus (Sullivan et al., 2011), and have been implicated to play a crucial role in the consolidation of episodic memory (Girardeau et al., 2009; see Section 1.1.2). SWRs are preserved across mammals and have been observed in rodents, humans, monkeys, cats, rabbits, and bats (for review, Buzsáki et al., 2013).

Recordings of hippocampal EFPs show SWRs as characteristic events that are composed of a strong deflection ($\approx$ 40–100 ms), the sharp wave, superimposed by fast oscillations, the ripples ($\approx$ 110–250 Hz, Buzsáki, 2015; Maier and Kempter, 2017). Typical SWRs are depicted in Fig. 1.4A and B in vivo and in vitro, respectively (Buzsáki et al., 1992; Maier et al., 2003). SWRs are most prominently observed in CA1 but can also be recorded in CA3, CA2, and the dentate gyrus (Fig. 1.4C, Sullivan et al., 2011).

SWRs were first reported by Buzsáki et al. (1992) in an in vivo study of the EFPs of CA1, even though earlier reports of sharp wave-like activity (Jouvet et al., 1959; Vanderwolf, 1969) and ripple oscillations (O'Keefe and Nadel, 1978) exist. SWRs are observed during consummatory behavior, resting, and slow-wave sleep (Buzsáki et al., 1992; Ylinen et al., 1995), which bolsters their role in memory consolidation according to the two-stage memory hypothesis (Section 1.1.2; Buzsáki, 1989).

In this section, I first present evidence that SWRs are important for memory consolidation, and subsequently, report where and under which conditions SWRs can be observed, and which neurons contribute to SWRs.

1.2.1 Sharp wave-ripples are important for memory consolidation

In 2009, Gabrielle Girardeau et al. did an exciting experiment. They let rats perform a spatial memory task and monitored their performance. In the phase of rest or sleep during the pauses between consecutive trials, they selectively interrupted online-detected SWRs by stimulating the commissural fibers, which silenced the hippocampal network including the SWR. The test group, in which SWRs were interrupted, performed significantly worse than the control group (Fig. 1.4D). They also excluded that the current injection itself was responsible for the memory deficit by showing that current injections that left SWRs intact (stimulated control; Fig. 1.4D) did not lead to performance deficits compared to unimplanted controls. Thus, Girardeau et al. concluded that SWRs are important for memory consolidation.

These findings have been reproduced and extended, showing explicitly that SWRs during the state of slow wave-sleep (Ego-Stengel and Wilson, 2010) and wakefulness (Jadhav et al., 2012) are both important for memory consolidation.

How do SWRs support memory consolidation? Past neuronal activity is reactivated during slow-wave sleep in SWRs (Wilson and McNaughton, 1994; Lee and Wilson, 2002). These studies have been made possible by the findings of place cells (O'Keefe and Dostrovsky, 1971; Section 1.1.2), which allow to translate neuronal activity to spatial coordinates. It was shown that during SWRs place cells are reactivated in the same sequence

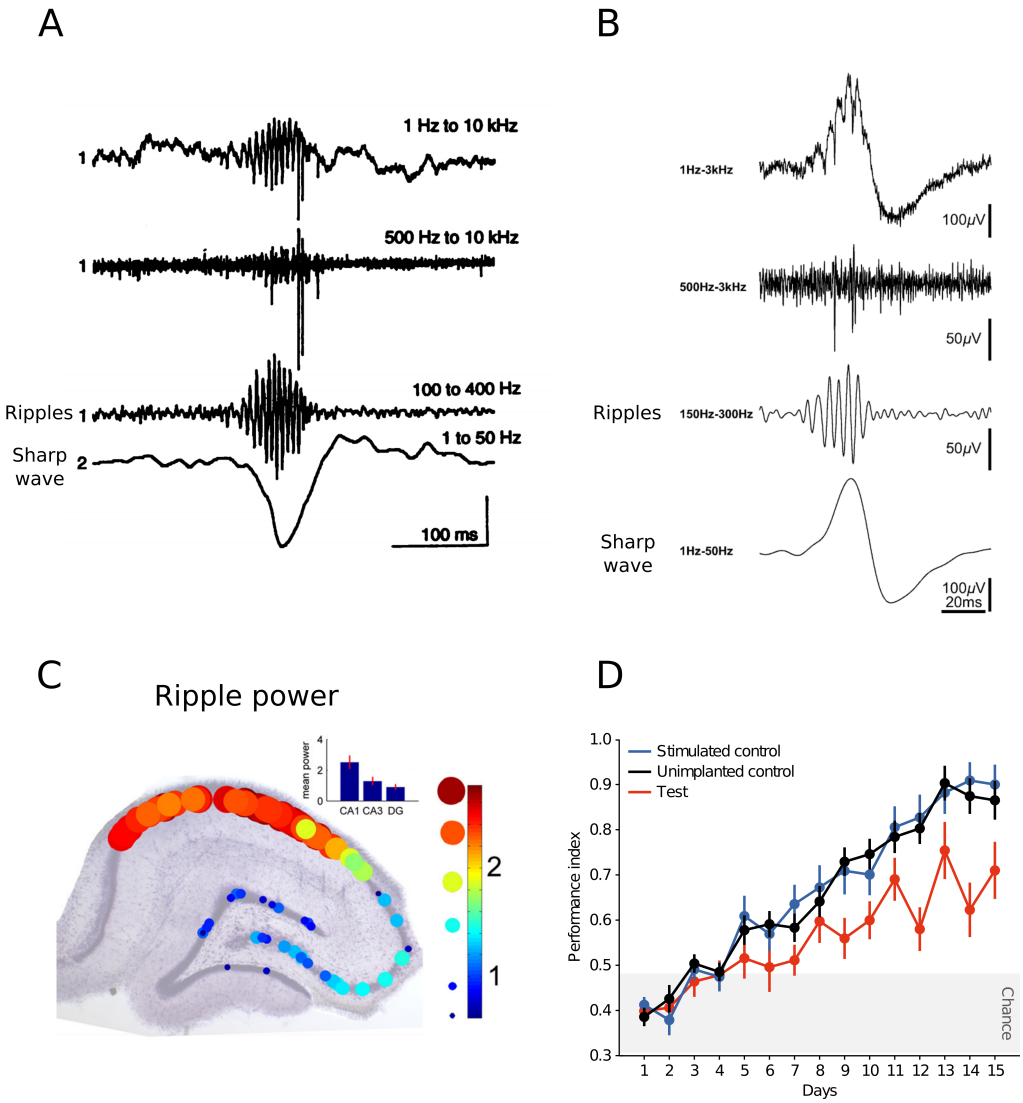

Figure 1.4: Sharp wave-ripples (SWRs) in the rodent hippocampus. **A**, SWR in vivo (Buzsáki et al., 1992; reprinted with permission from AAAS). EFP recordings in rat hippocampal region CA1. Electrode 1 (upper three traces) was positioned in st. pyramidale and electrode 2 (lowest trace) in st. radiatum. Band-pass filtered as indicated. Scale bars (from top to bottom): 0.5 mV, 0.25 mV, 0.25 mV, 1.0 mV. **B**, SWR in vitro (Maier et al., 2003; reproduced with permission). EFP recordings of mouse in st. pyramidale of hippocampal region CA1. Band-pass filtered as indicated. **C,** Normalized spectral power at ripple frequency ($\approx$ 170 Hz) in hippocampal areas CA1, CA3, and dentate gyrus (rat, in vivo; Sullivan et al., 2011; reproduced with permission). **D**, SWRs are important for memory consolidation (Girardeau et al., 2009. Reprinted by permission from Springer Nature: Nat Neurosci, Girardeau et al., ©(2009)). Rats in which SWRs were selectively shut down (Test) perform significantly worse in spatial memory task than two control groups (Stimulated control, Unimplanted control).

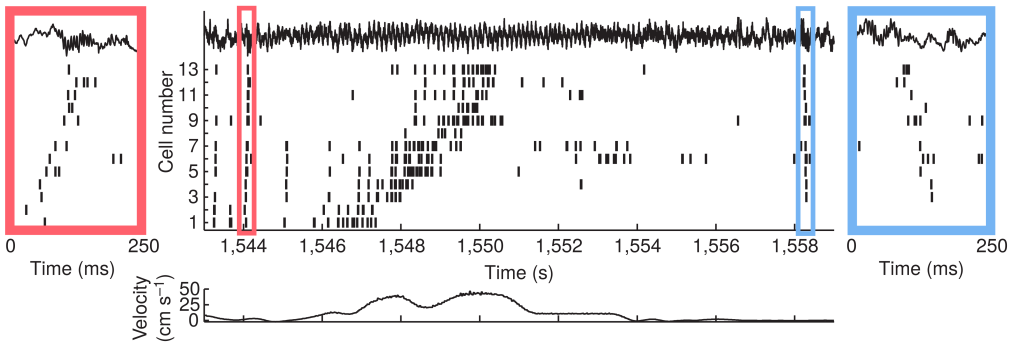

Figure 1.5: Preplay and reverse replay of place cell activity during sharp wave-ripples (SWRs) (Diba and Buzsáki, 2007). Recordings from hippocampal area CA1 of a freely moving rat that traverses a linear track for a water reward. Depicted are the spike trains of cells 1–13, which are place cells that code for locations with increasing spatial coordinates. Left (red) and right (blue) insets show time compressed preplay and reverse replay during SWRs of the place cell activity. Adapted by permission from Springer Nature: Nat Neurosci, Diba and Buzsáki, ©(2007).

as in the previous exploration (Lee and Wilson, 2002; Wilson and McNaughton, 1994). This sequence of place cells describes a trajectory of the animal in real space that the animal traversed before, and it is plausible that remembering spatial trajectories depends on such replays. It was also found that sequences of place cells are replayed in reverse order, and preplayed, i.e., activated before the animal is traversing the trajectory (Fig. 1.5; Foster and Wilson, 2006; Diba and Buzsáki, 2007; Gupta et al., 2010), which might be relevant for decision making. The sequences reactivated during SWRs are time compressed ($\approx$ 10–20-fold) compared to behavioral time scale of exploration (Buzsáki, 2015), which might allow for efficient memory consolidation because it matches the timescale of synaptic plasticity.

As mentioned earlier, the hippocampus is only temporarily involved in long-term memory consolidation, and more distant memories are stored in neocortical areas (Wiltgen et al., 2004). How does this transfer of memories from hippocampus to neocortex happen?

There is evidence that sleep, in particular, slow-wave sleep, plays an important role in consolidation and transfer of memory (see Diekelmann and Born, 2010; Rasch and Born, 2013 for reviews on the topic). During slow-wave sleep, hippocampal SWRs occur correlated with thalamic and neocortical activity, i.e., with neocortical slow waves and thalamic spindles. It is hypothesized that these correlated oscillatory activity is important for the redistribution of explicit memories across different brain regions (Wiltgen et al., 2004; Dudai et al., 2015; Maingret et al., 2016; Khodagholy et al., 2017). Memory consolidation is an exciting topic on its own, and for further reading on the topic of sleep and memory, I recommend the recent review by Rasch and Born (2013).

1.2.2 Sharp wave-ripples: extracellular field potentials and neuronal statistics

SWRs are the *default state* of the hippocampal network since they occur when no extrahippocampal input is present (Buzsáki, 2015). SWRs have been observed first in vivo (Fig. 1.4A; Buzsáki et al., 1992; Ylinen et al., 1995; Stark et al., 2014), and later in vitro (Fig. 1.4B; Maier et al., 2002, 2003, 2011; Nimmrich et al., 2005; Schlingloff et al., 2014; Hulse et al., 2016). In vivo and in vitro preparations allow for complementary observations: while in vivo correlations between behavior and SWRs can be observed, in vitro the cellular and network mechanisms are more accessible. SWRs show a great similarity in these two preparations, e.g., similar rates of occurrence (Buzsáki, 1986; Maier et al., 2003) and comparable frequencies of ripple oscillations (Buzsáki, 2015; Maier et al., 2003). Nevertheless, some properties of SWRs are different in in vivo and in vitro preparations, e.g., the firing rates of pyramidal cells during SWRs are higher in vivo (English et al., 2014) than in vitro (Bahner et al., 2011), and the occurrence of SWRs is more irregular in vivo (Buzsáki, 1986; Maier et al., 2003). These differences might be caused by the lack of extrahippocampal inputs and the reduced size of the networks in vitro (Maier and Kempter, 2017). For a more elaborate comparison of SWRs in vivo and in vitro see Maier and Kempter (2017) and Buzsáki (2015).

The sharp wave. The sharp wave is a strong voltage deflection (amplitude $\approx$ 1–2 mV, duration $\approx$ 40–100 ms) of the hippocampal EFP (Fig. 1.4A, B). In vivo or in intact horizontal hippocampal slices, the sharp wave originates from the local networks of CA3, and then propagates through the entire hippocampus (Sullivan et al., 2011). However, it has been shown that sharp waves and associated ripple oscillations can persist also in isolated CA1 slices (Maier et al., 2003). The sharp wave in CA3 is putatively facilitated by recurrent excitatory connections amongst the pyramidal cells (e.g., Wittner et al., 2007) but the mechanisms of its initiation and termination are still debated. From CA3, the sharp wave spreads to CA1 via the Schaffer Collaterals, where it arrives at the dendrites of CA1 pyramidal cells and causes these neurons to become active. This leads to current sinks in the dendritic region, and current sources in the stratum pyramidale (Ylinen et al., 1995; Sullivan et al., 2011), which is a hallmark of SWRs. This source-sink distribution is also reflected in the reversal of the EFP polarity of the sharp wave across the strata of CA1 (see sharp waves in Fig. 1.4A, B).

Ripple oscillations. Ripples are oscillations in the range of 110–250 Hz depending on preparation and species (Fig. 1.4A, B; Buzsáki et al., 2013; Buzsáki, 2015; Maier and Kempter, 2017). Ripples appear in association with sharp waves (Buzsáki et al., 1992; Ylinen et al., 1995; English et al., 2014). Despite their high frequency, ripple oscillations show a remarkable temporal coherence in CA1 (Sullivan et al., 2011), and are maybe the most synchronous events in the mammalian brain (Buzsáki, 2015).

In this thesis, I distinguish between ripple oscillations and ripple-like oscillations: Ripple oscillations are the oscillations that are occurring in combination with sharp waves both in vivo and in vitro. Ripple-like oscillations are oscillations at ripple frequently that

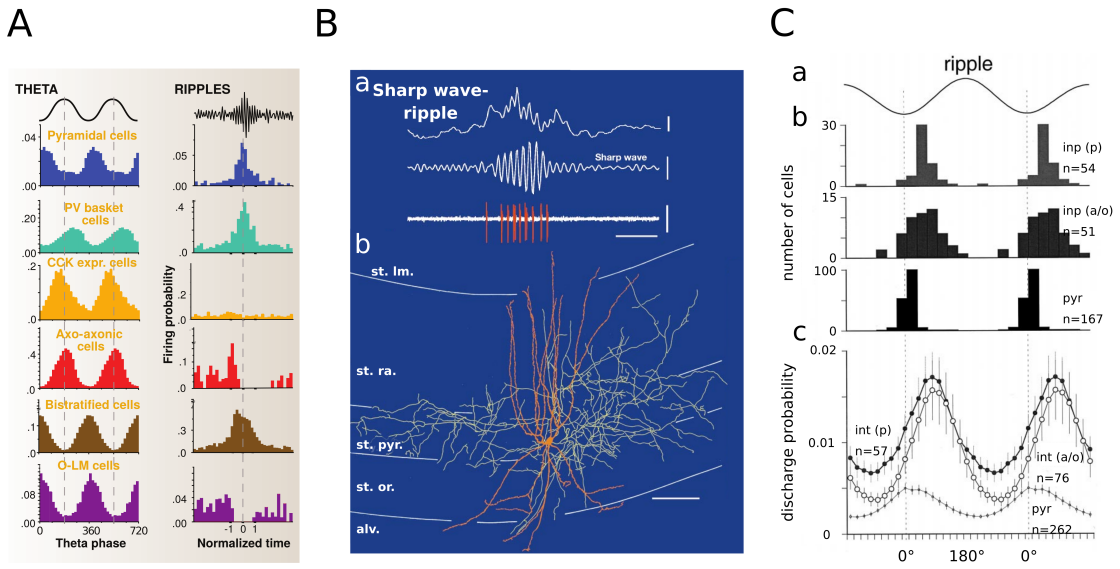

Figure 1.6: Activity of neurons during sharp wave-ripples (SWRs) in hippocampal area CA1. **A**, Activity of pyramidal cells and different interneurons during theta and ripples (Klausberger and Somogyi, 2008; reprinted with permission from AAAS). **B**, PV+BCs' activity during SWRs in vivo. **Ba**, PV+BCs fire phase locked to ripples during SWRs. The scale bars are: raw extracellular field potential (EFP), 0.5 mV; ripple oscillations (90–140 Hz), 0.2 mV; unit activity, 0.5 mV; time scale, 50 ms (Klausberger et al., 2003. Reprinted by permission from Springer Nature: Nature, Klausberger et al., ©(2003)). **Bb**, Reconstruction of a PV+BC. Soma and dendrites in red, axon net in yellow. st. lm., stratum lacunosum-moleculare; st. rad., stratum radiatum; st. py., stratum pyramidale; st. or., stratum oriens; alv., alveus. For details see (Fig. 1; Klausberger et al., 2003). **C**, Phased-locked activity of CA1 pyramidal cells and interneurons during SWRs. int(p) and int(a/o) describe interneurons recorded in the pyramidal layer and alveus and stratum oriens, respectively (Csicsvari et al., 1999b; reproduced with permission). **Ca**, Ripple cycle. **Cb**, Phase distribution of cells firing during ripple oscillations. Only neurons included that show significant phase modulations. **Cc**, Same as Cb but including all neurons and expressed as discharge probabilities. For more details see (Csicsvari et al., 1999b).

do not occur in combination with sharp waves.

Ripple-like oscillations, can be triggered by pharmacology in vitro (Draguhn et al., 1998; Nimmrich et al., 2005), or by optogenetic activation (in vitro, Fig. 1.8, Schlingloff et al. 2014; in vivo Stark et al. 2014). How ripple oscillations are generated is unknown, and hence also whether the underlying mechanism(s) for ripple-like oscillations and ripple oscillations are the same. Models for ripple generations are discussed in Section 1.3.

Activity of neurons during SWRs in CA1. During a SWR event, $\approx 10\,\%$ of the neurons throughout the hippocampus are active (Csicsvari et al., 1999b). CA1 pyramidal cells fire with a probability of $\approx 30\,\%$, which represents a ≈ 10 fold increase compared to periods without SWRs (Fig. 1.6A, C; Csicsvari et al., 1999b). The interneuronal population located around stratum pyramidal shows an even higher recruitment during SWRs; here,

$\approx 70\%$ of the interneurons are active, with about 4 times higher firing rates than during non-SWR activity (Csicsvari et al., 1999b; 2000). Expressed in explicit firing rates this yields ≈ 11 spikes/s for the pyramidal cells, and ≈ 40 spikes/s for interneurons (Csicsvari et al., 2000). Pyramidal cells and specific interneuron types fire phase locked to ripple oscillations (Fig. 1.6A–C; Csicsvari et al. 1999a,b). Relevant for the contribution of ripples to cognitive function might be that the replay of previous experiences by pyramidal place cells (Section 1.2.1) is also clocked by ripple oscillations.

Interneuron activity during ripples. Two interneuron types are particularly active during ripple oscillations: Parvalbumin-positive basket cells (PV+BCs) and bistratified cells (Fig. 1.6A, B; Klausberger et al. 2003, 2004). Both of these interneurons fire phase locked to the ripple oscillations, and they are hypothesized to be important for the generation of ripple oscillations. Interestingly, oriens lacunosum-moleclares cells and also axo-axonic cells are inhibited during SWRs and show very low firing rates (Klausberger et al., 2003). An overview of the active interneurons during SWRs is given in Fig. 1.6A and in the review of Klausberger and Somogyi (2008).

1.3 Models of ripple generation

Different theories for the origin of ripple oscillations have been formulated. The most common models for the origin of ripples are: recurrent interneuronal networks (Fig. 1.7A; INT-INT; Ylinen et al., 1995), the putatively gap junction (GJ) coupled pyramidal cells (Fig. 1.7B; Ylinen et al., 1995; Traub et al., 1999), supralinear dendritic integration in pyramidal cells (Fig. 1.7C; Memmesheimer, 2010), and pyramidal-interneuron feedback loops (Fig. 1.7D, E; PYR-INT; e.g., Buzsáki et al., 1992; PYR-INT-INT; Stark et al., 2014).

Given that excitatory (Csicsvari et al., 1999b) and inhibitory neurons (Klausberger et al., 2003, 2004) fire phase locked to EFP ripple oscillations we are faced with a classical "chicken or the egg causality dilemma". As a consequence, all possible interactions between these neurons have been proposed to be the pacemaker of ripple oscillations.

1.3.1 Interneuronal networks: parvalbumin-positive basket cells can generate ripple oscillations (INT-INT)

In 1995, Ylinen et al. proposed that ripple oscillations can be mediated by recurrently connected interneurons that receive strong excitatory drive during sharp waves (Fig. 1.7A; INT-INT, or fast inhibitory neuronal oscillation, FINO). The theoretical foundation for the INT-INT hypothesis is that recurrent interneuronal networks in combination with synaptic transmission delays can generate robust neuronal oscillations (Wang and Buzsáki, 1996; Brunel and Wang, 2003). The network frequency in an INT-INT network is predominately set by the synaptic time scales of the inhibition and by the excitatory drive depending on the firing regime (Brunel, 2000). An involvement of interneurons in the rhythmogenesis throughout the brain has been also shown experimentally, e.g., in

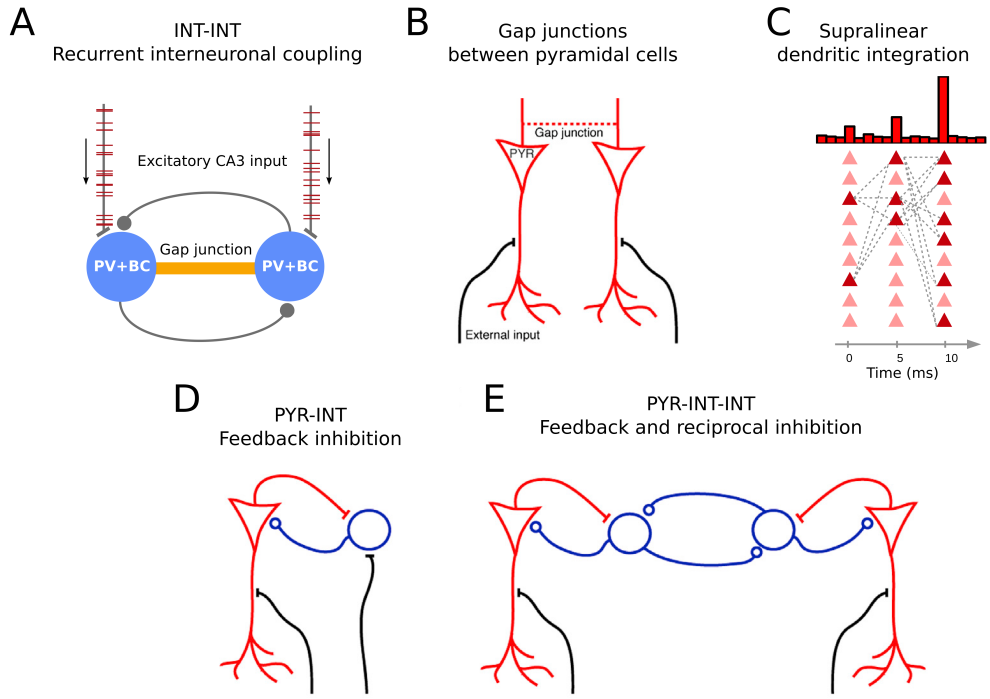

Figure 1.7: Models for the generation of ripples. **A**, Reciprocal inhibition (INT-INT) hypothesis (Ylinen et al., 1995; Chapter 3): networks of gap junction and inhibitory coupled PV+BCs. **B**, Gap junctions between axons of pyramidal cells (Traub et al., 1999). **C**, Supralinear integration in pyramidal dendrites (Memmesheimer, 2010). **D**, Pyramidal-inhibitory loop hypothesis (PYR-INT or PING; e.g., Buzsáki et al., 1992). **E**, Pyramidal-interneuron feedback loops in conjunction with inhibitory loop (PYR-INT-INT; Stark et al., 2014). For details of the models see Section 1.3. B, D, E adapted from Stark et al. (2014) with permission.

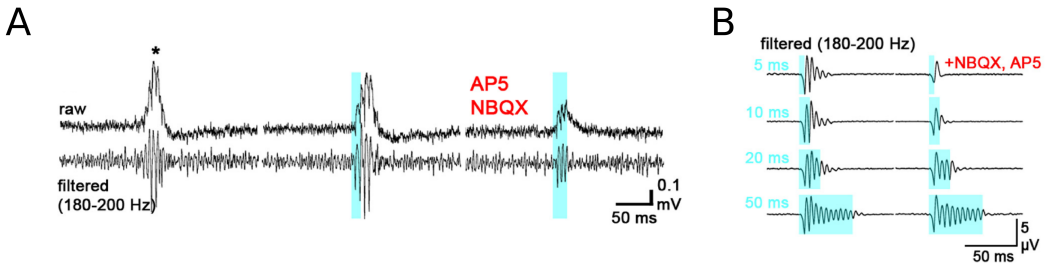

Figure 1.8: Optogenetic stimulation of PV+ interneurons can trigger ripple-like oscillations in vitro (Schlingloff et al., 2014). **A**, Spontaneous SWR (left), SWR triggered by optogenetic activation of PV+ interneurons (middle), and SWR triggered by optogenetic activation of PV+ interneurons (blue) under blockade of excitatory receptors (AMPA, NBQX; NMDA, AP5; right). **B**, Ripple oscillations in response to prolonged optogenetic activation of PV+ interneurons (blue). For details of the experiments see Schlingloff et al. (2014). Figure adapted from Schlingloff et al. (2014), their Figures 6D E, and reprinted with permission.

gamma oscillation in the hippocampus (for a review on oscillations in the hippocampus, see Colgin, 2016).

Even though interneurons represent only roughly 10 % of the hippocampal neurons they have a strong influence on the network because they are highly divergent (Bezaire and Soltesz, 2013). Parvalbumin-positive basket cells (PV+BCs) are the ideal candidate for clocking ripple oscillations in CA1 because they are abundant (Bezaire and Soltesz, 2013), fire phase locked during ripples (Fig. 1.2B, C; Klausberger et al., 2003, 2005), directly target the soma of the pyramidal cells (Sik et al., 1995), are organized in local recurrent networks with high connectivities (Bartos et al., 2002, 2007), and express fast GABAergic synapses that allow for oscillation frequencies in the ripple range (Bartos et al., 2002).

Furthermore, PV+BCs are also coupled by gap junctions (Katsumaru et al., 1988a; Galarreta and Hestrin, 2001a). Gap junctions are direct connections of the cytoplasms of two neurons that serve as electrical synapses (Chapter 2). GJs are usually implicated in synchronizing neuronal ensembles, which is particularly interesting because they might be contributing to the high synchrony of ripple oscillations. The influence of GJs on ripple oscillations in the framework of INT-INT networks is the main topic of this thesis.

Recent evidence for the INT-INT hypothesis

Recent optogenetic experiments allowed more insights in the mechanisms underlying SWRs, and specifically, ripple oscillations (Stark et al., 2014; Schlingloff et al., 2014). In hippocampal slice experiments, Schlingloff et al. (2014) showed that the optogenetic activation of PV+ interneurons in CA3 was sufficient to generate steady-state ripple-like oscillations, even if all excitatory synapses were blocked (Fig. 1.8). This demonstrates that the inhibitory network formed by the PV+ interneurons is able to generate rhythmic activity at 200 Hz by itself and does not require any excitatory pacemaker. In a further

experiment, they demonstrated that the optogenetic deactivation of PV+ interneurons interrupts SWRs, which shows that PV+ interneurons are also necessary for the observed fast oscillations.

Are these optogenetically triggered ripple-like oscillations the same as spontaneous ripple oscillations? A detailed comparison of optogenetically induced ripple-like oscillations and spontaneously occurring ripple oscillations by Stark et al. (2014) supports this view. However, in the experiments of Stark et al. (2014) the oscillations were caused by the activation of pyramidal cells in CA1 in vivo. While these oscillations could be also silenced by blocking $GABA_A$ synapses, the sole excitation of PV+ interneurons was not enough to generate EFP oscillations at ripple frequency. According to Stark et al. (2014), inhibitory interneurons are required, however, not sufficient for generation of ripple oscillations. This discrepancy might be explained by the fact that in the experiments of Stark et al. (2014) less interneurons were activated than in the experiments by Schlingloff et al. (2014). Furthermore, the experiments by Stark et al. (2014) were carried out in vivo and in CA1, whereas the experiments from Schlingloff et al. (2014) were in CA3 and in vitro. Additional evidence that inhibitory currents and hence inhibitory neurons are crucial for ripple oscillation was found by Gan et al. (2017). They demonstrated that phase-locked inhibition generated by PV+ interneurons is dominating excitation during ripple oscillations. For further discussion see Chapter 3.

1.3.2 Alternative models for ripple generation

Here, I present the principles of the alternative models for ripple oscillations (Traub et al., 1999; Memmesheimer, 2010; Stark et al., 2014).

GJ coupled axonal plexus of CA1 pyramidal cells

It has been shown that GJ blockers such as octanol and carbenoxolone can block ripple oscillations (Ylinen et al., 1995; Nimmrich et al., 2005; see also Chapter 4), and that fast oscillations can persist in the absence of chemical synaptic transmission (Draguhn et al., 1998). Stimulated by these findings, Traub et al. (1999) showed in simulations that GJs between axons of pyramidal cells can generate ripple oscillations (Fig. 1.7B; Traub et al., 1999, 2000, 2001, 2003, 2012).

The main idea is that axonal action potentials are transferred through pyramidal GJs that are putatively located in the axonal plexus in stratum oriens. Due to the anatomy of the pyramidal axons, the transmission is proposed to be delayed by a characteristic time, which sets the time scale for the ripple oscillations. These delays were estimated to be $\approx 5\,\mathrm{ms}$ leading to $\approx 200\,\mathrm{Hz}$ oscillations.

Recent reports suggest that experiments that rely on GJ blockers are inconclusive due to their strong side effects (Juszczak and Swiergiel, 2009; Behrens et al., 2011). Furthermore, the evidence for gap junctions between mature pyramidal cell is sparse (Schmalbruch and Jahnsen, 1981; Perez-Velazquez et al., 1994; Condorelli et al., 2000; Mercer et al., 2006; Hamzei-Sichani et al., 2007; Nagy, 2012).

Supralinear dendritic integration

Memmesheimer (2010) proposed that supralinear dendritic integration generates ripple oscillations (Fig. 1.7C). He showed that coincident inputs to pyramidal cells can cause potentiation in the recurrent networks of pyramidal cells in CA1. The network frequency is controlled by the time that an AP in one neuron needs to elicit an AP in a second neuron. This delay is determined by the axonal delays between excitatory neurons, dendritic delays and the time scale of the active dendrites in Memmesheimer's model (Memmesheimer, 2010, Supporting Information, Fig. S6, S7). Memmesheimer (2010) showed that even though the parameters are varied in quite a wide range, the network frequency is relatively stable. In a recent publication, Jahnke et al. (2015) extended this framework for ripple oscillations to explain replays of previous activity and learning.

This hypothesis relies crucially on the recurrent coupling of excitatory neurons. However, ripple-like oscillations can be also caused by the optogenetic activation of principal cells of dentate gyrus, which are known to have no recurrent connectivity (Stark et al., 2014; Buzsáki, 2015).

Pyramidal-inhibitory feedback loop

Ripple oscillations have been proposed to be generated by a pyramidal-interneuronal feedback loop (Fig. 1.7D; PYR-INT or PING), which is a common model for the origin of gamma oscillations (e.g., Whittington et al. 2000; Buzsáki and Wang 2012). A closely related idea is that pyramidal-interneuron feedback loops in conjunction with inhibitory loops (PYR-INT-INT) are the generator of ripples (Fig. 1.7E; Stark et al., 2014). Both of these models have been fueled by the observation that pyramids and interneurons fire phase locked to the ripples (Csicsvari et al., 1999b). Furthermore, Stark et al. (2014) argued that both pyramidal cells and interneurons are required for ripple oscillations (Section 1.3.1; but cf. Schlingloff et al., 2014).

It remains an open question whether neuronal loops that contain pyramidal cells and interneurons can oscillate fast enough to generate oscillations at ripple frequency (Brunel and Wang, 2003). According to simulations from Donoso et al. (2018), oscillations at ripple frequency are generated by INT-INT networks, and including pyramidal neurons in these networks (PYR-INT-INT) shifts the oscillation frequency from ripple frequencies to slower frequencies.

1.4 Scope of this thesis

In this thesis, I aim to understand the contribution of interneuronal gap junctions to ripple oscillations in the hippocampal area CA1. Ripple oscillations are occurring associated to sharp waves and form sharp wave-ripples (SWRs; Section 1.2). These characteristic events can be described as the default state of the hippocampal networks, and have been implicated to be important for memory consolidation and decision making (Section 1.2.1).

In consequence, if we would like to achieve a holistic theory for hippocampal dependent memory consolidation, we will need to understand how SWRs are created. Understand-

ing the generation of SWRs necessarily implies to figure out how ripple oscillation are generated.

Gap junction in the hippocampus. The next chapter of this thesis is devoted to gap junctions (Chapter 2), which are the second main neuronal messaging pathway next to chemical synapses. GJs had received much attention in the beginning of neuroscience, however, have received less in the last decades. Since GJs play an important role in my scientific work, I discuss their discovery, function, and abundance, in particular, for GJs between PV+BCs in CA1.

Function of gap junctions in hippocampal ripple oscillations. For me, it is intriguing that gap junctions are present between PV+BCs in the hippocampus, however, there function has not been understood. How do interneuronal GJs contribute to ripple oscillations? – In Chapter 3, I tackle this question and present results from my research on the effect of interneuronal GJs in ripple oscillation in the hippocampal area CA1.

Data analysis: ripple oscillation in the absence of chemical synaptic transmission. Many models for the generation of ripple oscillations exist as discussed in Section 1.3 of the Introduction. In Chapter 4, I discuss EFP data that shows ripple-like oscillations in the absence of synaptic coupling (Nimmrich et al., 2005), which was originally published in support of the pyramidal cell-GJ hypothesis (Traub et al., 1999). I reanalyze this data and evaluate the hypothesis whether these ripple-like oscillations could be mediated by interneuronal GJs.

2 Gap junctions in the mammalian brain and implications for sharp wave-ripples

Gap junctions (GJs) are present between neurons in the mammalian brain, in particular, between inhibitory neurons (Connors and Long, 2004). Although obvious from today's perspective, this statement was the bone of contention of a passionate debate about the basic structure of the central nervous system: Is the brain either compartmentalized in single interacting subunits, i.e., neurons, as we know today, or is it an electrical and chemical continuum?

This chapter is devoted to GJs, and the reader is provided with all information about GJs necessary for understanding my research. First, I briefly guide through the interesting episode at the beginning of neuroscience, which started with a controversy about the general structure of the brain and pathways of communication, and ended with the certainty that there are neurons in the brain that communicate primarily chemically but also electrically. After these historical considerations, I discuss the function of GJs as electrical synapses in the brain. Since I aim to understand the role of GJs within networks that are constituted by hippocampal parvalbumin-positive basket cells (PV+BCs), sound information about the GJ connectivity between these types of neuron is crucial. After reviewing morphological and electrophysiological findings, I consider the means of exploring GJ transmission experimentally, i.e., chemical gap junction blockers and Cx36 knockout studies, and discuss the implications that these experiments have for the role of GJs in sharp wave-ripples (SWRs).

2.1 The discovery of chemical synapses and gap junctions: soup vs. sparks

At the end of the 19th century, neuroscience was at its very beginning. It was a time of a passionate debate about the basic structure of the brain. The main question was whether the brain was built of compartmentalized units, today known as neurons, or whether it was an electrically continuous nerve net. Two of the most prominent (neuro)scientists at this time, Golgi and Ramón y Cajal, represented these two opposing hypotheses. While Golgi argued for an electrical continuum constituting the basis of the brain, Ramón y Cajal was convinced of the neuron doctrine, i.e., single neurons carrying out the computations in the brain (Valenstein, 2012). For "their work on the structure of the nervous system" the two researches were honored by a shared Noble Price in 1906 (The Nobel Prize, 1906). The severity of this conflict is emphasized by the fact that Golgi used this festive occasion to attack the recent advances of the neuron doctrine camp in his Noble Lecture with the title "The Neuron Doctrine - Theory and Facts" (Golgi, 1906).

Indeed, the two hypotheses pose different requirements for the signaling mechanisms within the brain: while the interaction between different regions is inherent to the electrical continuum hypothesis, the means of communication for the neuron doctrine were up to debate. More insights into the neuronal communication were given by Sir Henry Dale (Dale, 1914) and Otto Loewi (Loewi, 1921), who identified a chemical neuromuscular transmitter that mediated the signal transmission to the heart. This chemical transmitter, which Dale later identified as acetylcholine, marks the first evidence that neuronal communication could be mediated by chemical transmitters and "for their discoveries relating to chemical transmission of nerve impulses" (The Nobel Prize, 1936) Dale and Loewi were awarded with a Nobel Prize in 1936 (Dale and Loewi, 1936). Despite the growing evidence in favor of the neuron doctrine accompanied by chemical transmission, many neurophysiologists were convinced that only electrical signaling would guarantee a fast sufficient transmission since the diffusive process involved in chemical transmission would be too slow. This debate is known as the *war of soup and sparks* (Valenstein, 2012), where Henry Dale is one of the most representative figures of the *soup* team and John Eccles of the *sparks* team. The name *soup* originates from the application of homemade pharmaceutics and also from the cliché that pharmacologists turned their kitchen into a laboratory. The name *sparks* reflects the dependence of the electrophysiologist on electrical currents, which tend to throw out sparks.

In the following years, more neurotransmitters were found adding weight to the chemical transmission hypothesis. However, the breakthrough in the field was made possible by the introduction of electron microscopy. This technique allowed in 1954 the observation of the synaptic cleft (Palade and Palay, 1954), and in 1968 the discovery of the chemical carrying synaptic vesicles (PhD thesis by T. Hökfelt; Valenstein, 2012), which were considered as the final proofs for the neuron doctrine and chemical transmission. It seemed like the soup team had won. Ironically, the same technique, electron microscopy, enabled researchers at the same time to discover gap junctions in two different species: the crayfish (Furshpan and Potter, 1959) and the Japanese lobster (Watanabe, 1958). Stimulated by these findings, gap junctions were found in the mammalian central nervous system around a decade later (Hinrichsen, 1970).

Today, it is evident that chemical synapses are the predominant form of neuronal communication, however, there is no doubt that next to these chemical synapses there are electrical synapses in the brain, mostly located between inhibitory neurons. In conclusion, this interesting twist of history tells us that it is neither singly soup nor singly sparks but it is both: soup with sparks. In the next section, I provide more information about the morphology and function of GJs.

2.2 Gap junctions: the basic facts

This section answers the most basic questions about gap junctions: What are gap junctions? How do gap junctions contribute to the function of neuronal circuits?

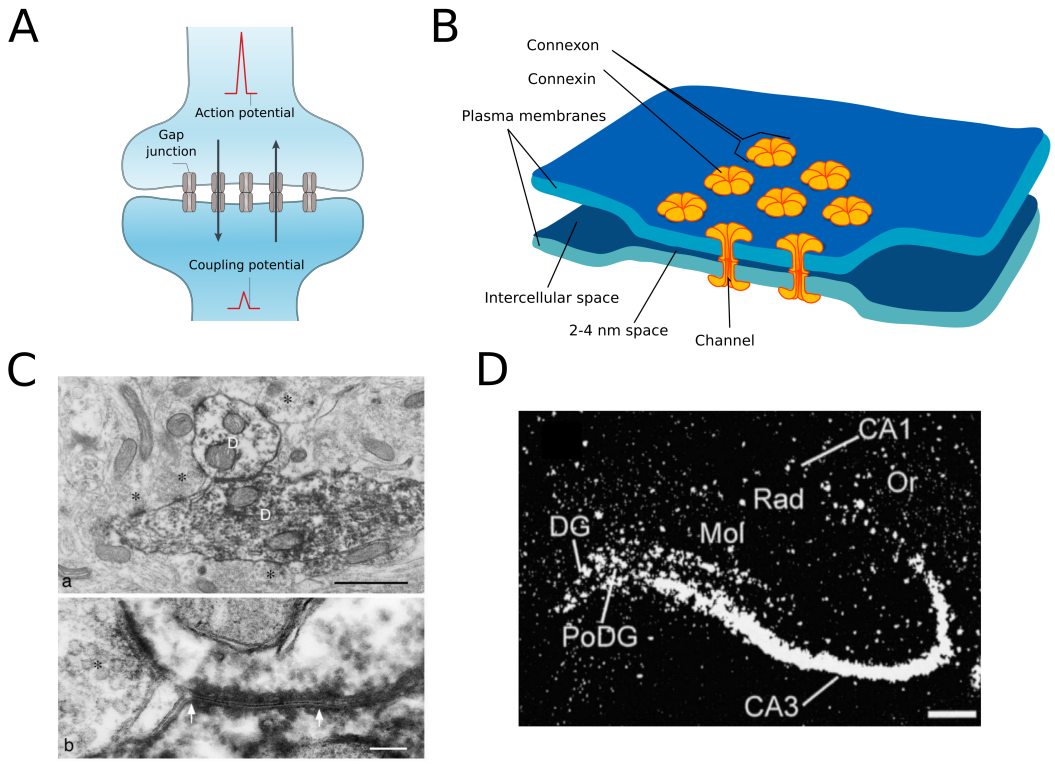

Figure 2.1: Morphology and abundance of gap junctions in the hippocampus. **A**, **B**, Schematics of gap junctions (Pereda, 2014, reprinted by permission from Springer Nature: Nat Rev Neurosci, Pereda, ©(2014); `https://en.wikipedia.org/wiki/File:Gap_cell_junction-en.svg` by LadyofHats, public domain). **C**, Electron micrograph of gap junction coupled dendrites (top, D) of parvalbumin-positive hippocampal interneurons in area CA1. Both dendrites receive postsynaptic terminals (*) and form direct gap junction contact (bottom, arrows). Scale bars, 1 μm (top), 0.1 μm (bottom) (Fukuda and Kosaka, 2000b; reprinted with permission). **D**, Expression of Cx36 RNA within the hippocampus. Scale bar, 200 µm. Picture includes dentate gyrus (DG), polymorph layer of DG (PoDG), stratum lacunosum-moleculare (Mol), stratum radiatum (Rad), stratum oriens stratum (Or, Condorelli et al., 2000; reprinted with permission).

2.2.1 Morphology of gap junctions

A gap junction is the direct connection between the cytoplasms of two cells, which bridges the 2–3 nm gap between the two cells (Fig. 2.1A, B; Connors and Long, 2004). GJs exist between different kinds of cells throughout the body, e.g., muscle cells in the heart and astrocytes or neurons in the brain (Dermietzel and Spray, 1993). Since my research is focused on neurons of the mammalian brain, I only provide information relevant for this topic.

GJs enable the flow of cytoplasm from one neuron to another. Therefore, molecules and ions that are present in the cell on one side of the GJ can diffuse to the other side of the GJ if they fit through the pore formed by the gap junctions ($\approx$ 12–14 Å, Connors and Long, 2004). Thus, ion concentration gradients across the membrane cause a current through the GJ. This is the reason why the terms *electrical synapse* and *electrically coupled* are used as synonyms for gap junction, which I also use throughout this thesis.

The size of a GJ pore depends on which molecular building blocks constitute the GJ. The most relevant of molecules establishing neuronal gap junctions are connexins (cf. Pereda, 2014). Different connexins exist and they are categorized by their weight in kDa. The most relevant connexins for mammalian neuronal coupling are connexin45 and connexin36 (Cx36). The latter, Cx36, is known to couple interneurons and is expressed abundantly in the neocortex and in the hippocampus (Fig. 2.1D, Connors and Long, 2004).

The Cx36 gap junctions have a relatively small unitary conductance of $\approx$ 10–15 pS (Srinivas et al., 1999). However, unitary conductances are seldom measured directly since gap junctions mostly form clusters, and their conductances add up linearly (Fig. 2.1B, C). Depending on the size of the GJ cluster, the distance of the cluster to the soma, and other electrophysiological parameters, the measured GJ conductances are distributed between 10–2100 pS (Galarreta and Hestrin, 2001a; Connors and Long, 2004). This range was obtained from multiple experiments in which the measurements were usually done from soma to soma. However, because measurements have to be compensated for the loss taking place within the dendritic trees of the neuron the real conductances of the GJs are potentially larger.

2.2.2 Function of gap junctions

There are two main messaging pathways between neurons: chemical synapses and gap junctions. Gap junctions can be described as ohmic conductors. They are not dependent on action potentials, are usually bidirectional, and enable subthreshold coupling. In contrast, chemical synapses are dependent on a presynaptic action potential, are unidirectional, and require the emission of a chemical neurotransmitter, which equips chemical synapses with their functional diversity.

Since gap junctions establish a direct connection between two neurons, they couple the cells both electrically and chemically. Their role for chemical messaging is especially important in early development when gap junctions outbalance chemical synapses. At this stage, GJs are relevant for the functional differentiation of neuronal circuits (Montoro

and Yuste, 2004; Shimizu and Stopfer, 2013). Here, also GJ coupling between excitatory neurons is commonly found. Additionally, the electrical function of gap junctions also might support the maturation of brain circuits by facilitating oscillatory activity (Yuste et al., 1992; Zhang and Poo, 2001). Moreover, increased gap junction expression is prevalent after traumatic brain injuries, possibly to rescue and repair neuronal circuits (Belousov and Fontes, 2013). These examples show that GJs as pathways for chemical messaging play an important role during development, and are probably still relevant throughout the entire life. However, since my research project is concerned with the functions of gap junctions as electrical synapses in the adult brain, I focus on this topic in the following.

In the mature brain, the number of GJs is decreased in comparison to the developing brain; however, a significant amount of GJs persist (Meyer et al., 2002). These GJs contribute to the network dynamics in the different parts of the brain, where they coexist with chemical synapses. Since these dynamics are complex, the role of gap junctions in neuronal circuits cannot be generalized easily. Nevertheless, in the upcoming paragraphs the most relevant functional aspects of GJs for my research are presented.

There have been substantial contributions using experimental, computational, and analytical approaches to understand the functional role of gap junctions as electrical synapses (e.g., Bennett, 1997; Galarreta and Hestrin, 2001b; Yang and Michelson, 2001; Traub et al., 2001; Maex and De Schutter, 2003; Bennett and Zukin, 2004; Kopell and Ermentrout, 2004; Saraga et al., 2006; Pfeuty et al., 2005; Ostojic et al., 2009; Guo et al., 2012; Tchumatchenko and Clopath, 2014). Synchrony is the most prominent GJ function found independently of the research methodology. The idea of this is straightforward: GJs act as ohmic conductors between the potentials of the neurons, hence equilibrate their membrane potentials, which in turn leads to synchronous activity (Bennett, 1997).

Synchronous neuronal activity often co-occurs with neuronal oscillations, which is another function that is strongly associated with gap junctions (Chapter 3). This has been investigated theoretically in the most reduced neuronal network: two coupled neurons (Kepler et al., 1990; Lewis and Rinzel, 2003; Bem and Rinzel, 2004; Kopell and Ermentrout, 2004; Pfeuty et al., 2005; Saraga et al., 2006). These studies found that depending on the choice of the parameters, GJs can have differential effects on two-neuron networks: GJs can stimulate oscillations and influence the oscillation frequency, synchronize and desynchronize/anti-synchronize the two-neuron network. These analytical and computational results have been bolstered by theoretical studies of networks that consist of more than two neurons (Ostojic et al., 2009; Guo et al., 2012). For instance, Ostojic et al. (2009) showed that a network exclusively coupled by GJs can oscillate but only at the mean firing rate of the single neurons. Simulations of more biologically realistic neuronal networks confirm that gap junctions increase synchrony and promote oscillatory activity (Maex and De Schutter, 2003; Bartos et al., 2007).

The strong link between GJs and oscillatory and synchronous activity has been investigated experimentally as well. It was found that gap junctions can facilitate different oscillatory patterns in the brain, e.g., theta oscillations ($\approx 10\,\mathrm{Hz}$; Konopacki et al., 2013), gamma oscillations ($\approx 70\,\mathrm{Hz}$; Traub et al., 2000; Yang and Michelson, 2001; reviewed by LeBeau et al., 2003), sharp wave-ripples ($\approx 200\,\mathrm{Hz}$; e.g., Draguhn et al., 1998; or

cf. Chapter 3) and epileptic discharges (reviewed by Carlen et al., 2000). Interestingly, it was also experimentally shown that gap junctions can desynchronize neuron ensembles, as predicted earlier by theoretical work (Vervaeke et al., 2010; Lewis and Rinzel, 2003; Saraga et al., 2006). Due to the short transmission delays of GJ potentials, GJs have not only been proposed to cause synchrony but also to detect synchronous, coincident activity (Galarreta and Hestrin, 2001b).

Recently, some assumptions about GJs have been shown to not be valid in general: GJ coupling can be asymmetric (Sevetson and Haas, 2014), plastic (Haas et al., 2011; Coulon and Landisman, 2017; Snipas et al., 2017), and delays can be long depending on the GJ position (Chapter 3).

In conclusion, gap junctions are used for chemical and electrical messaging between neurons, and their function comprises generation of synchrony and oscillatory activity but certainly also more complex functions, which are dependent on the specific network context.

In this thesis, I focus on the function of GJs as electrical synapses between interneurons. Thus, next I review experiments that report details on this connectivity.

2.3 Gap junctions between parvalbumin-positive basket cells

What is known about electrical connectivity depends strongly on the brain region, and is a matter of ongoing research. Because I follow the hypothesis that sharp wave-ripples are generated by PV+BCs in the hippocampal area CA1 (Chapter 1.1.1), my main focus is on gap junctions between PV+BCs in the hippocampal area CA1. However, since life is not always a bowl of cherries and such data is rare in CA1, I also review data from the entire hippocampus and neocortex.

In the following, I first present data from the hippocampus, which is based on electron microscopy, and then review findings from the hippocampus and the neocortex, which are based on dual-cell recordings. An overview of all the referenced experimental data on GJ connectivity can be found in Table 2.1.

Technique	Animal	Region	Cell type	Distance / Location*	Connectivity**	Reference
			Hippocampal formation			
EM	rat	CA1	non-pyr	-	-	Kosaka (1983)
EM	rat	CA1/CA3	non-pyr	70–27 µm	-	Kosaka and Hama (1985)
EM	rat	CA1	PV+	soma, dendrite	-	Katsumaru et al. (1988a)
EM	rat	CA1	PV+	proximal, distal	-	Fukuda and Kosaka (2000a)
DCEP	postnat. rat	DG	BC	10–40 µm	82% , $N = 11$	Venance et al. (2000)
DCEP	mice	HC	PV+BC	< 200 µm	29%, $N = 49$	Bartos et al. (2001)
DCEP	mice (KO36)	CA3	PV+FS	≈ 50 µm	62% , $N = 8$	Hormuzdi et al. (2001)
DCEP	mice (KO36)	DG	PV+FS	≈ 50 µm	92%, $N = 13$	Hormuzdi et al. (2001)
DCEP	mice	DG	PV+BC	< 100 µm	92%, $N = 13$, P14	Meyer et al. (2002)
"	"	"	"	"	50%, $N = 10$, P28	
DCEP	rat	DG	PV+BC	-	33%, $N = 9$	Bartos et al. (2002)
DCEP	rat	CA3	PV+BC	-	50%, $N = 6$	Bartos et al. (2002)
DCEP	rat	CA1	PV+BC	-	22%, $N = 9$	Bartos et al. (2002)
			Neocortex			
DCEP	rat	NC, L5	FS (9 of 12 PV+)	< 80 µm	66%,$N = 44$	Galarreta and Hestrin (1999)
DCEP	rat	L4/6	PV+FS	< 50 µm	62%, $N = 39$	Gibson et al. (1999)
DCEP/EM	rat	NC, L2/3	(PV+)BC	3.6 µm	not quantified	Tamás et al. (2000)
DCEP	rat	NC, Tha	FS	< 200 µm	59%, $N = 88$	Amitai et al. (2002)
EM	rat	NC	PV+BC	< 500 µm	< 10 GJs per neuron	Fukuda and Kosaka (2003)
EM	cat	L2/3	PV+BC	< 380 µm	≈ 60 GJs per neuron	Fukuda et al. (2006)

Table 2.1: Gap junction connectivity and estimates for the coupling distance between (potential) basket cells within hippocampus and neocortex. Connections between interneurons are most prominent within 0.2 mm. *, Distance measured from soma to soma if available, other position of the GJ in neuronal tree is given, e.g., soma; **, N given denotes the number of tested neuron pairs. EM, electron microscopy; DCEP, dual-cell recording electrophysiology; non-pyr, non-pyramidal cell; PV+, parvalbumin-positive; BC, basket cell; FS, fast spiking cell. NC, neocortex; L1–5, layer 1–5 in NC; Tha, thalamus. Cell type attribute in parenthesis was not tested for all the recorded neurons.

2.3.1 Proof of existence: gap junctions between hippocampal parvalbumin-positive basket cells in ultrastructural studies

Kosaka (1983) was the first researcher to report GJ coupling between putative interneurons in the hippocampal areas CA1 and CA3. He used electron microscopy to take high resolution micrographs on which gap junctions are visible as "a cytoplasmic semidense material [that] undercoats the whole length of the inner surfaces of the junctional plasma membrane" (Sotelo and Korn, 1978; see Fig. 2.1C to appreciate the art of identifying GJs on electron micrographs). He reported that there were GJs between non-pyramidal cells in 7 animals, and he hypothesized that the imaged cells were inhibitory interneurons. Later studies confirmed GJ coupling in dendrodendritic and dendrosomatic locations of hippocampal interneurons and indicated that these neurons were basket cells (Kosaka and Hama, 1985) and parvalbumin-positive (Katsumaru et al., 1988a). Interestingly, the establishment of the interneuron type "parvalbumin-positive basket cell" (PV+BC) is tightly interwoven with the discovery of GJs between this neuron type (Katsumaru et al., 1988a), and hence was introduced in the same year by the same researchers (Katsumaru et al., 1988b). Further studies confirmed GJ coupling between PV+BCs in the hippocampal area CA1 and additionally showed that GJ locations can be distal and proximal in the dendritic tree of the neurons (Fukuda and Kosaka, 2000b; overview in Table 2.1).

While these ultrastructural studies demonstrated that gap junctions are morphologically connecting PV+BCs in the hippocampus, electron microscopy does not allow judgements about the functionality of GJs as electrical synapses. Furthermore, it is difficult to draw strong empirical conclusions about the morphological connectivity due to the high complexity of the ultrastructural recordings. In most of the cases, the dendritic tree is visible only partially, and even if a dendrite is captured in its total on the micrograph, there is no guarantee that all GJs can be identified (Fig. 2.1C).

2.3.2 Quantitative assessment: gap junction coupling potentials in dual-cell recordings

The findings in Section 2.3.1 are based on ultrastructural micrographs that provide high-resolution morphology data, but only electrophysiological data can show whether GJs are functional. In consequence, direct measures of the GJ coupling potentials, e.g., via dual-cell recordings, are necessary. Since such recordings have been difficult to obtain at the time when the interest in GJ connectivity in the hippocampus was at its peak, there are not many hippocampal dual-cell recordings of GJ coupling potentials available (Venance et al., 2000; Bartos et al., 2001, 2002; Hormuzdi et al., 2001; Meyer et al., 2002). To nevertheless get an idea of the delay and the shape of GJ coupling potentials, data not only from areas CA1 and CA3 but also from the whole hippocampal formation and neocortex is reviewed (Galarreta and Hestrin, 1999, 2001b; Gibson et al., 1999; Tamás et al., 2000; Amitai et al., 2002; see Table 2.1).

The first intracellular dual-cell recordings of GJ coupling potentials between parvalbumin-positive, fast-spiking interneurons were made simultaneously by Galarreta and Hestrin

(1999) and Gibson et al. (1999) in the neocortex. A third study from Tamás et al. (2000) confirmed these results and showed that the neurons are PV+BCs, which might also be true for the previous findings. These studies report that neurons further than 200 µm apart are only rarely coupled by GJs, since for dendritic GJ coupling the dendritic processes must overlap (reviewed in Galarreta and Hestrin, 2001a). Indeed, when two PV+BCs are within a radius of 200 µm the GJ connection probability is high: 59 % (Amitai et al., 2002), 61 % (Gibson et al., 1999), and 66 % (Galarreta and Hestrin, 1999). Moreover, the coupling potentials show minimal delays of $\lesssim 0.5$ ms (Galarreta and Hestrin, 1999; Tamás et al., 2000). As previously found in the hippocampus, the coupling is both somatodendritic and dendrodendritic. Interestingly, interneurons seem to sustain GJ connection preferentially to the same neuron subtype (Gibson et al., 1999) even though exceptions have been shown recently (Hatch et al., 2017).

In the hippocampal loop, GJ coupling potentials have been measured in dentate gyrus (Bartos et al., 2001; Meyer et al., 2002; Bartos et al., 2002; Hormuzdi et al., 2001), in CA3 (Hormuzdi et al., 2001; Bartos et al., 2002) and CA1 (Bartos et al., 2002). In contrast to the studies from neocortex, these hippocampal studies are less detailed. The reported GJ connection probability in dentate gyrus varies from 29 % (Bartos et al., 2001) to up to 92 % (Hormuzdi et al., 2001). For CA3, GJ connection probabilities of 63 % (5 of 8; Hormuzdi et al., 2001) and 50 % (3 of 6; Bartos et al., 2002) have been found for fast-spiking, PV+ interneurons and PV+BCs, respectively. To our knowledge, the only study which explicitly showed GJ coupling between PV+BCs in CA1 is from Bartos et al. (2002), who showed that 22 % (2 of 9) PV+BCs are GJ coupled.

2.4 Experimental evidence for the functional role of (interneuronal) gap junctions in hippocampal ripple oscillations

In the previous section, evidence that GJs exist in the hippocampal area CA1 between PV+BCs is presented, which are hypothesized to be the pacemaker of ripple oscillations (Ylinen et al., 1995; also Chapter 3). In this section, I review the experiments that have investigated the effect of GJs on ripple oscillations. This research was primarily triggered by experiments from Draguhn et al. (1998), who proposed that gap junctions between excitatory pyramidal cells generate ripple oscillations (Traub et al., 1999, 2000). However, reproducible sound evidence for GJ coupling of mature pyramidal cells is still missing (Schmalbruch and Jahnsen, 1981; Condorelli et al., 2000; Mercer et al., 2006; Wang et al., 2010). Interestingly, the means for blocking GJs in experiments are not specific to putative GJs between pyramidal cells but also block GJs between interneurons (Section 2.3).

In general, two major approaches exist to manipulate the function of gap junctions (Table 2.2; see review by Posłuszny, 2014). The first method is to use drugs that block or uncouple GJs (Pais et al., 2003; Hormuzdi et al., 2001; Draguhn et al., 1998; Traub et al., 2003; D'Antuono et al., 2005; Behrens et al., 2011). The second method is to delete GJ proteins genetically, so that animals grow up without GJs (Hormuzdi et al.,

2001; Buhl et al., 2003; Maier et al., 2002). This section gives an overview of experiments that have applied these GJ deactivation techniques to probe the effect of GJs on SWRs, and discusses the limitations of such experiments. The results of these experiments are summarized in Table 2.2.

2.4.1 Gap junction deletion

Gap junctions between hippocampal inhibitory neurons are predominantly formed by connexin36 proteins (Cx36; Section 2.2.1). Genetic manipulation allows to create Cx36 knockout (Cx36KO) mice (Hormuzdi et al., 2001; Güldenagel et al., 2001). These mice express no active Cx36, and consequently, there are no Cx36-based electrical synapses in the brain (Hormuzdi et al., 2001). Here, I review the studies that analyzed SWRs in Cx36KO mice (Table 2.2, top).

Using Cx36KO mice, Hormuzdi et al. (2001) experimentally analyzed the functional role of GJs in SWR oscillations in the hippocampal area CA3 in vitro. They found that SWRs are still present in Cx36KO mice. Interestingly, these SWRs can be blocked by octanol, a GJ blocker. The persistence of SWRs in Cx36KO mice was backed up by an in vivo study from Buhl et al. (2003), who showed that SWRs are not significantly altered in CA1 region. Additionally, they could neither find a change of ripple frequency (150 Hz) nor of the ripple amplitude in Cx36KO mice. In contrast, a detailed in vitro study showed that the incidence of SWRs and the frequency of the ripple oscillations are significantly altered in CA1 (192 $\rightarrow$ 176 Hz, Maier et al., 2002). A further study from Pais et al. (2003) showed that "fast ripples" (60–115 Hz) evoked by kainate were present only in the Cx36KO mice and not in the control group. Because this study did not report SWRs in the wild type and the observed oscillation frequencies were well below ripple range, we might not consider this study for further analysis.

In conclusion, the studies do not deliver a coherent picture of the role of Cx36 gap junctions between PV+BCs. These contradicting results might be explained by the fact that the experiments suffer from confounding factors. Most importantly, the genetically modified mice grow up without GJs. As a result, regulatory mechanisms might induce compensatory effects during development.

2.4.2 Gap junction blockers

An alternative approach to test the function of gap junctions is to block or uncouple them pharmacologically. For this purpose, different drugs are available (Juszczak and Swiergiel, 2009). Secondary effects have to be taken into consideration when interpreting data from these studies because GJ blockers are unspecific, have strong side effects, and the particular mechanisms by which they block GJs are largely unknown. So, I first discuss the findings of experiments studying the effects of chemical GJ blockers (Table 2.2, bottom), and thereafter, I consider the confounding factors that accompany the available drugs.

The most common gap junction blockers are carbenoxolone, octanol, halothane, and mefloquine. Carbenoxolone was used in multiple studies that investigated the functional

role of GJs in SWRs. Three of these studies found that it completely abolished SWRs in vitro (Draguhn et al., 1998, 100 μM, CA3; Pais et al., 2003, 200 μM, CA3, triggered by kainate; Behrens et al., 2011, 200 μM, CA3). These findings were to some extent confirmed by other studies that found high-frequency oscillations to be strongly reduced (Maier et al., 2003, 200 μM, CA1) or significantly reduced (Traub et al., 2003, 200 μM, CA1, evoked by GABA). In contrast, in another in vitro experiment the ripple-like oscillations were only mildly affected (D'Antuono et al., 2005, 200–600 μM, DG, evoked by picrotoxin).

Similar results have been obtained by the GJ blocker octanol. While Draguhn et al. (1998) found that octanol "repeatedly blocks SWRs" (1 mM, CA3, normal ACSF), others found that it strongly reduces SWRs (Maier et al., 2003, 1 mM, CA1, normal ACSF) or only leads to a mild reduction (D'Antuono et al., 2005, 0.2–0.5 mM, DG, evoked by picrotoxin).

The first evidence that blocking GJ leads to a consistent block of SWRs were achieved using halothane (Ylinen et al., 1995, 1-3 % (of ACSF), CA1; Draguhn et al., 1998, 5 mM, CA3).

In contrast to all these drugs, mefloquine, the GJ blocker that was shown to be most specific (Cruikshank et al., 2004), did not significantly affect SWRs (Behrens et al., 2011, 50 μM, CA3).

In conclusion, different studies show very different effects of GJ blockers on SWRs. On the one hand, this might be caused by the different preparations of the neuronal tissue and different means to evoke the SWRs. On the other hand, we assume that the multiple side effects of GJ blockers are responsible for the diverse results. These side effects are the topic in the next section.

Area	Drug/Method	Stimulation	Effects on SWRs	Effect on ripples	Ripple freq. (Hz)	Reference
			Cx36 knockout			
CA3	Cx36KO	Ca^{2+} - free	No effect/no detailed analysis	n.m.	n.m.	Hormuzdi et al., 2001
CA1	Cx36KO	-	Significant small effect	reduced incident	significant 192 → 176	Maier et al., 2002
CA1*	Cx36KO	-	No significant effect	no effect	149 → 150	Buhl et al., 2003
CA3	Cx36KO	Kainate	**	n.m.	71	Pais et al., 2003
			GJ blockers			
CA3	Carbenoxolone	-	Abolishment	-	-	Draguhn et al., 1998
CA1	Carbenoxolone	GABA	Significant Reduction	n.m.	broad, 120–400	Traub et al., 2003
CA1/3	Carbenoxolone	-	Strong Reduction	n.m.	unchanged 193 (CA1)	Maier et al., 2003
DG	Carbenoxolone	Picrotoxin	Mild reduction	decreased duration	unchanged ≈ 200	D'Antuono et al., 2005
CA3	Carbenoxolone	-	Abolishment	-	-	Behrens et al., 2011
CA3	Cx36KO + Carbenoxolone	Kainate	Abolishment	-	-	Pais et al., 2003
CA3	Octanol	-	Abolishment	-	-	Draguhn et al., 1998
CA1/3	Octanol	-	Strong Reduction	n.m.	unchanged 193 (CA1)	Maier et al., 2003
DG	Octanol	Picrotoxin	Mild reduction	decreased duration	unchanged ≈ 200	D'Antuono et al., 2005
CA1	Octanol	KCl***	Strong Reduction	strong reduction	n.m.	Nimmrich et al., 2005
CA3	Cx36KO + Octanol	Kainate	Abolishment	n.m.	n.m.	Hormuzdi et al., 2001
CA1*	Halothane	-	Abolishment	-	-	Ylinen et al., 1995
CA3	Halothane	-	Abolishment	-	-	Draguhn et al., 1998
CA3	Mefloquine	-	No significant effect	not sign. reduction	183 → 177	Behrens et al., 2011

Table 2.2: Overview of studies of GJ blockers and Cx36 knockout studies. All experiments are carried out in vitro, except for the ones marked by (*), which are in vivo. Cx36KO, Connexin36 knockout, i.e., the genetic deletion of the most relevant gap junctions protein for coupling between interneurons. "-" quantities that could not be given; "n.m." not measured. (**), the fast oscillations are only present in the Cx36KO so we cannot compare the wild type oscillation to the Cx36KO oscillations. (***) Additional to the KCl puff all synaptic transmission is blocked by 10 µmol SR-95531, 20 µmol CNQX, and 30 µmol DL-APV. Extended from Posłuszny (2014).

2.4.3 Confounding factors of gap junction blockers

How much can we learn from the studies that are based on blocking GJs chemically? To be able to answer this question, we need to know which effects the pharmaceutics have beyond GJ blocking.

Carbenoxolone has a strong influence on excitatory and inhibitory synaptic currents. Tovar et al. (2009) came to the strong conclusion that

> "CBX [Carbenoxolone] broadly affects several neuronal membrane conductances independent of its effects on gap junctions. Thus effects of carbenoxolone on network activity cannot be interpreted as resulting from specific block of gap junctions."
>
> – Tovar et al. (2009)

These results have been confirmed by a study from Maier et al. (2011, Supplemental Information, Fig. S9). If synaptic currents, which are dependent on synaptic conductances, are affected that strongly, carbenoxolone has a strong effect on SWRs even if GJ are not important for the oscillations. This fits well to observations from Pais et al. (2003) who found that carbenoxolone also blocks SWRs in Cx36KO mice.

For octanol, many side-effects have been found as well, in particular it was reported that

> "[...] octanol enhances the GABAA (0.01–0.05 mM) and glycine receptor responses (0.006–0.05 mM) and, with lower potency, it inhibits the responses of the NMDA (0.1–0.4 mM), AMPA (0.2– 0.5 mM) and kainate (0.1–0.4 mM) receptors."
>
> – Juszczak and Swiergiel (2009)

Maybe these side effects could explain that octanol, like carbenoxolone, can abolish SWRs even in Cx36KO mice (Hormuzdi et al., 2001). This raises the question whether the abolishment or the strong suppression of SWRs found in the studies using octanol are caused by the GJ blocking effect (see Table 2.2; e.g., Draguhn et al., 1998; Maier et al., 2003). There are (at least) two possible explanations for this observation: either there were other GJ types present that were constituted by connexins different than Cx36, which were blocked by octanol (Traub et al., 2000), or a non-specific side effect of octanol, not the GJ blocking effect, caused the abolition of the SWRs.

Halothane, another gap junction blocker, is known to block GJs only if the concentration is high enough to induce anesthetic effects (Wentlandt et al., 2006). Assuming that the loss of conscience is not a direct consequence of GJ blocking, this drug probably affects a broad range of neuronal dynamics, and hence might as well affect SWRs.

Even mefloquine, probably the most specific blocker for Cx36 and Cx50 GJs (Cruikshank et al., 2004),

> "[...] significantly increased the afterhyperpolarization following evoked action potentials (APs) resulting in reduced probability of AP firing during depolarizing current injection."
>
> – Behrens et al. (2011)

Furthermore, the intake of mefloquine, which is a common malaria medication, is known to cause psychological side effects, which are putatively not singly caused by the blocking of gap junctions (Juszczak and Swiergiel, 2009), and is known to block potassium channels (Gribble et al., 2000).

In sum, all the used gap junction blockers are not specific and have side effects that might alter SWRs. For a more detailed account of the specific effects of different GJ blockers I refer the reader to the review by Juszczak and Swiergiel (2009). In face of the results from the GJ blocker and Cx36KO experiments, it seems to be difficult to deduce the role of GJs in SWRs experimentally since neither the GJ blocker studies nor the Cx36KO studies delivered a clear result.

2.5 Summary

In this chapter, gap junctions are introduced as a basic pathway for neuronal communication. The existence of GJs was firstly demonstrated by electron microscopy. Later, these findings have been confirmed by dual-cell recordings, which allowed to directly measure GJ coupling potentials. Since then electrical synapses have been found in multiple locations in the brain, frequently between various types of interneurons.

Gap junctions might be relevant for SWRs because they couple PV+BCs that have been identified to fire phase locked to hippocampal ripple oscillations, and hence are an ideal candidate for pacemaking these fast oscillations (Chapter 3). GJs are also hypothesized to generate ripple oscillations by coupling pyramidal cells (Traub et al., 1999). Unfortunately, experiments that probed the functional role of gap junctions in SWRs could not clarify their contribution. I assume that this is mostly caused by the side effects of the GJ manipulation methods on the neuronal tissue.

Due to these experimental limitations, it is relevant to analyze the effect of interneuronal GJ coupling on hippocampal SWRs within a theoretical framework. This is the topic of the next chapter.

3 Interneuronal gap junctions increase synchrony and robustness of hippocampal ripple oscillations

Sharp wave-ripple (SWRs) are important for memory consolidation. Their signature in the hippocampal extracellular field potential (EFP) can be decomposed into a $\approx 100\,\text{ms}$ long sharp wave superimposed by $\approx 200\,\text{Hz}$ ripple oscillations. How ripple oscillations are generated is currently not well understood. A promising model for the genesis of ripple oscillations is based on recurrent interneuronal networks (INT-INT). According to this hypothesis, the INT-INT network in CA1 receives a burst of excitation from CA3 that generates the sharp wave, and recurrent inhibition leads to an ultrafast synchronization of the CA1 network causing the ripple oscillations; fast-spiking parvalbumin-positive basket cells (PV+BCs) may constitute the ripple-generating interneuronal network. PV+BCs are also coupled by gap junctions (GJs) but the function of GJs for ripple oscillations has not been quantified. Using simulations of CA1 hippocampal networks of PV+BCs, we show that GJs promote synchrony and increase the neuronal firing rate of the interneuronal ensemble, while the ripple frequency is only affected mildly. The promoting effect of GJs on ripple oscillations depends on fast GJ transmission ($\lesssim 0.5\,\text{ms}$), which requires proximal gap junction coupling ($\lesssim 100\,\mu\text{m}$ from soma). [1]

3.1 Introduction

Sharp wave-ripple (SWRs) are transients of the extracellular field potential (EFP) in the hippocampus that occur in rest and slow-wave sleep (Buzsáki et al., 1992). SWRs consist of $\approx 200\,\text{Hz}$ ripple oscillations that are enveloped by the $\approx 100\,\text{ms}$ long sharp wave (O'Keefe, 1976; O'Keefe and Nadel, 1978). Different computational tasks are associated with SWRs, e.g., decision making via preplaying future trajectories (Diba and Buzsáki, 2007) or memory consolidation (Girardeau et al., 2009) putatively via replay of past events (Wilson and McNaughton, 1994), which underlines their role for the two-stage model of memory consolidation (Buzsáki, 1989, see also Chapter 1.2.1).

The underlying mechanism that is responsible for generating ripples is debated (Traub et al., 2000; Memmesheimer, 2010; Ylinen et al., 1995). Three distinct origins of ripples were proposed, which could also coexist: (1) the axonal plexus of pyramidal neurons, which is putatively densely coupled by GJs (Draguhn et al., 1998; Traub et al., 1999), (2) supralinear synaptic integration in feedforward excitatory networks (Memmesheimer,

[1] The content of this chapter was developed together with Richard Kempter. A preprint of the resulting article is avaiable online (Holzbecher and Kempter, 2018).

2010; Jahnke et al., 2015) and (3) fast recurrent interneuronal networks (INT-INT, Ylinen et al., 1995). In silico, all of these models can create ripple-like oscillations (see also Chapter 1.3).

Recent experiments support the INT-INT hypothesis. In CA3, Schlingloff et al. (2014) showed in vitro that optogenetic activation of PV+ interneurons leads to ripple-like oscillations, even with excitatory chemical transmission blocked. This matches well the results from an in vivo study by Stark et al. (2014), where blocking of the interneurons abolished ripple oscillations in CA1. Following this hypothesis, evidence accumulates that from the zoo of interneurons (Chamberland and Topolnik, 2012; see also 1.1.1) fast-spiking parvalbumin-expressing basket cells (PV+BCs) are a key component of the INT-INT ripple-generating network (Klausberger et al., 2003; Schlingloff et al., 2014). PV+BCs are highly active during SWRs and fire phase-locked to ripple oscillations (Klausberger et al., 2003). Furthermore, INT-INT networks can explain intraripple frequency accommodation (Donoso et al., 2018), an experimental hallmark of SWRs (Ponomarenko et al., 2004).

Additional to the strong and fast GABAergic synapses, PV+BCs are coupled by gap junctions (GJs; Fukuda and Kosaka, 2000b; Tamás et al., 2000; Galarreta and Hestrin, 2001a,b; Bartos et al., 2002). Two major categories of experiments exists to determine the function of GJs in SWRs (Chapter 2.4; Table 2.2): pharmacological GJ blockers (Ylinen et al., 1995) and genetic knockouts of GJ proteins (Hormuzdi et al., 2001; Güldenagel et al., 2001). However, the experimental results prove ambiguous and hence inconclusive, i.e., many of the experiments that use GJ blockers find a strong suppression of SWRs (Ylinen et al., 1995; Draguhn et al., 1998; Hormuzdi et al., 2001; Maier et al., 2003; Pais et al., 2003; Traub et al., 2003; Buhl et al., 2003; Behrens et al., 2011), while the studies relying on GJ knockout mice find a rather mild effect (Hormuzdi et al., 2001; Pais et al., 2003; Buhl et al., 2003; Behrens et al., 2011).

In addition to experiments, there are also substantial contributions from theoretical neuroscience to understand the function of GJs in oscillations. These results were derived by both analytical (Lewis and Rinzel, 2003; Pfeuty et al., 2005; Ostojic et al., 2009; Tchumatchenko and Clopath, 2014) and numerical means (Traub et al., 2001; Maex and De Schutter, 2003; Bartos et al., 2007; Guo et al., 2012; Fink et al., 2015).

On the analytical side, studies from Lewis and Rinzel (2003) and Pfeuty et al. (2005) of two-neuron systems have shown that the effect of GJs on synchrony depends on the proportions of electrical and chemical coupling. Using mean-field analysis, Ostojic et al. (2009) showed that oscillations can arise in a neuronal network that is exclusively coupled by GJs but the network frequency equals the mean firing rate of the neurons.

While these studies provided a sound theoretical basis, they were not specifically tailored to reproduce biologically realistic networks. Numerical simulations give more insights on this issue, e.g., GJs were found to increase synchrony in gamma oscillations (30–70 Hz, Traub et al. 2001; Bartos et al. 2007; Guo et al. 2012) and ripple oscillations (Maex and De Schutter, 2003). However, Maex and De Schutter restricted their analysis to one set of GJ parameters, which does not satisfy the variability found in the GJ connectivity data (Chapter 2.3 and Table 2.1).

Even though there is evidence that PV+BCs are coupled by GJs and that PV+BCs

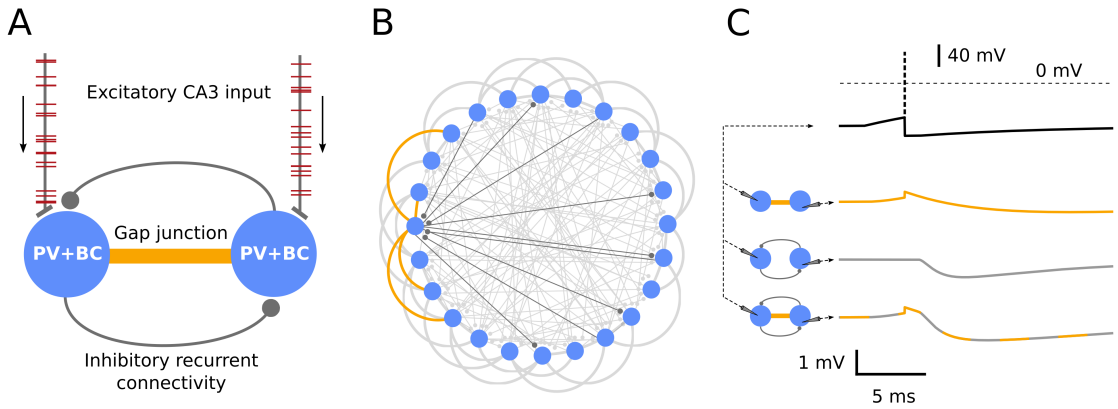

Figure 3.1: Network architecture. **A**, Network schematic of the CA1 PV+BC network that receives Poisson distributed excitation representing inputs from the CA3 region (arrows). The CA1 neurons are coupled by gap junctions (orange) and inhibitory synapses (gray lines with circles at their ends). **B**, More detailed scheme of connectivity. To resemble an in-vitro slice preparation, the network is chosen to consist of 200 neurons (here only 24 shown). Gap junctions are introduced with a connectivity of 0.3 between the 20% nearest neighbors, i.e., 0.06 overall connectivity (curves, highlighted in orange for one neuron on the left). Interneurons are randomly connected with a probability of 0.2 by inhibitory synapses (gray lines; highlighted in dark gray for one neuron on the left). **C**, Membrane potentials of a postsynaptic neuron show the response to a presynaptic action potential (top, black) when neurons are connected by only a gap junction (orange), only an inhibitory synapse (gray) or both (orange/gray). Standard parameters of all simulations are displayed in Tables 3.1 and 3.2.

are the generator of ripples, the implications of interneuronal GJ-coupling for ripple oscillations have not been investigated in depth. Thus, here we study how interneuronal GJs of different coupling probabilities, conductances, and delays impact the primary properties of hippocampal ripple oscillations, which advances our understanding about this phenomenon.

3.2 Methods

Since we want to investigate the influence of interneuronal GJs on hippocampal ripple oscillations, we first present the network model that we use for our analysis. Subsequently, we introduce the measures used to characterize ripple oscillations. Finally, we present the multicompartment models of hippocampal PV+BCs that are used for measuring the amplitudes and the delays of the GJ coupling potentials between two neurons. A summary of all standard parameters is given in Table 3.1, and an overview of all the varied parameters for each figure is given in Table 3.2.

3.2.1 CA1 network model

Hippocampal PV+BCs are highly active during SWRs and fire phase locked to ripple oscillations. Thus, we consider a minimal model for ripple generation in the CA1 hippocampal area that only consists of PV+BCs, and neglects all other neuron types as motivated by Donoso et al. (2018).

In this network model, the neurons are approximated by point-like leaky integrate-and-fire (LIF) neurons to set the focus on the network dynamics. In total, we simulate 200 neurons, which resembles the average number of PV+BCs in an in vitro slice preparation of the hippocampal area CA1 (Nimmrich et al., 2005; Donoso et al., 2018). The interneurons are coupled by gap junctions and inhibitory synapses, and they receive Poisson distributed excitation (Fig. 3.1A).

3.2.2 Neuron and synapse model

The dynamics of the membrane potential v_i of neuron i is modeled by

$$C \frac{\mathrm{d}}{\mathrm{d}t} v_i(t) = I_i(t)$$

for v_i that is below the firing threshold of $-52.0\,\mathrm{mV}$ (Wang and Buzsáki, 1996). When the membrane voltage reaches this threshold the neuron fires an action potential (AP). Subsequently, the neuron is reset to $-67.0\,\mathrm{mV}$ and remains inactive for a refractory period of $1.0\,\mathrm{ms}$ (Wang and Buzsáki, 1996). The capacitance is set to $C = 100\,\mathrm{pF}$ for all neurons (Buhl et al., 1996). Further, the current $I_i(t)$ that is received by the ith neuron is given by

$$I_i(t) = I_i^{\mathrm{GJ}}(t) + g_i^{\mathrm{inh}}(t)\left(v^{\mathrm{inh}} - v_i(t)\right) + g^{\mathrm{leak}}\left(v^{\mathrm{leak}} - v_i(t)\right) + g_i^{\mathrm{exc}}(t)\left(v^{\mathrm{exc}} - v_i(t)\right).$$

Here $g^{\mathrm{leak}} = 10\,\mathrm{nS}$ and $v^{\mathrm{leak}} = -65.0\,\mathrm{mV}$ (Buhl et al., 1996) are the leak conductance and the leak reversal potential, respectively. The analogous functions and parameters for inhibition and excitation are $g_i^{\mathrm{inh}}(t)$ and $v^{\mathrm{inh}} = -75.0\,\mathrm{mV}$ (Buhl et al., 1995), and $g_i^{\mathrm{exc}}(t)$ and $v^{\mathrm{exc}} = 0\,\mathrm{mV}$ (Taxidis et al., 2012), respectively. The membrane time constant set by this leak conductance and the membrane capacitance is $10\,\mathrm{ms}$ (Buhl et al., 1996).

The gap junction current $I_i^{\mathrm{GJ}}(t)$ is realized following an approach from Lewis and Rinzel (2003) and Ostojic et al. (2009). In this model, the current transferred through the gap junction to neuron i from all GJ coupled neurons j is given as (Fig. 3.1C)

$$I_i^{\mathrm{GJ}}(t) = \sum_{j \neq i}^{\#\mathrm{neurons}} \left(\gamma (v_j - v_i) + \beta C \sum_n^{N_j} \delta\left(t - t_n^{(j)} - \delta_{\mathrm{GJ}}\right) \right). \tag{3.1}$$

Here, the first term in the sum accounts for the passive subthreshold coupling. The bidirectional current is assumed to be ohmic, and hence given by the multiplication of the GJ conductance γ and the membrane potential difference of cell j and cell i. Since LIF neurons do not model the spiking dynamics of the membrane potential, the

postsynaptic potential caused by a *presynaptic* action potential is introduced manually by the second term. Naturally, gap junctions are bidirectional, and *postsynaptic* refers to the neuron, which receives a GJ potential and elicits no spike. Analogously, *presynaptic* is used hereafter to describe the neuron that elicited an action potential. Here, β is the amount of voltage added to the postsynaptic membrane potential of the neuron i at each presynaptic spiking event n ($n = 1, ..., N_j$) at times $t_n^{(j)} + \delta_{\mathrm{GJ}}$ of presynaptic neuron j. For this to hold true, the neuronal capacitance C is introduced in the expression, so that the product of C and β has the dimension of a charge. The parameter δ_{GJ} delays the response of the postsynaptic neuron to a presynaptic action potential and accounts for dendritic latencies. Since the active-spike component β mediates fast potentials, and hence more sensitive to a delay, the delay is only included in the active-spike component β. Biologically realistic values for β and γ can be extracted from electrophysiological studies (Galarreta and Hestrin, 1999; Tamás et al., 2000; Galarreta and Hestrin, 2001a), and here we use $\beta = 0.25\,\mathrm{mV}$ and $\gamma = 1.0\,\mathrm{nS}$ in most simulations. When we explore the effects of β and γ on the network dynamics, β is varied in the range $[0, ..., 0.5]\,\mathrm{mV}$ and γ in the range $[0, ..., 2.0]\,\mathrm{nS}$.

The inhibitory GABAergic conductances are modeled by a biexponential function (Fig. 3.1C)

$$g_i^{\mathrm{inh}}(t) = g^{\mathrm{peak}}\, K \left(\mathrm{e}^{-(t-\tau_{\mathrm{l}})/\tau_{\mathrm{d}}} - \mathrm{e}^{-(t-\tau_{\mathrm{l}})/\tau_{\mathrm{r}}} \right) \tag{3.2}$$

for a spike event at $t = 0$ and $t > \tau_{\mathrm{l}}$, otherwise $g_i^{\mathrm{inh}}(t) = 0$. Here, $\tau_{\mathrm{l}} = 1.0\,\mathrm{ms}$ sets the latency till the onset of the response, $\tau_{\mathrm{r}} = 0.45\,\mathrm{ms}$ is the rise time constant, and $\tau_{\mathrm{d}} = 1.2\,\mathrm{ms}$ is the decay time constant of the conductance. The peak conductance is given by $g^{\mathrm{peak}} = 5\,\mathrm{nS}$, and K is a normalization chosen such that the maximal value of the $g_i^{\mathrm{inh}}(t)$ is g^{peak} (Bartos et al., 2002).

Moreover, each neuron receives an excitatory Poisson-like input, which is mediated by the time dependent conductance $g_i^{\mathrm{exc}}(t)$. Here, we use the same model as for the inhibitory synapses but with $g^{\mathrm{peak}} = 1\,\mathrm{nS}$, $\tau_{\mathrm{l}} = 1.0\,\mathrm{ms}$, $\tau_{\mathrm{r}} = 0.5\,\mathrm{ms}$, and $\tau_{\mathrm{d}} = 2.0\,\mathrm{ms}$ (Taxidis et al., 2012).

3.2.3 Network connectivity

There are in total three types of different synaptic connections in the network model: feedforward excitation, recurrent inhibition, and bidirectional gap junctional coupling. Here, we briefly motivate the connectivities used in our model. For a more comprehensive overview of the GJ coupling between PV+BC, I refer the reader to Chapter 2.3 and Table 2.1.

Most of the studies of gap junctional coupling between PV+BC investigated neocortical areas (Tamás et al., 2000; Galarreta and Hestrin, 1999, 2001a; Amitai et al., 2002). They found that interneurons that are further than 200 µm apart are only rarely coupled by GJs since for dendritic GJ coupling the dendritic fields of the neurons have to overlap. However, within a radius of 200 µm the values found for the connection probability of PV+BCs are high: 59 % (Amitai et al., 2002), 61% (Gibson et al., 1999) and 66 % (Galarreta and Hestrin, 1999). Data for hippocampal networks is less abundant. The

GJ connection probability found in dentate gyrus varies from 29 % (Bartos et al., 2001) to up to 92 % (Hormuzdi et al., 2001). Data for the hippocampal area CA3 is provided by Hormuzdi et al. (2001) and Bartos et al. (2002), who found 5 of 8 (63 %) and 3 of 6 (50 %) fast spiking, parvalbumin-positive neuron pairs to be GJ coupled, respectively. Bartos et al. (2002) found in CA1 that 2 of 9 basket cell pairs were electrically coupled. Further evidence for GJ coupling in the area CA1 comes from ultrastructural studies (Katsumaru et al., 1988a; Fukuda and Kosaka, 2000b), which show the existence of GJ coupling, however electrophysiological studies that quantify GJ coupling in CA1 in more detail are, to our knowledge, not available (Bartos et al., 2002).

In conclusion, we set the standard connection probability for neurons within a distance of 200 µm to 30 %, and to 0 % otherwise. Note that in our network model a spatial structure is only introduced by GJs, which couple neurons to their nearer neighbors (Fig. 3.1B). When we explore the influence of the GJ connection probability on the network dynamics, we vary the connection probability in the range from 0 to 100 %.

The number of nearest neighbors in a vicinity of 200 µm is around 40 interneurons, since the total extent of the ventral hippocampal CA1 slice is around 1.1 x 0.4 x 0.1 mm^3 (Dougherty et al., 2012). For this approximation, we assume that the 200 neurons of the model are distributed homogeneously in space, but we neglect the 0.1 mm width of the pyramidal cell layer. Moreover, we take into account the effective size of the dendritic field in the 0.4 mm direction of the slice that is reduced by cutting the slices, i.e., most of the dendritic trees will not lie completely within the slice.

When we combine the number of neurons that are within a sphere of 200 µm with the assumed connectivity of 30 %, we find the overall GJ connectivity in the network to be $p_{GJ} = 0.06$ (Fig. 3.1B), i.e., one neuron is coupled to 12 other neurons via GJs on average.

Furthermore, the interneurons are coupled by random recurrent inhibition with 20 % connectivity according to estimates by Donoso et al. (2018) for ventral hippocampal slices. Excitation, of which 10 % is shared, is fed into the interneurons in form of Poisson distributed spike trains at 4000 spikes/s per interneuron in the simulations of the steady-state dynamics. In the case of the transient dynamics, each neuron receives 35 APs, whose times are drawn from a Gaussian distribution (width of 7 ms) to model a sharp wave-like excitation (Fig. 3.2). At the peak of the transient excitation the rate is ≈ 2000 spikes/s.

3.2.4 Simulation routine

The simulation time is 1 s for the steady state simulations, and 0.3 s for the transient SWR oscillation. At the start of each simulation, all neurons are initialized at a random membrane potential between reset and threshold voltage. For each network simulation the connectivities of inhibition and gap junctions are set randomly.

The network simulations are carried out using the spiking network simulator “Brian” (Goodman and Brette, 2008) and provenance is ensured by using pypet (Meyer and Obermayer, 2016).

3.2.5 How to characterize the network oscillations?

Measures that we use to quantify the simulated neuronal activity are: (1) the firing rate, (2) the network frequency, (3) the oscillation strength, and (4) the synchrony index.

The firing rate denotes how many times a neuron spikes per second, and it is computed over the whole time of the simulation, and averaged over the whole neuronal ensemble.

For the calculation of the network frequency, we combine the binary spike trains of the single neurons to one network spike train. Consequently, the network frequency is given by the frequency at the maximal power spectral density, i.e., the Fourier transformation of the autocorrelation function. To ignore the low-frequency components of the spectrum, we consider only frequencies $> 30\,\mathrm{Hz}$.

The oscillation strength is computed from the peak of the power spectral density as the product of the amplitude and the FWHM of that peak. This gives an estimate of the area under the peak that corresponds to how much power is distributed in the frequency modes around the network frequency.

The synchrony index we use is based on the pairwise event synchronization measure proposed by Quian Quiroga et al. (2002) and refined by Kreuz et al. (2007, 2015). For a spike i from spike train $t^{(1)}$ the coincidence with a (non-empty) second spike train $t^{(2)}$ is calculated by taking the minimum of the distances to each spike j in $t^{(2)}$ and comparing it with a coincidence window τ_c

$$A_i = \begin{cases} 1 & \text{if } \min_j \left(|t_i^{(1)} - t_j^{(2)}| \right) < \tau_\mathrm{c} \\ 0 & \text{otherwise} \end{cases} .$$

Here $\min_j$ means that the minimum is calculated over all the spikes of $t^{(2)}$. In contrast to (Kreuz et al., 2007), we use a fixed coincidence window $\tau_\mathrm{c} = 0.5\,\mathrm{ms}$. The coincidence indicator A_i is calculated for every spike i of every neuron. Then, all the A_i's are summed and divided by the total number of spikes N in all spike trains to obtain the synchrony index, and a such defined synchrony index would be between 0 and 1. To correct for spike events that are coincident by chance, which is determined by the product of $2\tau_\mathrm{c}$ and the average firing rate f, is subtracted. This yields for the synchrony index S

$$S = \frac{1}{N} \left(\sum_i^N A_i - 2\tau_\mathrm{c} f \right) . \tag{3.3}$$

The synchrony index is a measure that is used to compare the synchrony in different configurations of the network. Accordingly, the window size of 0.5 ms is chosen such that the synchrony index leads to well distinguishable values for oscillations at ripple frequency. For a comparison of different synchrony measures please see Section 7 in the Supplementary Material.

For the simulation of the transient SWRs, we calculate the time-resolved spectrograms of the network activity additionally to the periodogram. This analysis is carried out in Python using the inbuilt spectrogram function from the module SciPy (Jones et al., 2001–).

3.2.6 Multicompartment models for determining the gap junction transmission delay

Since there is no experimental data for the delays of GJ coupling potentials in hippocampal area CA1, we use multicompartment models of hippocampal PV+BCs to calculate these. For an estimate of the properties of the GJ coupling potentials, it is important that the shape of the action potential is as close as possible to the one in real PV+BCs. Using realistic spiking dynamics as a criterion, we selected two models with a simplified basket cell morphology (Lee et al., 2014; Saudargiene et al., 2015) from ModelDB (McDougal et al., 2017; Fig. 3.5A). Note that the model from Saudargiene et al. (2015) has a morphology similar to the model from Lee et al. (2014) but is scaled up by roughly a factor of two (Fig. 3.5A). The FWHMs of the PV+BC action potential that are measured in experiments are around 0.3 ms (Buhl et al., 1996; Kohus et al., 2016) while the FWHMs for the two models are ≈ 0.6 ms (Lee et al., 2014; Saudargiene et al., 2015). The impact of this mismatch between the widths of the action potentials is discussed further in the Results.

We used the multicompartment models for calculating three different characteristics of the GJ coupling potentials. First, the delay from the maximum of the presynaptic action potential to the maximum of the postsynaptic GJ potential, i.e., the peak delay (Fig. 3.5B left). Second, the delay from the maximal rise of the action potential to the maximal rise of the GJ coupling potential, i.e., the maximal-rise delay (Fig. 3.5C left). And third, the amplitude of the postsynaptic GJ coupling potential (Fig. 3.5D left). All these quantities are measured in dependence upon the soma–GJ distance. The GJ is modeled as a resistor coupling the two neurons with a conductivity of 1 nS (Galarreta and Hestrin, 2001b). For simplicity, all GJs are positioned symmetrically in the two coupled neurons, i.e., in the same dendrite and with the same distance to the soma in the respective neuron (Fig. 3.5A).

The three quantities, the peak delay, the maximal-rise delay, and the GJ amplitude, are estimated from the simulations, i.e., determined from the simulated voltage traces. The two coupled neurons are initialized at their equilibrium potentials, and then a current is injected in the presynaptic neuron until it elicits an action potential. More specifically, we inject a current of 0.95 nA for a duration of 4 ms into the model from Lee et al. (2014), and a current of 0.5 nA for 4 ms into the model from Saudargiene et al. (2015). These currents are chosen such that the action potential has a smooth onset. The membrane potentials of both somata are recorded while the action potential propagates from the pre- to the postsynaptic neuron.

Since the action potentials of the neuron models are too wide, we repeat the same analysis but with the AP replaced by a short, bipolar current pulse that resembles a (very) fast AP. This current pulse is generated by injecting a positive current, 0.1 ms long with an amplitude of 30 nA, and a negative current, 0.6 ms long and amplitude of -5.25 nA, into the soma of the model from Saudargiene et al. (2015), and currents of the same durations but amplitudes of 45 nA and -7.875 nA into the Lee et al. (2014) model. The bipolar current pulses are chosen such that the peak of the membrane potentials has approximately the same amplitude as an AP and the same value for both current

pulses, a small afterhyperpolarization, and a minimal width. Note that for this analysis, all active conductances were switched off. The action potentials and the bipolar current pulses for both models are depicted in Section 1 in the Supplementary Material.

Name	Symbol	Value	Reference
Gap junctions			
Active-spike component	β	0.25 mV	Galarreta and Hestrin, 2001a
Passive conductance	γ	1 nS	Galarreta and Hestrin, 2001a
Multicompartment GJ conductance	g^{GJ}	1 nS	Galarreta and Hestrin, 2001a
Inhibitory synapses			
Latency	τ_{l}	1.0 ms	Bartos et al., 2002
Rise time	τ_{r}	0.45 ms	Bartos et al., 2002
Decay time	τ_{d}	1.2 ms	Bartos et al., 2002
Peak conductance	g^{peak}	5 nS	Bartos et al., 2002
Reversal potential	v^{inh}	−75.0 mV	Buhl et al., 1995
Excitatory synapses			
Latency		1 ms	Taxidis et al., 2012
Rise time		0.5 ms	Taxidis et al., 2012
Decay time		2 ms	Taxidis et al., 2012
Peak conductance		1 nS	Taxidis et al., 2012
Reversal potential	v^{exc}	0 mV	Taxidis et al., 2012
Membrane properties of PV+BCs			
AP threshold		−52 mV	Wang and Buzsáki, 1996
Reset potential		−67 mV	Wang and Buzsáki, 1996
Refractory period		1.0 ms	Wang and Buzsáki, 1996
Leak reversal potential	v^{leak}	−65.0 mV	Buhl et al., 1996
Leak conductance	g^{leak}	10 nS	Buhl et al., 1996
Capacitance	C	100 pF	Buhl et al., 1996
Membrane time constant		10 ms	Buhl et al., 1996
Network properties			
Network size		200	Donoso et al., 2018
Overall GJ connectivity	p_{GJ}	0.06	Methods
GJ connectivity to nearest neighbor		0.3	Methods
GJ nearest neighbors		40	Methods
Inhibitory connectivity		0.2	Donoso et al., 2018
Averaged drive per neuron		4000 spikes/s	Donoso et al., 2018

Table 3.1: Standard parameters for all simulation except stated otherwise. If the "Methods" are referenced, a further explanation for the value of the parameter is given therein.

		p_{GJ}	β (mV)	γ (nS)	g^{GJ} (nS)	N_{excited}	δ_{GJ} (ms)	Input*
Fig. 1	**C**	-	0.25	1	-	-	0	AP
Fig. 2	**A**	0.06	0.25	1	-	200	0	Transient
	B	0	0.25	1	-	200	0	Transient
Fig. 3	**A**	0, 0.06, 0.12	0.25	1	-	200	0	Steady-state
	B	0–0.2	0.25	1	-	200	0	Steady-state
	C, D, E	0.06	0–0.5	0–2	-	200	0	Steady-state
Fig. 4	**A**	0	0.25	1	-	56	0	Steady-state
	B	0.06	0.25	1	-	56	0	Steady-state
	C–F	0, 0.06	0.25	1	-	0–200	0	Steady-state
	G	0	0.25	1	-	80	0	Steady-state
	H	0.06	0.25	1	-	80	0	Steady-state
Fig. 5		-	-	-	1	-	-	AP
Fig. 6		0–0.12	0.25	1	-	200	0–2.2	Steady-state

Table 3.2: Parameters varied across figures. Note that g^{GJ} is only used in the multicompartment model. (*) Input to the neuron or the interneuronal network. Here, "AP" stands for a sufficient input to stimulate an action potential; "Transient" for transient sharp wave-like excitation at a peak rate of ≈ 2000 spikes/s and a background Poisson rate of 750 spikes/s; "Steady-state" for Poisson steady-state input at 4000 spikes/s.

3.3 Results

The central question of our work is how gap junctions (GJs) between interneurons influence hippocampal ripple oscillations. We follow the hypothesis that hippocampal ripple oscillations are generated by recurrently connected interneurons (INT-INT), in particular, by parvalbumin-positive basket cells (PV+BCs) (Ylinen et al., 1995; Klausberger et al., 2003). Morphological and electrophysiological evidence suggests that PV+BCs are coupled by GJs (Katsumaru et al., 1988a; Galarreta and Hestrin, 2001a) but their importance for ripple oscillations has not been analyzed in detail. As depicted in Fig. 3.1, we use a network model of 200 leaky integrate-and-fire neurons that are tuned to reproduce PV+BCs characteristics to simulate ripple oscillations as observed in acute hippocampal slice preparations (Nimmrich et al., 2005; Donoso et al., 2018).

3.3.1 Interneuronal gap junctions increase synchrony of ripple oscillations during sharp wave-like activation

To demonstrate that the PV+BC network model generates SWR-like events, the PV+BC network is first stimulated with a transient sharp wave-like input (Fig. 3.2). This input is modeled by a Gaussian burst of excitation (half width 7 ms, peak rate $\approx$ 2000 spikes/s) that resembles the excitatory inputs from area CA3 (see Methods). To this transient burst of activity a homogeneous Poisson input at 750 spikes/s is added (Fig. 3.2A).

Because we are interested in the difference in the network activity caused by GJs, we contrast the network dynamics of the GJ coupled network (hereafter named GJ network; Fig. 3.2A1–E1; GJ connection probability $p_{\mathrm{GJ}} = 0.06$), with the network that is lacking GJ coupling (hereafter named GJ-free network; Fig. 3.2A2–E2; $p_{\mathrm{GJ}} = 0$). In this example, we find that the GJ network generates ripple-like oscillations, while the GJ free network does not.

For the GJ network (Fig. 3.2A1–E1), we find that the neuronal population synchronizes rapidly, and collective oscillations emerge within the interneuronal population (Fig. 3.2B1) as a response to the Gaussian burst of excitatory input (Fig. 3.2A1). These oscillations are also visible in the membrane potentials of the neuronal ensemble (Fig. 3.2C1). The simultaneous spiking of a large fraction of the interneurons causes coincident inhibition, which leads to a strong transient hyperpolarization of the membrane potentials. The spectrogram (Fig. 3.2D1) shows that during the oscillation the maximal spectral power is at $\approx$ 200 Hz, i.e., in the biologically realistic range for ripple oscillations (Maier et al., 2003). The spectrum of the full simulated network activity is shown in Fig. 3.2E1 to allow for a more quantitative estimate of the spectral composition of the network activity.

In contrast, in the GJ-free network, the sharp wave-like excitation does not evoke prominent ripple oscillations (Fig. 3.2B2 & C2). The spectral analysis reveals that there are some elevated frequency modes around 180–220 Hz (Fig. 3.2D2 & E2) but with an amplitude that is much lower than in the GJ network.

In summary, the GJ network in Fig. 3.2 generates prominent oscillations in the ripple frequency range whereas oscillations are weak in the GJ-free network. In these exam-

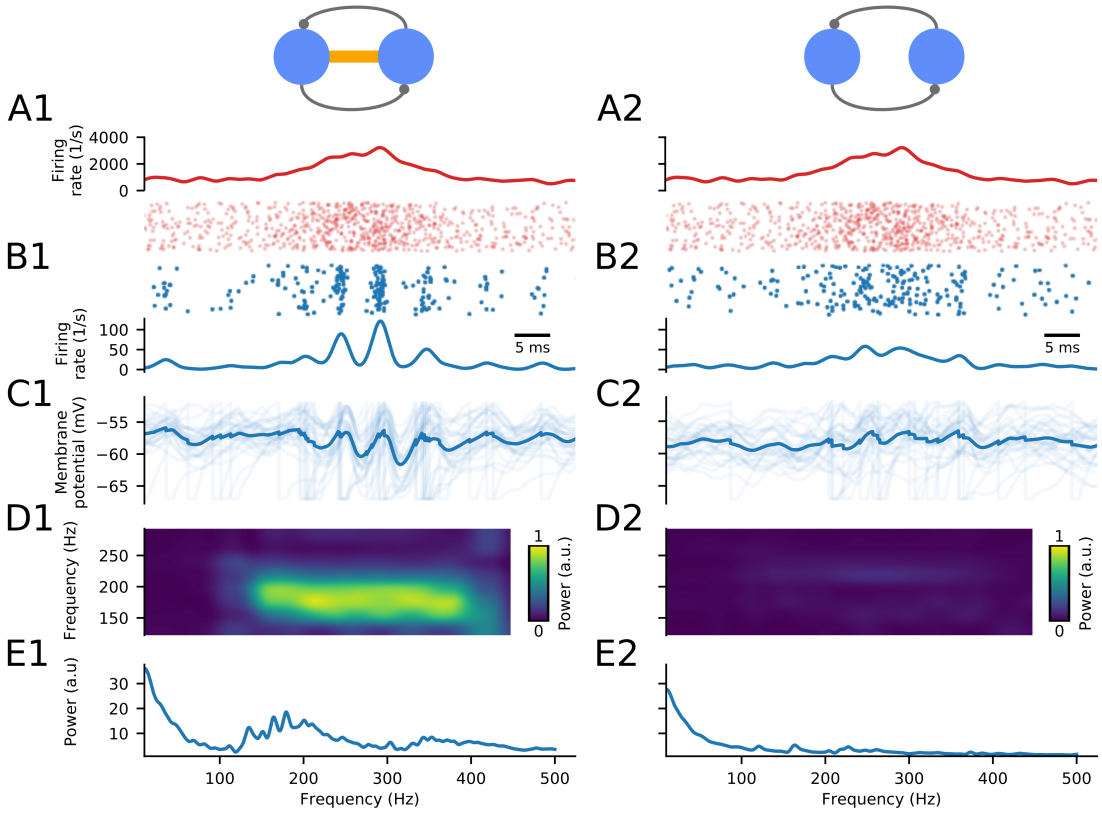

Figure 3.2: Gap junction (GJ) coupling promotes ripple oscillations during transient excitation. Ripple oscillations are much stronger in an interneuronal network ($N = 200$) with GJs (left column; $p_{\mathrm{GJ}} = 0.06$) than in a network without GJs (right column; $p_{\mathrm{GJ}} = 0$). **A**, Excitatory input to the interneuronal network. APs of the total excitatory population are shown in a rastergram, and average excitatory firing rates received by one interneuron (smoothed by a Gaussian filter with 1 ms width) are depicted in the plot above. Note that A–D share a common time scale. **B**, Same quantities as A but for the response of the interneuron network. **C**, Membrane potentials of interneurons. Dark blue lines represent the population average, lighter blue lines correspond to individual neurons. **D**, Spectrogram of the population activity showing elevated activity for the GJ network at ≈ 200 Hz. **E**, Power spectrum. For an overview of the parameters see Tables 3.1 and 3.2.

ple networks, GJ parameters were set to reasonable values (Table 3.2). However, the electrophysiological parameters of GJs coupling of PV+BCs in hippocampal area CA1 are largely unknown (see Methods), and are object to natural variability. Thus, a more thorough analysis of a wider range of GJ parameters is necessary to account for this undetermined variability, and to test the putative role of GJs in ripple oscillations.

3.3.2 Interneuronal gap junctions synchronize steady-state ripple oscillations

To get a more quantitative estimate for the effect of GJs on the ripple oscillations generated by the CA1 network model, we explore in Fig. 3.3 the influence of the GJ connection probability p_{GJ} (for details on p_{GJ} see Fig. 3.1B). GJs can be further characterized by their active-spike component β and their passive conductance γ (Fig. 3.1C, and Eq. (3.1)). The active-spike component β models the amount of voltage that is added to the postsynaptic membrane potential at each presynaptic spike, and the passive conductance γ describes the ohmic subthreshold coupling.

To explore how p_{GJ}, β, and γ affect ripple oscillations, we reduce the complexity of the transient network activity and analyze the network in its steady state. For example, if the network receives Poisson input at 4000 spikes/s, it oscillates at ripple frequencies (Fig. 3.3A) that are similar to the transient state (Fig. 3.2). Due to the longer temporal extent of the neuronal activity, the analysis of the network activity is more precise compared to the transient state. Simulations by Donoso et al. (2018) suggest that the results that we obtain from the steady-state ripple oscillations are transferable to transient SWR oscillations.

Examples of the steady state spiking activities of the interneuron network are shown in Fig. 3.3A at GJ connection probabilities $p_{\mathrm{GJ}} = 0$, $p_{\mathrm{GJ}} = 0.06$ (standard parameter), and $p_{\mathrm{GJ}} = 0.12$. The networks are oscillating at 183, 163, and 159 Hz with mean interneuron firing rates of 90, 115, and 142 spikes/s for $p_{\mathrm{GJ}} = 0$, $p_{\mathrm{GJ}} = 0.06$, and $p_{\mathrm{GJ}} = 0.12$, respectively. This indicates that GJs decrease the network frequency and increase the average firing rate.

In Fig. 3.3B, the GJ connectivity p_{GJ} is varied systematically, and we compute its impact on three basic network properties: the network frequency, the average firing rate, and the synchrony index. The synchrony index is a pairwise measure between 0 and 1 that counts the coincident events (coincidence window = 0.5 ms) in the neuronal spike trains; see also Methods. Simulation results are shown as the relative change of network properties with respect to their reference value at standard parameters ($p_{\mathrm{GJ}} = 0.06$, $\beta = 0.25\,\mathrm{mV}$, $\gamma = 1.0\,\mathrm{nS}$; see Methods).

The synchrony index shows the strongest dependence on the GJ connectivity. We find that an increased number of GJs in the network leads to more coincident spikes; despite a temporally compressed period of spiking activity in each oscillation cycle, also the firing rate is increased, i.e., more neurons are recruited in each cycle. Interestingly, the network frequency shows only a rather small decrease for increasing GJ connectivity ($p_{\mathrm{GJ}} \in [0, ..., 0.2]$).

In Fig. 3.3C–E, we vary the two GJ parameters β and γ independently [even though

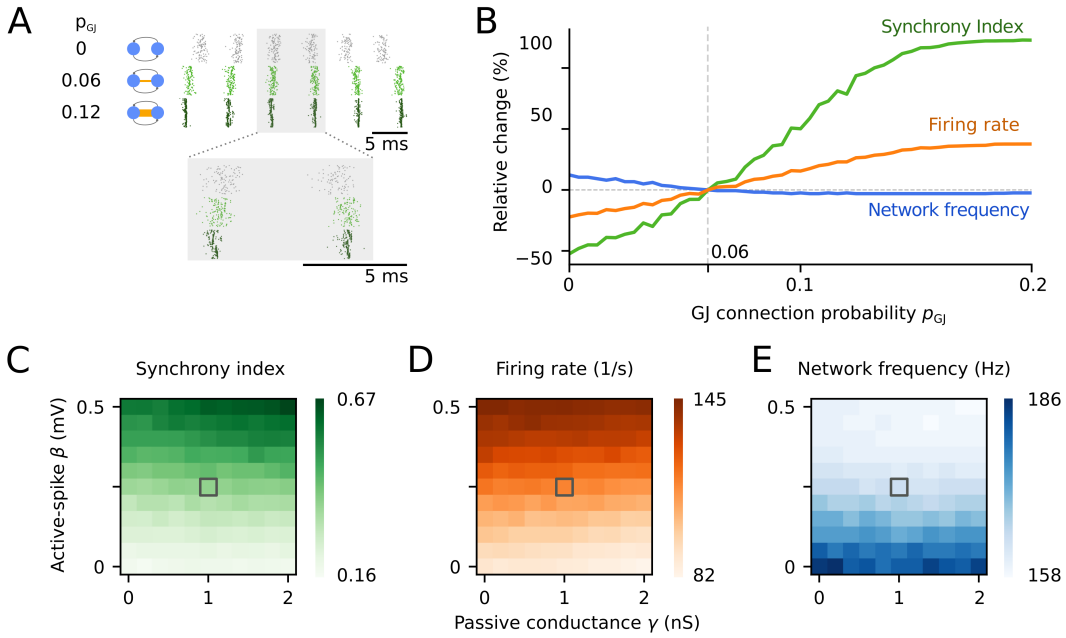

Figure 3.3: Gap junctions (GJs) increase synchrony and firing rates during ripple oscillations in interneuron networks. **A**, Rastergrams show the activities of networks without GJs ($p_{GJ} = 0$, gray, top), with standard GJ connectivity ($p_{GJ} = 0.06$; light green; middle), and with strong GJ connectivity ($p_{GJ} = 0.12$; dark green; bottom). Neurons receive Poisson input with a constant mean (4000 spikes/s). GJ parameters are $\beta = 0.25$ mV and $\gamma = 1.0$ nS. **B**, The relative change of the synchrony index, the average firing rate, and the network frequency is depicted for different values of the GJ connection probability p_{GJ}. Quantities are normalized by their respective values at $p_{GJ} = 0.06$. GJ parameters as in A. **C**–**E**, GJs parameters β and γ contribute differentially to the network dynamics for fixed $p_{GJ} = 0.06$. **C**, Synchrony index as function of β and γ. **D**, Firing rate. **E**, Network frequency. Gray squares denote the GJ standard parameters as used in A and B. For an overview of the parameters see Tables 3.1 and 3.2.

the two GJ parameters are correlated (Lewis and Rinzel, 2003; Ostojic et al., 2009)], to disentangle their effects on the synchrony index (Fig. 3.3C), the firing rate (Fig. 3.3D), and the network frequency (Fig. 3.3E). For all three quantities, we find that the active-spike parameter β has a strong influence whereas the passive parameter γ has only mild effects.

The synchrony index increases with increasing β (Fig. 3.3C). The same trend holds true for γ, however, the increase is much less pronounced. The synchrony index reaches its maximum for the maximal values of GJ parameters at $\beta = 0.5\,\mathrm{mV}$ and $\gamma = 2\,\mathrm{nS}$, which is at the corner of the investigated parameter range. The average firing rate of the neuronal population also increases with increasing β but slightly decreases with increasing γ (Fig. 3.3D). Finally, the network frequency decreases with increasing values of β, and it is mildly reduced by increasing values of γ (Fig. 3.3E).

In summary, we find that introducing GJ coupling into our model network increases the synchrony. In the Supplementary Material of this thesis, I additionally show that this increase in synchrony cannot be achieved by increasing the inhibitory coupling (Fig. S5). Thus, the high synchrony observed in the ripple oscillations is specific to GJs. We further find that the neuronal firing rates also increase, whereas the network frequency decreases mildly. Our simulations show that from the two GJ parameters, which describe the GJ currents (Eq. (3.1); Lewis and Rinzel (2003); Ostojic et al. (2009)), the active-spike component β is mainly responsible for the effects of the GJs on the network dynamics. The active-spike component increases the synchrony and the firing rates because it effectively acts as a precisely timed excitation that is fed into the neuronal population at the oscillation phase in which the network is on average close to spiking threshold. This increase of the interneuron firing rates leads in turn to a decrease of the network frequency because more inhibitory currents are fed back into the network. Consequently, the hyperpolarization of the membrane potentials following an oscillatory phase of spiking is stronger, hence the population needs a longer time to recover to spiking threshold, i.e., the network frequency is decreased.

For large values of β, the network frequency is similar to the firing rate of the neurons, i.e., every neuron is firing in almost every oscillation cycle. Rephrased in the terms introduced by Brunel (2000), this means that the increase of β corresponds to a transition from a synchronous irregular regime to a synchronous regular regime. Our results are in agreement with the results from Ostojic et al. (2009) who found that networks that are exclusively coupled by GJs can only globally oscillate at the firing rate of the single neurons.

3.3.3 Interneuronal gap junctions reduce the minimal number of neurons required for ripple oscillations

So far, the number of interneurons that received excitation was kept constant. However, it is not known how many interneurons are recruited during ripple oscillations and how many are required. Stark et al. (2014) optogenetically excited pyramidal cells in hippocampal networks in vivo and estimated that there are ≈ 80 pyramidal cells and ≈ 20 interneurons within the volume illuminated by the light source. Upon optic stim-

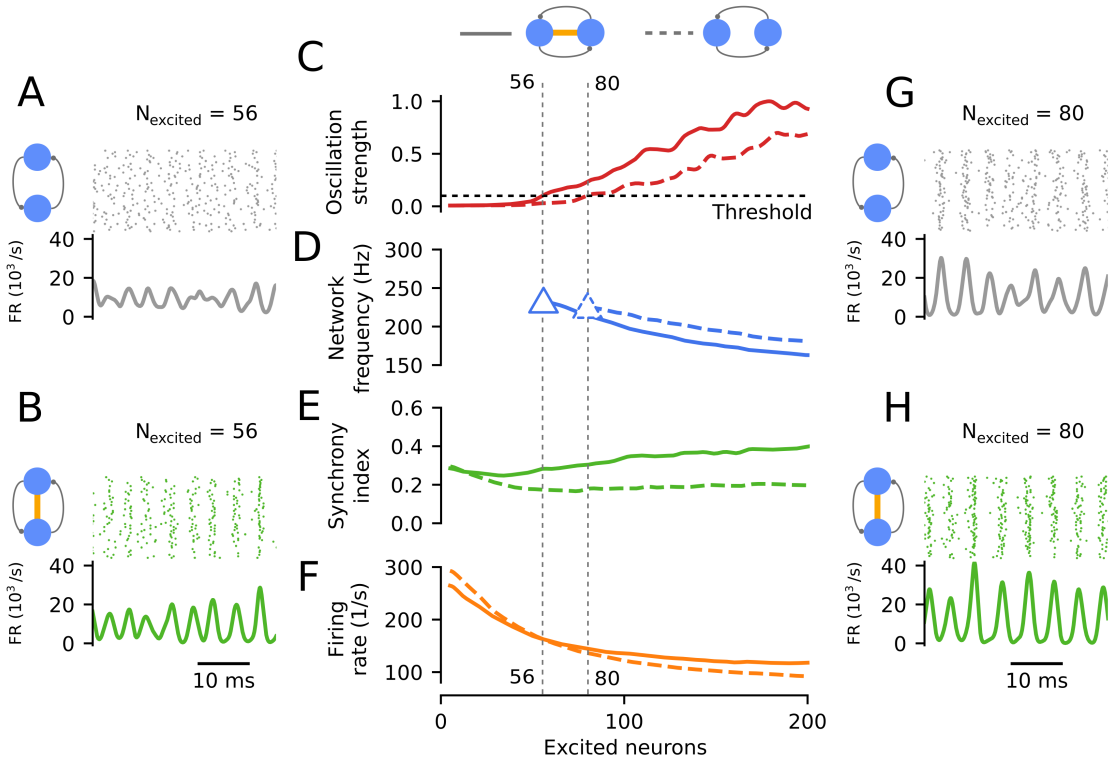

Figure 3.4: Interneuronal gap junctions (GJs) decrease the minimal number of neurons required for ripple oscillations. **A**, Example of spiking activity and network firing rate of a GJ-free network when only 56 neurons out of 200 receive excitation: oscillations are weak and unsteady. **B**, Same as A, but including GJs: oscillations are stronger and reliable. **C**, Oscillation strength as a function of the number of excited neurons of the GJ network (solid line), and of the GJ-free network (dashed line, see Methods for details). GJs decrease the number of neurons that is required to reach a certain threshold (here 0.1) of the oscillation strength. Note that **C**–**F** share their x-axes. **D**, Network frequency, displayed for suprathreshold oscillation strengths (solid triangle for GJ network, dashed triangle for GJ-free network). **E**, Synchrony index. **F**, Firing rate. **G**,**H**, Identical to A,B but for 80 excited interneurons, which is sufficient for the GJ-free network to reach the oscillation strength threshold. Plots in C–F are smoothed by a Gaussian function with a width of 5 "excited neurons". For an overview of the parameters see Tables 3.1 and 3.2.

ulation of the pyramidal cells, Stark et al. (2014) could observe fast oscillations despite the small number of pyramidal cells. However, if they optogenetically excited the ≈ 20 interneurons they could not observe oscillatory activity. In a similar experiment in vitro, Schlingloff et al. (2014) optogenetically excited ≈ 150 interneurons and showed that this number is sufficient to generate ripple-like oscillations.

Motivated by these experiments, we analyze the effect of a partial activation of the network. Therefore, the same Poisson input that was used for computing the steady-state activity in Fig. 3.3 is now fed into a fraction of the population of the in total 200 interneurons. The response of the interneuron network is then characterized by four properties: oscillation strength, network frequency, synchrony index, and firing rate. Moreover, we compare the dynamics of the GJ and the GJ-free network (Fig. 3.4).

Four examples of the network activities with 56 and 80 excited neurons for the GJ vs. the GJ-free network are shown in Fig. 3.4A, B, G, H. These examples already illustrate the general trend: First, the GJ networks show stronger oscillations; second, the more neurons receive excitatory input the stronger the oscillation. Additionally, we find that only excited neurons are spiking during these simulations.

These observations are first quantified by computing the oscillation strength, which is a measure for the size of a peak in the power spectral density (see Methods for details). We introduce this measure here to be able to quantify how strong a putative network oscillation is. A reliable estimate of the network frequency is possible only if the oscillation strength is above a certain threshold (here arbitrarily chosen as 0.1; results do not critically depend on this value).

Figure 3.4C shows the oscillation strength as a function of the number of driven interneurons. If the oscillation strength is above the depicted threshold (0.1), oscillations are generated reliably and we consider the activity to be oscillatory, and otherwise not. The threshold is reached for the GJ network at 56 active neurons, and for the GJ-free network at 80 active neurons.

In Fig. 3.4D, the network frequency is displayed for suprathreshold oscillation strength. In both networks, for values larger than the threshold, the network frequency is decreasing from $\approx 220\,\mathrm{Hz}$ to $\approx 170\,\mathrm{Hz}$ with increasing number of active neurons. For a fixed number of excited neurons, the network frequency is $\approx 20\,\mathrm{Hz}$ lower in the GJ network than in the GJ-free network.

In Fig. 3.4E, the effect of the partial activation of the network on the synchrony index is shown. We find that for more than ≈ 10 excited neurons the GJ network is more synchronous than the GJ-free network.

In Fig. 3.4F, the influence of the number of excited neurons on the firing rate is depicted. Increasing the number of excited neurons decreases the firing rate from $\approx 280\,\mathrm{Hz}$ to $\approx 100\,\mathrm{Hz}$ for both networks. This decrease of the firing rate with growing number of active neurons can be explained by the fact that the feedforward, synaptic excitatory input per neuron is kept constant while the number of neurons receiving input is increased. So, increasing the number of active neurons is effectively shifting the inhibition-excitation balance to more recurrent, synaptic inhibition that, in turn, leads to lower firing rates.

In conclusion, we find that for an increasing number of active neurons the oscillation strength increases whereas the network frequency and the firing rate decrease. Addition-

ally, GJs promote the oscillatory activity (larger oscillation strength), hence oscillations are possible at smaller numbers of active neurons (Fig. 3.4A&B). Moreover, GJs increase the synchrony in oscillating networks (Fig. 3.4E).

3.3.4 Delays of gap junction coupling potentials

Figures 3.2–3.4 have demonstrated that gap junctions between interneurons increase neuronal oscillation strength and synchrony. Synchrony, in turn, is strongly dependent on neuronal timing. Up to this point, we have assumed that gap junctions transfer their coupling potentials instantaneously. However, dendritic trees may cause delays of the GJ coupling potentials. Dendritic filtering should also affect amplitudes of GJ coupling potentials. To be able to assess the influence of delay and amplitude of GJ coupling potentials on network oscillations, an evaluation of the typical range of values is necessary.

To quantify GJ delays and amplitudes, we numerically simulate two GJ coupled multicompartmental neurons for variable GJ locations in the dendritic tree. Note that the coupling location is, for simplicity, always the same in both neurons (Fig. 3.5A). The neurons are coupled by a GJ that is modeled by an ohmic conductance of 1 nS. An action potential is generated in the presynaptic neuron, and the GJ coupling potential is measured in the soma of the postsynaptic neuron (for illustration of APs see Supplementary Material, Section 1). In the following, we compare results from two different standard models of hippocampal PV+BCs (Saudargiene et al., 2015; Lee et al., 2014; see Methods for details).

Results of simulations of two GJ coupled PV+BCs are depicted in Fig. 3.5B–D. We first calculated the peak delay, i.e., the delay from the peak of the presynaptic somatic AP of the first cell to the peak of the postsynaptic GJ potential in the soma of the second cell (Fig. 3.5B, left). This peak delay is calculated for different locations of the GJs in the dendritic tree, and hence different distances to the soma (Fig. 3.5B, right). The peak delay monotonically increases with increasing distance of the GJ from the soma. At the most distal ends of the dendrites, the measured delays are 2.7 ms and 3.2 ms for the Lee et al. (2014) and the Saudargiene et al. (2015) models, respectively (solid lines, Fig. 3.5B).

Surprisingly, even the peak delay at GJ locations close to the soma ($< 50\,\mu m$) is > 0.5 ms. The main reason for this large minimum is that the peak delay is sensitive to the width of the presynaptic AP. Since the changes of the postsynaptic membrane potential ($\lesssim 1$ mV, see also Fig. 3.5D) are small in comparison to the amplitude of the action potential (≈ 100 mV), the width of the AP is a lower bound for the delay of the two peaks. Thus, the large delays for even short GJ–soma distances are the result of the broad action potentials of the two models (≈ 0.6 ms FWHM; see Methods), which are around double of what was measured in experiments (≈ 0.3 ms FWHM; Buhl et al., 1996; Kohus et al., 2016).

In essence, the delays at all distances, but most prominently at short distances, are overestimated in our simulations. This hypothesis is tested by replacing the presynaptic action potential by a fast bipolar current injection (FWHM< 0.1 ms) in a neuron model

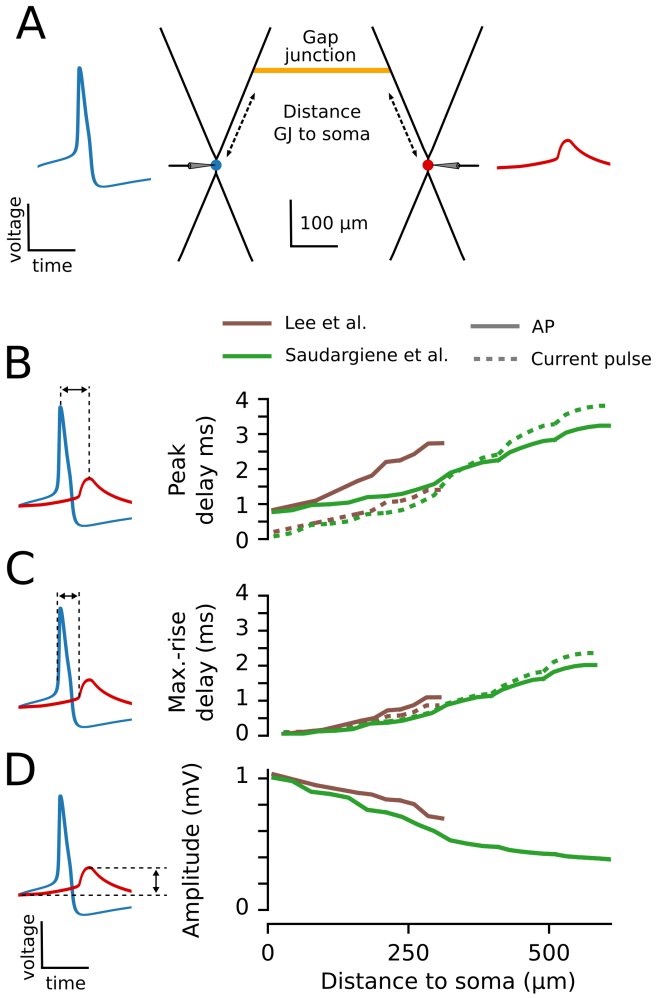

Figure 3.5: Delays and amplitudes of GJ coupling potentials in PV+BC multicompartment models. **A**, Schematic of two GJ coupled PV+BCs with simplified morphologies (model from Lee et al., 2014). AP (blue trace) in the left neuron (blue), and GJ coupling potential (red trace) in the right neuron (red). The position of the GJ is the same for both neurons. Thus, the distance that the AP has to travel from the soma to the GJ is the same as the distance the GJ coupling potential has to travel from the GJ to the soma. **B**, Left, The peak delay is calculated as the time between the maxima of the presynaptic AP (blue) and the postsynaptic GJ potential (red). Potentials not to scale. Right, peak delays for APs (solid lines) and waveforms evoked by short current pulses (dashed lines) for different values of GJ-soma distance as depicted in A (see Methods for details) for two different models (Lee et al. 2014; Saudargiene et al. 2015). The displayed delays in B correspond to GJ-coupling in the longer branches in the dendritic trees of the neurons in A, and delays are qualitatively similar for the shorter branches. B–D share the same x-axis. **C**, Same as B but for the maximal-rise (max.-rise) delay, i.e., the delay between the times of maximal rise of the potentials. **D**, Same as B and C but for the amplitude of the gap junction coupling potential. Here, only amplitudes of the action potential stimulus are displayed. For an overview of the parameters see Tables 3.1 and 3.2.

without active conductances in soma or dendrites (for illustration of bipolar current pluses see Supplementary Material, Section 1). This change of the presynaptic pulse leads to very short peak delays at proximal GJ distances for both models ($\approx 0.2\,\mathrm{ms}$, dashed lines, Fig. 3.5B). For larger GJ-soma distances, we find that the signal generated by the current injection leads to longer delays than the AP for the Saudargiene et al. (2015) model. This behavior is caused by the lack of active conductances within the dendrites, which decelerates the transmission for longer distances.

Another way to remove the dependence of the delay on the width of the action potential is to measure the delay between the maximal rise of the AP and the maximal rise of the postsynaptic GJ potential. This maximal-rise delay is plotted in Fig. 3.5C. Resulting values are small ($< 0.5\,\mathrm{ms}$) at short distances ($< 50\,\mu\mathrm{m}$). The maximal-rise delay is also insensitive to the different presynaptic activations: action potentials and bipolar current pulses lead to similar delays. Furthermore, the estimated propagation speeds of signals within the dendritic tree, i.e., the slopes of the lines in Fig. 3.5B and C, are similar.

Finally, we measure the dependence of the amplitude of the GJ coupling potential on the location of the GJ (Fig. 3.5D). The amplitude of the postsynaptic GJ potential varies between 1.1–0.4 mV, and amplitudes monotonically decrease for increasing GJ–soma distance in both models. Amplitudes have to be treated with care because they also depend on the width of the presynaptic action potential, which is overestimated in the models used here. When we assume that the action potential would be half as wide, what is biologically plausible (Buhl et al., 1996; Kohus et al., 2016), and that the transferred current scales linearly with the width of the action potential, the amplitudes would be half as large. Explicitly, this scaling would lead to corrected GJ coupling potential amplitudes between $\approx 0.6\,\mathrm{mV}$ and $\approx 0.2\,\mathrm{mV}$.

We conclude from the simulations that GJ delays in PV+BCs are short ($\lesssim 0.5\,\mathrm{ms}$) for proximal locations ($\lesssim 100\,\mu\mathrm{m}$) and can be quite long ($> 1\,\mathrm{ms}$) for distal locations ($> 200\,\mu\mathrm{m}$). While delays $\lesssim 0.5\,\mathrm{ms}$ were found in experiments (Galarreta and Hestrin, 1999; Tamás et al., 2000; Galarreta and Hestrin, 2001a), values $> 1\,\mathrm{ms}$ have not been reported to the best of our knowledge. Further, simulations show that a presynaptic action potential elicits a gap junction coupling potential with an amplitude $\lesssim 0.6\,\mathrm{mV}$, which is in agreement with experiments ($\approx 0.5\,\mathrm{mV}$, Tamás et al., 2000; $\approx 1\,\mathrm{mV}$, estimated from Gibson et al., 1999; $\approx 0.5\,\mathrm{mV}$ estimated from Galarreta and Hestrin, 2001a).

3.3.5 Effect of gap junctions on ripple oscillations depends on gap junction delays

Having approximated the range of the delays for the GJ coupling, we can now analyze their effect on the steady-state ripple oscillations (Fig. 3.6). We vary the GJ delay δ_{GJ} from 0 to 2.4 ms, which shifts the point in time, when the active-spike component β increases the postsynaptic membrane potential (Eq. (3.1), Methods). In Fig. 3.3, we showed that the passive conductance γ has little effect on the network properties for zero delay, and hence we did not include nonzero delays in γ here. Otherwise we use the standard GJ parameters as in Figs. 3.1–3.4: $\beta = 0.25\,\mathrm{mV}$ and $\gamma = 1\,\mathrm{nS}$. Furthermore, the GJ connection probability p_{GJ} is varied from 0 to 0.12 to provide a reference for the

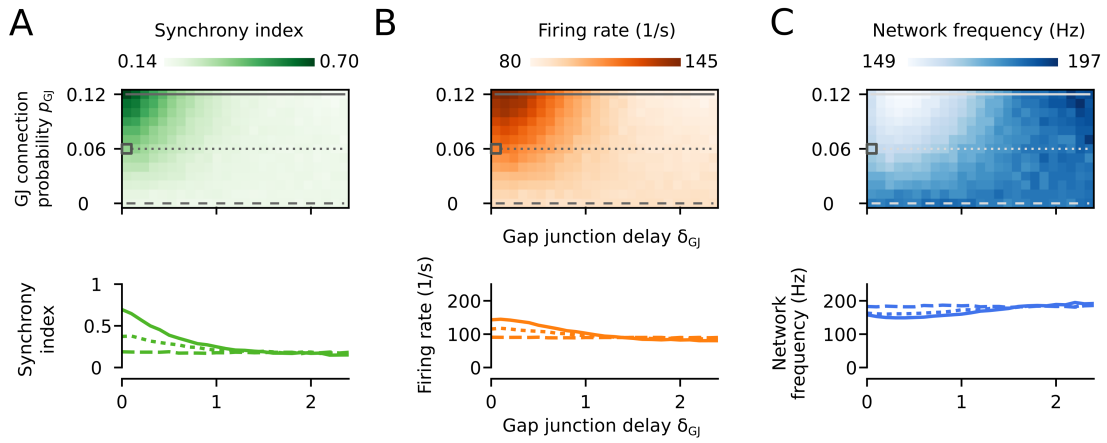

Figure 3.6: Small gap junction (GJ) delays only mildly decrease the impact of GJs on the network activity. Synchrony index (**A**), firing rate (**B**), and network frequency (**C**) as functions of the GJ connection probability p_{GJ} and the GJ delay δ_{GJ}. The gray squares denote the standard parameters. Bottom row, Example traces at p_{GJ} fixed to 0, 0.06 and 0.12, as denoted by gray lines in the graphs at the top. Standard GJ parameters are used, i.e., $\beta = 0.25\,\text{mV}$ and $\gamma = 1.0\,\text{nS}$. For an overview of the parameters see Tables 3.1 and 3.2.

strength of the effect on the network properties that is caused by the delay.

The synchrony index is shown in Fig. 3.6A. We find an elevated level of synchrony in the network only for low values of the delay ($\lesssim 1\,\text{ms}$). For longer delays ($> 1.0\,\text{ms}$), the synchrony index is similar to the value in the GJ-free network ($p_{GJ} = 0$).

The neuronal firing rate varies from 80–145 Hz over the full range of the parameters (Fig. 3.6B). The firing rate is maximal at $\delta_{GJ} \approx 0.1\,\text{ms}$, decreases for larger delays, and reaches the value of the GJ-free network at $\approx 1.3\,\text{ms}$.

The network frequency varies between $\approx 150\,\text{Hz}$ and $\approx 200\,\text{Hz}$ within the whole parameter range of δ_{GJ} and p_{GJ} (Fig. 3.6C). For high values of p_{GJ}, the network frequency reaches its minimum at $\delta_{GJ} \approx 0.3\,\text{ms}$. For $\delta_{GJ} > 1.3\,\text{ms}$ the network frequency is at its reference value at $p_{GJ} = 0$.

Interestingly, we find the extremal values of the different network properties at different values of δ_{GJ}: the firing rate and the network frequency reach their extremal values at $\approx 0.1\,\text{ms}$ and $\approx 0.3\,\text{ms}$, respectively.

In conclusion, GJ potentials have to fall into a narrow time window ($\lesssim 0.5\,\text{ms}$) of the oscillation cycle, at which the average membrane potential is close to spiking threshold, to promote synchrony, increase the firing rates, and decrease the network frequency. This temporal window is short since it is only a fraction of the total period ($\approx 5\,\text{ms}$) of the ripple oscillations.

3.4 Discussion

Parvalbumin-positive basket cells (PV+BCs) are coupled by gap junctions (GJs; Katsumaru et al. 1988a; Fukuda and Kosaka 2000a; Galarreta and Hestrin 2001a), and in the hippocampal area CA1 they form recurrently coupled interneuron networks (INT-INT) that are hypothesized to generate ripples (Ylinen et al., 1995; Klausberger et al., 2003). To test the functional relevance of these GJs for ripple oscillations, we used a biologically plausible network model of PV+BCs that reproduced ripple oscillations under transient and steady-state input (Donoso et al., 2018).

Our simulations showed that interneuronal GJs, especially action potentials transmitted by GJs, increase the synchrony and the mean firing rate of the interneuronal network during ripple oscillations, but only mildly decrease the frequency of the ripple oscillations. Furthermore, GJs reduce the minimum number of active interneurons required for ripple oscillations in such INT-INT networks. Finally, GJ transmission delays can vary from 0 to $\approx 3\,\text{ms}$, which depends on the somatodendritic GJ location and on the PV+BC model. We demonstrated that only small GJ delays ($\lesssim 0.5\,\text{ms}$) promote ripple oscillations.

We predict that hippocampal ripple oscillations that are generated by INT-INT networks are affected by deactivation of the interneuronal GJs (Ylinen et al., 1995). To test this hypothesis, we propose to record the spiking activity of CA1 hippocampal PV+BCs, e.g., by extracellular multi-electrode recordings or by intracellular recordings of membrane potentials, while the properties of gap junctions among PV+BCs are selectively altered.

3.4.1 Experimental evidence for the function of gap junctions in ripple oscillations

Many studies have already tried to test the functional relevance of GJs for hippocampal ripple oscillations, using either chemical GJ blockers (Ylinen et al., 1995; Draguhn et al., 1998; Hormuzdi et al., 2001; Maier et al., 2003; Pais et al., 2003; Traub et al., 2003; Buhl et al., 2003; D'Antuono et al., 2005; Behrens et al., 2011) or connexin36 knockout (Cx36KO) mice (Hormuzdi et al., 2001; Maier et al., 2002; Pais et al., 2003; Buhl et al., 2003) lacking the GJ protein Cx36, which has been found in pyramidal cells (Condorelli et al., 2000) and interneurons (Venance et al., 2000). Most studies that rely on the chemical GJ blockers octanol, carbenoxolone, or halothane (Ylinen et al., 1995; Draguhn et al., 1998; Hormuzdi et al., 2001; Maier et al., 2003; Pais et al., 2003; Traub et al., 2003; Buhl et al., 2003; Behrens et al., 2011) find a strong suppression or abolishment of SWRs (but cf. D'Antuono et al., 2005), and, hence, do not allow conclusions about changes of the frequency of ripple oscillations. These findings are contrasted by experiments using Cx36KO mice (Hormuzdi et al., 2001; Pais et al., 2003; Buhl et al., 2003) or the GJ blocker mefloquine (Behrens et al., 2011) that only find mild effects on SWRs. In the studies in which ripple oscillations were still observed after a putative GJ block, the ripple frequency was not affected (Maier et al., 2003; Buhl et al., 2003; D'Antuono et al., 2005; Behrens et al., 2011; but cf. Maier et al., 2002).

These contradictory results might be explained by several confounding factors: GJ blockers are not specific and have strong side-effects (Juszczak and Swiergiel, 2009), SWRs were stimulated by different means (GABA, Traub et al., 2003; kainate, Hormuzdi et al., 2001; Pais et al., 2003; picrotoxin, D'Antuono et al., 2005, KCl, Nimmrich et al., 2005, Ca^{2+} - free ACSF, Hormuzdi et al., 2001), and networks of Cx36KO might be altered due to compensatory effects during development. Moreover, GJ blocker and Cx36KO experiments are not specific for GJs between PV+BCs but also interfere with putative GJs between pyramidal neurons.

GJs between pyramidal cells are the major element of an alternative theory for the origin of ripple oscillations (Traub et al., 1999), albeit evidence for pyramidal GJs is sparse for mature pyramidal cells (Rash et al., 1997; Condorelli et al., 2000; Mercer et al., 2006; Wang et al., 2010). According to the hypothesis from Traub et al. (1999) a block of GJs between pyramidal cells would abolish ripple oscillations, which is in contrast to experiments that observed only mild effects on the network dynamics (Hormuzdi et al., 2001; Pais et al., 2003; Buhl et al., 2003; Behrens et al., 2011).

3.4.2 How many interneurons are necessary to generate ripple oscillations?

Our simulations showed that GJs decrease the minimal number of excited interneurons that is required to generate ripple oscillations (Fig. 3.4), and the minimum number is on the order of tens of neurons. For a sufficiently large number of interneurons, ripple oscillations can be more robustly generated when GJs are present. Our estimates depend on a specific set of parameters, yet, the qualitative observations that GJs decrease the number of necessary neurons was true for all tested sets of biologically plausible parameter ranges. In the Supplementary Material of this thesis, I also show that gap junctions decrease the minimal required excitatory input (Fig. S4), and the minimal required inhibitory coupling (Fig. S5) that is necessary to generate ripple-like oscillations in our INT-INT network model. These findings support the notion that gap junction increase the robustness of ripple oscillation.

Some experimental constraints for the minimum number of interneurons required for ripple-like oscillations were obtained via optogenetics. Schlingloff et al. (2014) found that the activation of ≈ 150 PV+BCs in hippocampal CA3 slices was enough to generate ripple-like steady-state oscillations (see Fig. 1.8). While this supports the INT-INT hypothesis, it was challenged by the in vivo study by Stark et al. (2014) in CA1, where the optogenetic excitation of $\lesssim 20$ PV+BCs was not sufficient to generate ripple-like activity. In the light of our findings, we argue that the number of directly activated interneurons by Stark et al. (2014) was still below the threshold of neurons required for ripple-like oscillations, and consequently the results by Stark et al. (2014) do not necessarily reject the INT-INT hypothesis for ripples.

To test our prediction that a certain minimal number of PV+BCs is necessary for ripple oscillations, we propose the following experiment. The EFP is recorded in a hippocampal slice during an optogenetic direct activation of a variable number of PV+BCs. There are three specific predictions: First, ripple-like oscillations require the activation of more than a sufficient (minimal) number of PV+BCs. Second, this minimum is smaller for

wild-type mice with intact GJs in comparison to Cx36KO mice. Third, the firing rate and the network frequency decrease with an increasing number of activated neurons.

3.4.3 Gap junction transmission delays

We calculated the delays of GJ potentials between hippocampal PV+BCs to be in the range 0–3 ms, which depends on the GJ location in the dendritic tree (Fig. 3.5) and on the specific neuron model (Lee et al., 2014; Saudargiene et al., 2015). In contrast, only delays below $\lesssim$ 0.5 ms have been found experimentally (Galarreta and Hestrin, 1999; Tamás et al., 2000; Galarreta and Hestrin, 2001a). Such short delays require proximal GJ coupling ($\lesssim$ 100 µm from soma; Fig. 3.5) as observed between neocortical PV+BCs in ultrastructural studies (Tamás et al., 2000). Our analysis showed that with such small delays GJs can still promote ripple oscillations (Fig. 3.6). Conversely, if the GJs are located more distally, as found in ultrastructural studies in the hippocampus ($>$ 200 µm; Fukuda and Kosaka, 2000b), the delays of the GJ potentials were long ($>$ 1 ms). In our network simulations, we found that GJs with such long delays do not promote ripple oscillations, possibly because the GJ potentials are outside of the time window within each oscillation cycle in which neurons are spiking.

Motivated by our simulations (Fig. 3.5) and experimental evidence of distal GJ coupling (Fukuda and Kosaka, 2000b), we predict that GJ potentials with long delays ($>$ 1 ms) do exist between PV+BCs. Such long delays have not been observed in experiments to the best of our knowledge. Moreover, we predict fast GJ potentials ($\lesssim$ 0.5 ms) between hippocampal PV+BCs in CA1 (Bartos et al., 2002) in analogy to neocortical findings (Galarreta and Hestrin, 2001a) because proximal GJ coupling ($\lesssim$ 100 µm) of PV+ interneurons was shown in ultrastructural studies (Fukuda and Kosaka, 2000b).

3.4.4 Limitations of this study

Our network simulations are based on single-compartment leaky integrate-and-fire neurons, which is a major simplification of the neuronal dynamics because such models do not include action potentials. To be able to include GJs in this network model and to simulated coupling potentials evoked by action potentials, we used the two-parameter model for the GJs by Lewis and Rinzel (2003). Further, the neurons in our network model do not have any physical extension, and hence cannot describe propagation of signals within the neurons. To account for such delays, we included them in electrical and chemical couplings.

3.4.5 Comparison to other theoretical studies

We found that GJs increase the synchrony of neuronal oscillations. This confirms results of previous approaches that either employed analytical methods on idealized networks (Lewis and Rinzel, 2003; Kopell and Ermentrout, 2004) or computational methods on more biologically plausible networks (Traub et al., 2001; Bartos et al., 2002; Maex and De Schutter, 2003; Guo et al., 2012). While all of these studies showed that GJs can increase synchrony for various network settings, none of these studies had a focus on

hippocampal ripple oscillations nor considered different strengths and connectivities of GJ coupling. We showed that GJs increase the synchrony of ripple oscillations for a large range of realistic GJ parameters. Further, we provided explicit predictions for the role of interneuronal GJs in ripple oscillations, and systematically studied the size and impact of GJ delays, which has only been considered implicitly (Traub et al., 2001; Maex and De Schutter, 2003) or has been neglected (Bartos et al., 2002; Guo et al., 2012) in previous studies.

3.4.6 Conclusion

GJs between PV+BCs promote and stabilize hippocampal ripple oscillations if the GJ delay is $\lesssim 0.5\,\mathrm{ms}$. We find that for such short delays the GJ coupling has to be proximal ($\lesssim 100\,\mu\mathrm{m}$ from soma). We confirm that such interneuronal GJs have a weak effect on the ripple frequency, and that they are not the primary pacemaker of the ripple oscillations. These findings support the INT-INT hypothesis of ripple oscillations, which assumes that recurrent chemical connections of interneurons set the oscillation frequency.

4 Data analysis: ripple oscillations in the absence of chemical transmission

How are hippocampal ripple oscillations generated? As lined out in the Introduction to this thesis (Chapter 1), there is dissent about this question up to date.

A prominent model for ripple oscillations assumes that gap junctions (GJs) between axons of pyramidal cells generate ripple oscillations (Traub et al., 1999). As evidence for this model, Traub et al. refer to in vitro studies in which ripple oscillations persist in absence of all chemical synaptic transmission (e.g., Draguhn et al. 1998; Nimmrich et al. 2005). Here, I reassess the recordings by Nimmrich et al. (2005), and checked whether GJs between interneurons (Chapter 3) could clock the observed oscillations.

To test this hypothesis, I reanalyze data[1] from recordings of the extracellular field potential (EFP) from in vitro experiments by Nimmrich et al. (2005), in which all chemical synaptic interactions were blocked (Fig. 4.1). In these recordings, oscillations were stimulated using KCl pressure injections.

Here, I quantify the evolution of the ripple-like oscillations taking into account the multiple effects that KCl has on the neuronal networks. Furthermore, I test whether the observed oscillations could be generated by GJ-coupled networks of interneurons, which is a contrasting hypothesis to Traub et al. (1999), who assume that pyramidal GJs are responsible for ripple oscillations.

4.1 Methods

Here, I briefly present the experiments carried out by Nimmrich et al. (2005) and introduce the data analysis methods. For a detailed description of the experiments the reader is referred to Nimmrich et al. (2005).

4.1.1 Experiments of Nimmrich et al., 2005

In total, I analyzed seven experiments of extracellular field potential recordings that were made in acute, horizontal minislices of the isolated hippocampal area CA1 of mice (Fig. 4.1A, rat's hippocampus in Fig. 1.1). The EFP electrode was positioned in st. pyramidale, and the needle for the pressure injection was located in the st. radiatum. Recording sessions had a duration of up to 3000 s, and contained multiple KCl pressure injections

[1] The data analyzed in this chapter was cordially provided by Dr. Nikolaus Maier and published in Nimmrich et al. (2005). In particular, data from seven experiments in 2004 has been used: 8th Oct, slice 1 (recording 1); 8th Oct slice 2 (recording 2); 4th Oct, slice 1 (recording 3); 3rd Oct, slice 3 (recording 4); 30 Sep, slice 2 (recording 5); 1st Oct, slice 2 (recording 6); 1st Oct; slice 3 (recording 7). Terms in parentheses refer to labels for the data used throughout this chapter.

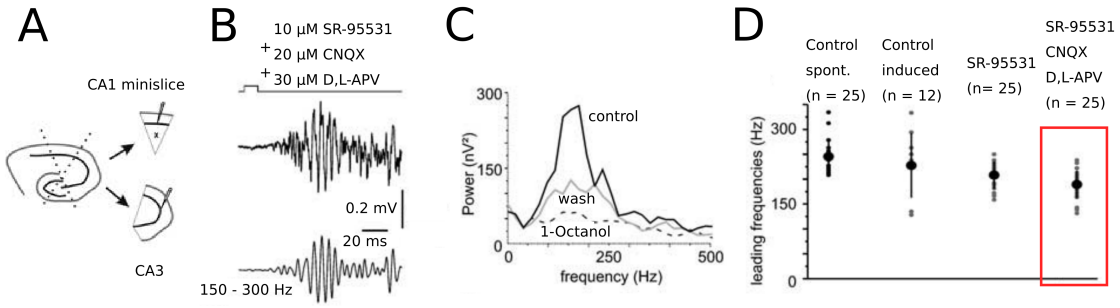

Figure 4.1: Oscillations in the absence of chemical synaptic transmission in hippocampal area CA1. **A**, Minislice preparation. Locations of electrode and injection needle (x) are indicated in CA1. **B**, Example traces of a KCl-induced event, where all synaptic transmission is chemically blocked. Time of KCl injection (top), raw EFP trace (middle), and band pass filtered EFP traces (150–300 Hz, bottom). **C**, Average power spectrum from 10 KCl-induced events. In control condition (solid line), all chemical transmission is blocked as in B. The other two lines represent the same preparation in which octanol, a GJ blocker, is applied (dashed line), and after wash out of octanol (gray line). **D**, Leading frequencies of the power spectral densities for spontaneous control, KCl-induced control, KCl-induced events during block of inhibition, and KCl-induced events with block of all synaptic transmission (from left to right). Recordings analyzed in this chapter are marked in red. Data from Nimmrich et al. (2005), their Figure 1A, 4D1, 4E, 4C here A, B, C, D, respectively. Reproduced with permission.

that were optimized to lead to strong activity bursts, which were typically accompanied by oscillations. Different injection pressures (12–30 psi) and different injection durations (4–30 ms) were used. Further details of the KCl injections are discussed in the Results (Section 4.2.1). Recordings were done at a sampling frequency of 10 kHz.

4.1.2 Data analysis

To analyze the time course of the KCl-triggered activity, the standard deviation of EFPs was calculated in 50 ms bins for the 5 s epochs that followed each KCl-puff. Consequently, the KCl-stimulated epochs were cut individually for each recording session, i.e., data was selected from the time point of KCl-injection until the time when the standard deviation had decayed back to 25% of the maximal value, measured from the peak of the amplitude to baseline variability (Fig. 4.2; Section 4.2.1). I excluded epochs in which no activity elevation followed the KCl-injection ($N = 4$ out of in total 91). Additionally, I excluded epochs in which the activity following a KCl-application was very high and not characteristic ($\gtrsim$ 2-fold higher than in recordings in the same session; $N = 2$ out of in total 91), which left in total $N = 85$ epochs for further analysis.

Two methods of frequency analysis were applied. First, I calculated the time-resolved spectrograms using the inbuilt function for spectrograms of Python with a window of 100 ms in steps of 5 ms. Second, I calculated the power spectral density of whole epochs using *Welch's method* (Python inbuilt periodogram). This yielded a periodogram for each

recorded epoch that was used to calculate the recording session average, and further the average periodogram of all sessions. The leading frequency of a periodogram was calculated as its first positive peak.

4.1.3 Network model

To test whether the observed oscillations could be clocked by interneuronal GJs, I used our interneuronal network model presented in Chapter 3.2. In this model, I set all the inhibitory conductances to zero (Eq. (3.2)), so that the neuronal coupling was exclusively electrical. The KCl injections, which increase the extracellular concentration of K^+-ions, and hence primary depolarize the neurons (see Section 4.2.1), were modeled as a Poisson-distributed excitatory input. Thus, to investigate the effect of a changing KCl concentration, I varied the excitatory current that was fed into the neurons.

4.2 Experimental results

The data presented in the following is exclusively from experiments that were performed on acute hippocampal slices of mice (Nimmrich et al., 2005). The recordings of the extracellular field potential were published by Nimmrich et al. (2005).

Here, I test the hypothesis that the ripple-like oscillations in the hippocampal region CA1, which were recorded in the absence of chemical coupling, could be clocked by interneuronal GJs. Therefore, I analyze the time course of the KCl-triggered activity, the frequency composition of the data, and the stability of the oscillation over time. Finally, I compare the experimental data to simulations of a network that is solely coupled by electrical synapses.

4.2.1 Potassium-triggered neuronal activity

Understanding the mechanism by which KCl increases the neuronal activity is a prerequisite for interpreting the data. Thus, I first study how a change of extracellular KCl concentration is affecting neuronal activity in the experiments by Nimmrich et al. (2005), and consequently discuss the results in a more general context of potassium triggered activity.

Time course of the KCl-triggered ripple-like oscillations

Fig. 4.2 shows the standard deviation of the EFP following a KCl injection. I found that $\approx$ 50–100 ms after a focal application of KCl the standard deviation increased strongly. The time that passed from the injection of the KCl solution (at $t = 0$ in the dendritic layer of CA1), over the consequent increase of activity, and to the return of the activity back to baseline was $\approx$ 1–5 s. The data epochs recorded from the time point of the KCl-puff ($t = 0$ s) until the time when the signal's variability decreased to 25 % (red dots in Fig. 4.2) of the maximal standard deviation (above baseline) were retained for further analysis to ensure that activity levels were sufficiently high. The resulting epoch lengths varied between 0.3–3.2 ms.

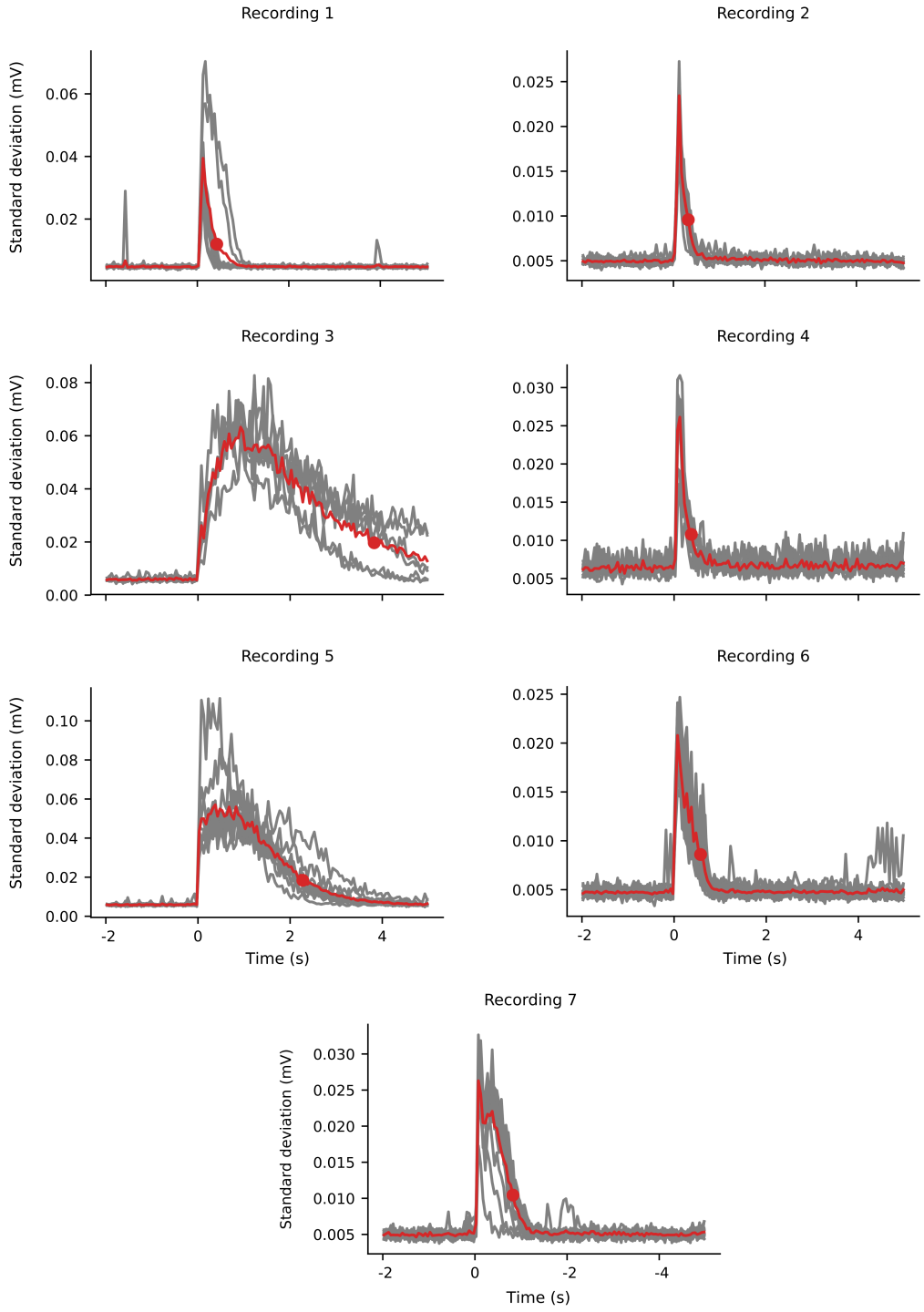

Figure 4.2: Standard deviation of unfiltered EFP in response to KCl injection. The standard deviation of the EFP was computed in 50 ms bins around the time point when potassium was injected (−2 s before; 5 s after). Each plot shows a different recording session, i.e., a different slice and/or different animal. Gray lines mark individual runs, and the average is shown in red. The red dot marks the data point at which the standard deviation has fallen to 25 % of its maximal value, which is measured above baseline variability.

This variable duration of elevated activity across the recording sessions might be explained by the fact that different slices were used. Another factor adding to the observed variability are the variability of experimental parameters, e.g., the location for the pressure injection, the location of the recording electrode, the distance between recording electrode and pressure injection, the pressure and the duration of the KCl injections. A conclusive relation between the pressure and duration of KCl-puff and the duration of the elevated activity could not be found (data not shown), possibly due to the limited amount of data. Additionally, the concentration of potassium might fluctuate because potassium accumulates in the slices.

How does extracellular potassium affect neuronal activity?

The actions of potassium on the neuronal activity depend on the concentration and location of the application (Somjen, 1979). The normal potassium concentration $[K^+]_o$ in the mammalian cerebrospinal fluid is about 2.8–3.2 mM (Somjen, 1979). An increase of the concentration leads to bursts of activity, which increase in frequency and strength with increasing concentration (Somjen, 2002). When the concentration is raised further above the *Lux-Heinemann ceiling*, all activity declines since the neurons go into excitation block (Heinemann and Lux, 1977).

The primary effect of a higher extracellular potassium concentration $[K^+]_o$ is that the equilibrium potential for potassium increases to less negative values (Fröhlich et al., 2008). This leads to an influx of potassium into the neurons via the partially opened potassium channels, which in turn leads to a depolarization of the neurons. Since most of the potassium channels are opening with an increasing membrane potential, this might even lead to a self-enhancing, higher influx of potassium (Johnston et al., 2010). This process is reversible, i.e., when $[K^+]_o$ returns to baseline, the equilibrium potential and the membrane potential of the neuron return to their initial values.

However, increasing $[K^+]_o$ has also been shown to cause bursting activity in pyramidal neurons and to lower the input resistance. Additionally, higher values of $[K^+]_o$ result in a higher reversal potential of $GABA_A$ synapses, which reduces the hyperpolarizing function of the inhibitory synapses. This effect is mediated by the potassium-chloride cotransporter KCC2, which transports less chloride out of the cell at high $[K^+]_o$ (Fröhlich et al., 2008). Since the ion cotransporter KCC2 is slow the decrease of inhibitory efficiency also takes effect on a slow time scale.

So, what sets the duration of activation following a KCl puff? The duration of the KCl-triggered activity depends on the mechanisms that regulate the extracellular concentration of potassium. Different mechanisms might contribute, most prominently, absorption by neurons and astrocytes, and extracellular diffusion (Fröhlich et al., 2008). In the experiments by Nimmrich et al. (2005), the neuronal tissue was mounted on a perfusion chamber, where the neuronal tissue was object to an ongoing flow of a thin layer of fluids. As a result, the local application of KCl was washed out of the slice in the course of time. However, this washing out is assumed to contribute on the time scale of minutes, i.e., a slower time scale than aforementioned effects.

In conclusion, the primary effect of increasing extracellular potassium is the increase of

excitability. How long this phase of excitability lasts is determined by a complex interplay of different mechanisms, which regulate the extracellular potassium concentration in the neuronal tissue.

Synthesis

In the experiments by Nimmrich et al. (2005), KCl was locally applied to the stratum radiatum of the CA1 region. The concentration was applied in an unphysiological high concentration of 1 M. As a result, the dendrites of pyramidal cells were exposed to this high KCl concentrations and received strong depolarizing currents (see Section 1.1.1 for anatomy of the slice). However, interneurons such as parvalbumin-positive basket cells (PV+BCs) are also known to extend their dendrites up to stratum lacunosum-moleculare (Klausberger et al., 2003), so they also receive excitatory currents. Thus, I assume that the observed activity was caused by both excitatory and inhibitory neurons.

Another interesting aspect of the Nimmrich et al. (2005) experiments is the generation of the EFP. Under normal conditions the EFP is dominated by synaptic currents (Buzsáki et al., 2012), here however, all synaptic currents were blocked (Nimmrich et al., 2005), and hence the EFP must be generated by different current sources.

I hypothesized that in the present experiments the contributions to the EFP can be attributed to two different sources that are distinct by their time scales. I assume that the slow components of the EFP ($\lesssim 20$ Hz) were primarily contributed by the currents directly caused by the KCl injection, i.e., excitatory currents received mostly in the dendritic region that mimic the excitatory inputs from the Schaffer collaterals during sharp waves (Ylinen et al., 1995). In contrast, the fast components of the EFP ($\gtrsim 20$ Hz) were primarily caused by the APs and by the AP associated currents in the pyramidal cell layer.

In the reasoning above, I considered only the primary effects of the increased KCl concentration on neuronal activity, i.e., the increase of neuronal excitability. However, the side effects of the potassium application, e.g., the bursting of pyramidal neurons and change of the membrane conductance, might also influence the network dynamics and hence shape the EFP as discussed in the previous section.

In conclusion, my working hypothesis is the following: Potassium activated both pyramids and interneurons in CA1 by means of depolarizing currents. These currents (slow, $\lesssim 20$ Hz) together with the action potential currents (fast, $\gtrsim 20$ Hz) were the main contributors to the EFP. The duration of the activation was set by the diffusion and the mechanisms of absorption of potassium, the time scale of the fluid exchange, and the amount of KCl injected into the slice. After the concentration of potassium declined, the neuronal activity returned back to equilibrium.

4.2.2 Oscillations in the extracellular field potential

In Fig. 4.3, I give an overview of the EFP recorded from a hippocampal slice when all chemical transmission was blocked by 20 µM AMPA/kainate receptor antagonist CNQX, 30 µM NMDA receptor antagonist D,L-APV and 10 µM gabazine (SR-95531).

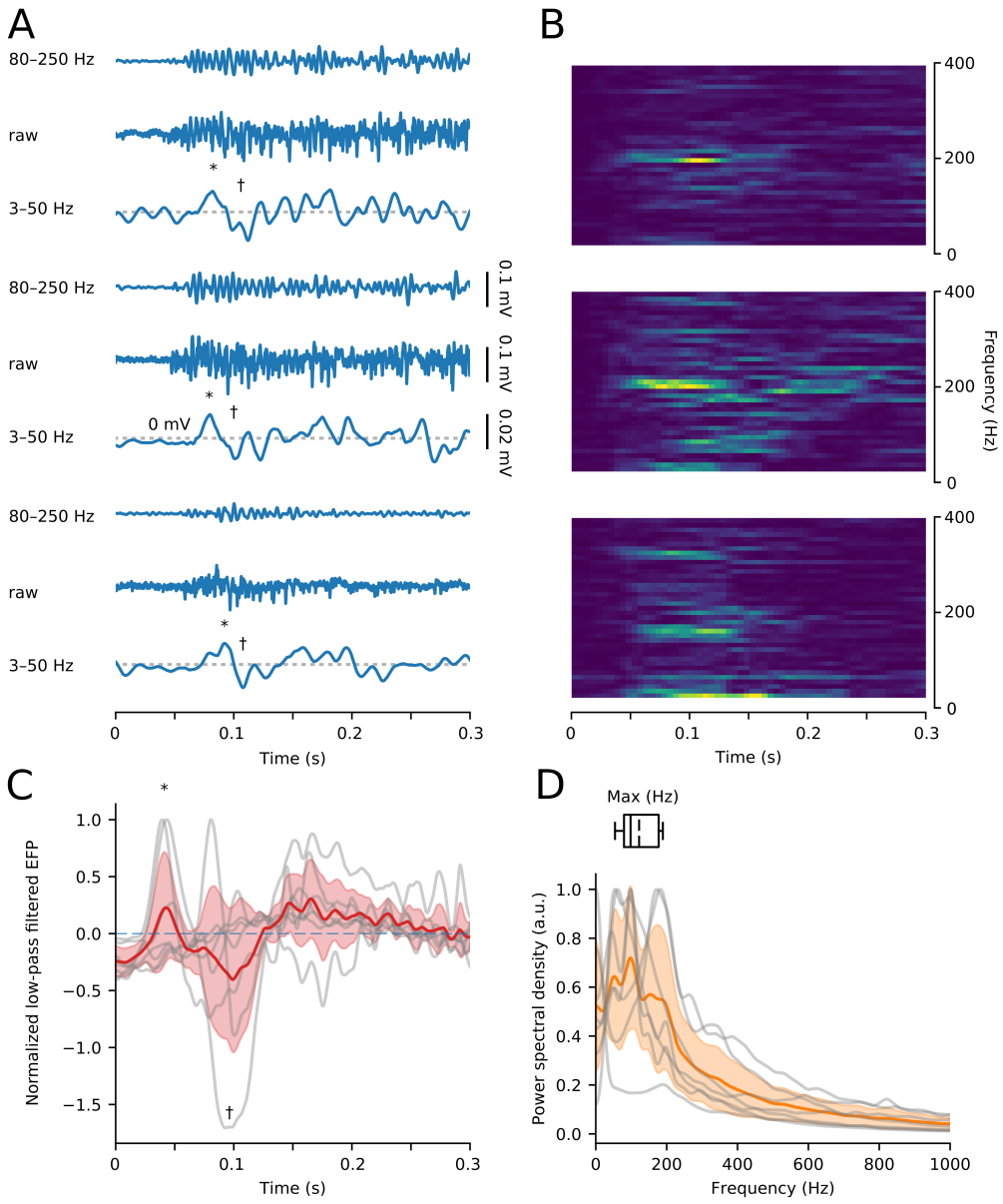

Figure 4.3: Oscillations in the absence of chemical synaptic transmission. Overview of raw data and frequency composition of the activity for all recordings. Synaptic transmission was blocked by SR-95531, CNQX, D,L-APV. **A**, Three example epochs (of in total $N = 13$ epochs in session 2; Fig. 4.2) evoked by KCl pressure injections at $t = 0$. Traces filtered as indicated. Here, (∗) and (†) denote positive and negative characteristic deflections, respectively. For details, see text in Section 4.3. **B**, Spectrograms of the data in A. Dark, blue colors code for low values, and bright, yellow colors for high values. **C**, Low-pass filtered (3–50 Hz) data averaged for each recording session (gray), and overall average (with its standard error) of the 7 recording sessions (red). Average EFP is normalized by its maximal value. **D**, Periodograms of all KCl events from the seven different recordings sessions and their mean (orange; with its standard error). The leading frequencies are visualized by a boxplot, that shows the mean (122 Hz), median (100 Hz), and the span of the maxima.

Fig. 4.3A shows three KCl-induced epochs of raw EFP data from one recording session (middle traces). Band-pass filtered EFP recordings depicting the fast (80–250 Hz) and slow (3–50 Hz) frequency components are plotted above and below the raw data, respectively. Within $\approx$ 50–100 ms, the KCl pressure injections (at $t = 0$ ms) showed an effect, and neuronal networks became strongly active. Interestingly, the period of elevated activity started with a slight positive voltage deflection, ($*$) in Fig. 4.3A, that was followed by a negative deflection, (†) in Fig. 4.3A.

Fig. 4.3A also shows EFP oscillations during the periods of elevated activity. In Fig. 4.3B, the spectrograms of the epochs in Fig. 4.3A are shown. I often found elevated spectral power in the frequency band around 200 Hz, however, most prominently within the first $\approx$ 150 ms of an epoch.

To further test the observations from the example traces about frequency content and slow bipolar onset (Fig. 4.3A and B), I extended my analysis to the entire dataset. First, I calculated the average of the low-pass filtered traces of all the seven available recording sessions, which were normalized by their maximal values (Fig. 4.3C). Here, a strong variability across the different recordings sessions was evident. Despite this variability, there was a weak trend of an initial positive deflection, ($*$) in Fig. 4.3C, followed by negative one, (†) in Fig. 4.3C, which lasted $\approx$ 100–150 ms. The duration and the general shape of the EFP deflection remind vaguely of the characteristics of a sharp wave (Maier et al., 2003; see also Fig. 1.4). This is probably due to the fact that the input in the dendritic region of CA1 was similar to the input during sharp waves, i.e., (inward) currents in st. radiatum caused by high $[K^+]_o$ and (outward) return currents in the stratum pyramidale (Section 4.2.1).

The frequency spectrum averaged across all seven sessions is presented in Fig. 4.3D.The strongest frequency modes are in the range of 100–200 Hz as depicted by the boxplot at the top of Fig. 4.3D. This confirms the original analysis by Nimmrich et al. (2005), and is in agreement with ripple frequencies observed in other experiments (Draguhn et al., 1998; Maier et al., 2003; Buhl et al., 2003; Maier et al., 2011; Behrens et al., 2011; Sun et al., 2012; Maier et al., 2012; Simeone et al., 2013; Maier et al., 2013; Aivar et al., 2014). However, in contrast to these experiments, I found a lot of spectral power at higher frequencies ($>$ 200 Hz).

4.2.3 Leading frequencies are stable over time

In Fig. 4.3, I analyzed the frequency composition of the activity. Here, I quantified the stability of the oscillations over time because this might give interesting insights into the mechanisms underlying the ripple-like activity (Fig. 4.4).

In Fig. 4.4, I show the evolution of the leading frequencies during single epochs of KCl-induced events (Fig. 4.4A), which had a total length on the order of a second. I also show the leading frequencies during the whole recording session (Fig. 4.4B), which had a total length on the order of one hour.

The leading frequencies found in Fig. 4.3D were relatively stable over the entire recording. Most importantly, I did not find any systematic trend neither within epochs nor across epochs within a recording session. This is an interesting finding since the oscil-

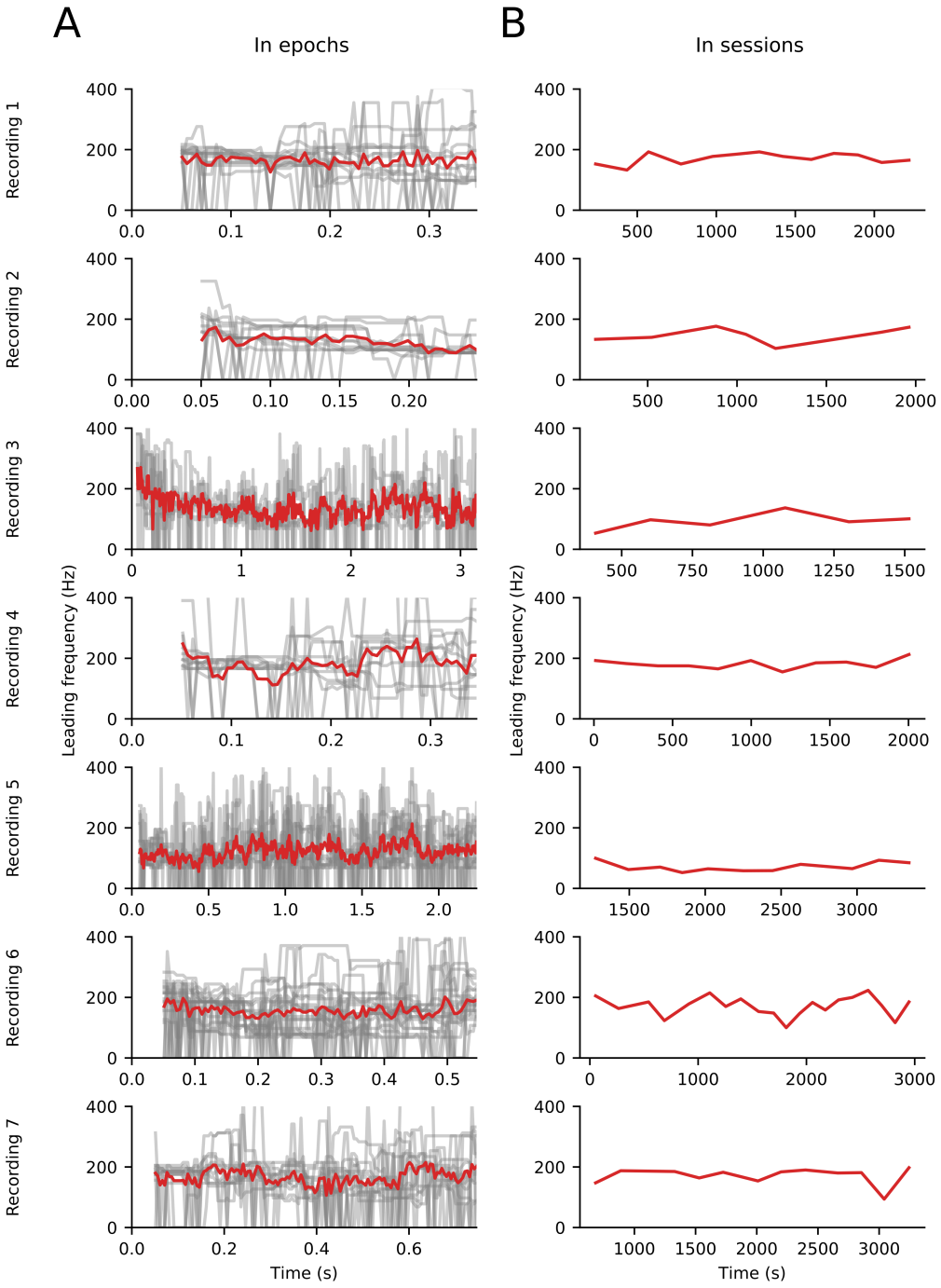

Figure 4.4: Time evolution of the leading frequencies of the EFP. **A**, Leading frequencies of the EFP as a function of time during a single KCl-induced epoch. The leading frequency are calculated the first positive peak of the EFP's periodogram. The average is plotted in red and single epochs in gray. Frequencies are calculated for overlapping bins of 0.1 s. **B**, Leading frequencies as a function of time during a whole recording session in the same slice. Each data point represents the average leading frequency of one KCl-induced event. Each plots shows one session.

lation frequency remains stable although the activity is expected to vary over time. I assume that the firing rates of the neurons are correlated to the standard deviation of the neuronal activity (Fig. 4.2). If this assumptions holds true, this results show that the network frequency is not affected by a change of the neuronal firing rates.

4.2.4 Activity of a network exclusively coupled by gap junctions

In Chapter 3, I have shown that a network of interneurons can oscillate at ripple frequency, and that GJs promote these oscillations. In the view of the experimental data analyzed in Sections 4.2.1, 4.2.2, and 4.2.3, it is interesting to know if, and under which conditions this network model can generate oscillatory activity without chemical synapses. To shine light on this question, I used the very same network model as described in Section 3.2 and set the peak conductance of the inhibitory chemical synapses to zero (Eq. (3.2)).

In Fig. 4.5, the response of the network to different input strengths is depicted with only electrical coupling amongst the neurons. Figure 4.5A1–D1 show the spiking activity and the instantaneous firing rate for an average interneuron in the network with standard GJ connectivity ($p_{\mathrm{GJ}} = 0.06$; Table 3.1). The firing rates indicate that the network starts to oscillate weakly for high values of the drive (4500 spikes/s). Increasing the GJ connectivity ($p_{\mathrm{GJ}} = 0.12$, Fig. 4.5A2–D2) leads to a change of regime: the network shows strong oscillations. I do not find an abrupt transition from a non-oscillating regime to an oscillating regime, but a gradual development from local synchronous bursts to network-wide oscillations.

These observations are further quantified by computing the oscillation strength, the firing rate, the network frequency, and the synchrony index in Fig. 4.5E-G (details for these measures are given in Section 3.2). Fig. 4.5E demonstrates that the oscillation strength, i.e., a measure for the spectral power distributed around the network frequency, increases drastically when the GJ connection probability is doubled from $p_{\mathrm{GJ}} = 0.06$ to $p_{\mathrm{GJ}} = 0.12$; note the logarithmic scale. Here, the oscillation strength is normalized by the same value as in Fig. 3.4, and consistently, the same threshold of the oscillation strength (0.1) is used to assess whether oscillations are generated reliably (gray line in Fig. 4.5E; Fig. 3.4). Notably, the weakly-connected network ($p_{\mathrm{GJ}} = 0.06$) does not cross the oscillation strength threshold, while the strongly-connected network ($p_{\mathrm{GJ}} = 0.12$) crosses the threshold at at $\approx 2000\,1/\mathrm{s}$.

Accordingly, the network frequency is only depicted for the strongly-connected network for suprathreshold oscillation strength (triangle in Fig. 4.5F). The network shows fast oscillations, whose frequency increases from $\approx 200\,\mathrm{Hz}$ to $\approx 400\,\mathrm{Hz}$ with increasing values of the excitatory input. The network firing rate is depicted in the same plot. I observe that the network frequency and the firing rate are almost identical for strong GJ coupling as predicted by a theoretical study from Ostojic et al. (2009).

In the strongly-coupled network, the synchrony index generally increases with increasing excitatory drive, however, also shows some non-monotonic behavior (Fig. 4.5G). In contrast, I observe no increase of synchrony in the weakly GJ coupled network.

In conclusion, I find that oscillations can arise in a network exclusively coupled by

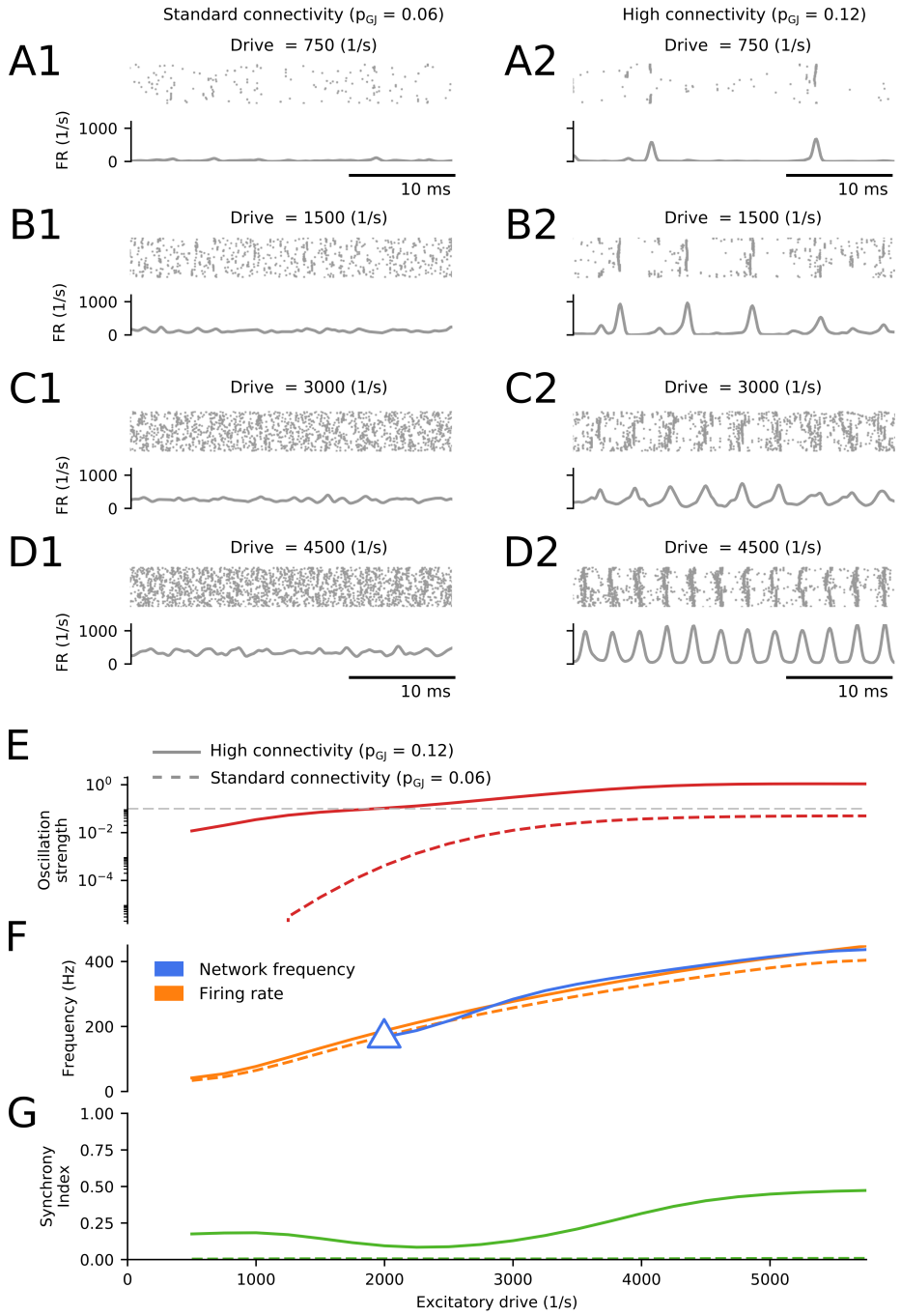

Figure 4.5: Simulation of an interneuronal network exclusively coupled by electrical synapses for two different GJ connectivities. **A1-D2**, Examples of network activities, i.e., rasterplots and average firing rates (FRs), with different excitatory input drive for $p_{\mathrm{GJ}} = 0.06$ (left) and $p_{\mathrm{GJ}} = 0.12$ (right). **E**, Oscillation strength as a function of the excitatory drive for $p_{\mathrm{GJ}} = 0.06$ and $p_{\mathrm{GJ}} = 0.12$. Note that the y-axis is on a logarithmic scale. The gray line marks the oscillation strength threshold above which oscillations are considered to be reliably. **F**, **G**, Same as E but for firing rate and network frequency (F), and synchrony index (G). The network frequency is displayed for suprathreshold oscillation strength (E). The point, where the threshold is crossed, is marked by a triangle for $p_{\mathrm{GJ}} = 0.12$. See Tables 3.1 and 3.2 for parameter values.

GJ, as predicted theoretically (Ostojic et al., 2009). These oscillations are within the synchronous regular regime, where the average firing rate of the neurons determines the network frequency. The implications of these findings for the interpretation of the experimental data analyzed in this chapter are discussed in the next section.

4.3 Discussion and conclusion

The analysis of the EFP data – cordially provided by Dr. Nikolaus Maier (see also Nimmrich et al., 2005) – showed that even without chemical synapses ripple-like oscillations can be triggered by KCl-injections in hippocampal CA1 minislices. I confirmed that the leading frequencies of these oscillations are in a range of 100–200 Hz (Fig. 4.3 and Fig. 4.4; Nimmrich et al., 2005), which is in good agreement with ripples (Draguhn et al., 1998; Maier et al., 2003; Buhl et al., 2003; Nimmrich et al., 2005; Maier et al., 2011; Behrens et al., 2011; Sun et al., 2012; Maier et al., 2012; Simeone et al., 2013; Maier et al., 2013; Aivar et al., 2014).

Interestingly, the leading frequencies of the oscillations remained stable within and across epochs during the elevated activity following the KCl pressure injections in the same recording session (Fig. 4.4), but showed a strong variability across the seven different recording sessions (Fig. 4.2 and 4.3). This variability might be caused by the natural variability of the slices, by the different durations and pressures of the KCl injections, or by the different times that were needed to optimize the stimulation parameters.

Another important observation is that the spectra of the extracellular field potentials did not consistently show pronounced peaks, and there was a relatively large amount of power at higher frequencies, in contrast to the spectra from other experiments that analyzed sharp wave-ripples (Draguhn et al., 1998; Maier et al., 2003; Buhl et al., 2003; Nimmrich et al., 2005; Maier et al., 2011; Behrens et al., 2011; Sun et al., 2012; Maier et al., 2012; Simeone et al., 2013; Maier et al., 2013; Aivar et al., 2014).

According to my simulations (Fig. 4.5) and previous theoretical predictions (Ostojic et al., 2009), a network of leaky integrate-and-fire point neurons that is exclusively coupled by gap junctions can collectively oscillate only at the average firing rate of the individual neurons (cf. Traub et al., 1999). How does this relate to our experimental observations?

In the experiments, I observed that the mean network frequency remained constant during epochs of elevated activity (Fig. 4.4A). The firing rates were not measured within the neuronal slice, but I expect them to be highest at the peak of the activity (Fig. 4.2) when the maximal effect of the elevated potassium concentration is observed. As time passes, the concentration of the KCl decreases, and so should the firing rates of the neurons. According to my theoretical results from Fig. 4.5, I postdict that the oscillation frequency follows the evolution of the firing rates. In the experiments, however, the network frequency stays constant (Fig. 4.4), which contradicts the results of my simulations. This argues against an involvement of interneuronal GJs in the generation of the ripple-like oscillations observed in the experiments by Nimmrich et al. (2005).

Further, the functional role of the GJs was tested experimentally by applying GJ

blockers (octanol and carbenoxolone), which led to an abolishment of the fast oscillatory activity (Fig. 4.1C) and hence argues in favor of a functional role of GJs between pyramidal cells (Traub et al., 1999). However, both GJ blockers induce strong side effects as discussed in more detail in Chapter 2, which renders the GJ blocker experiments inconclusive.

Another explanation for the ripple-like oscillations observed in the experiments might be provided by Fink et al. (2015), who show that uncoupled pyramidal neurons driven by uncorrelated Poisson noise at a constant rate could generate coherent network oscillations. Recent evidence also suggests that dendrites of fast spiking parvalbumin-positive interneurons can produce oscillations at ripple frequency (Chiovini et al., 2014). For all these hypotheses, it would be interesting to access the spike times of neurons in slices explicitly. Maybe, spike times could be still extracted from the existing data using spike sorting techniques (Rey et al., 2015). It is also possible that the remaining inhibitory connectivity was still strong enough to generate ripple-like oscillations because not 100 % of the inhibitory coupling might be blocked in the experiments of Nimmrich et al.. A further hypothesis for the origin of the ripple-like oscillations are pyramidal GJs as proposed by Traub et al. (1999) – a theory that is discussed in more detail in Chapter 1, Chapter 3, and Nimmrich et al. (2005).

5 Discussion and outlook

In this thesis, I investigated how interneuronal gap junctions affect hippocampal ripple oscillations. Ripple oscillations occur in combination with sharp waves as sharp-wave ripples (SWRs). SWRs have been implicated to be of great importance for memory consolidation (Girardeau et al., 2009), however, how exactly they contribute to memory is not known. It is very likely that (reverse) replays of previous neuronal activity, e.g., of place cells, contribute to memory consolidation (Wilson and McNaughton, 1994; Diba and Buzsáki, 2007). Such replays of cellular activity occur phase-locked to ripple oscillations during SWRs. Interestingly, previous activity is not only replayed but future activity is also preplayed during SWRs, which might be relevant for decision making. It is crucial to unravel the mechanisms that underlie SWRs, sharp waves, and ripples to understand their function in cognition.

In Chapter 1, I presented the different hypothesized theories for the generation of ripples that favor inhibition or excitation as their primary pacemaker. A differentiation between these hypotheses has posed a challenge for experimentalists because both pyramidal cells and interneurons fire phase-locked to ripple oscillations. However, advances in experimental techniques in the last decade, especially optogenetics, have allowed to collect evidence that argues more in favor of interneurons as the primary pacemaker of ripple oscillations (Schlingloff et al., 2014; Gan et al., 2017). These interneurons, in particular parvalbumin-positive basket cells (PV+BCs), are recurrently coupled not only by inhibitory synapses but also by gap junctions (GJs; Fukuda and Kosaka, 2000b; Galarreta and Hestrin, 2001a). It is unknown how exactly GJs between PV+BCs influence ripple oscillations.

In Chapter 2, I synthesized experiments that analyzed GJ coupling: PV+BCs throughout the whole mammalian brain are connected via gap junctions. They act as chemical and electrical pathways, however, their specific functions in the neuronal circuits of the brain – beyond increasing synchrony – remain elusive. Experimental efforts to understand the specific function(s) of gap junctions in SWRs have been inconclusive.

In Chapter 3, I took the controversial results of the GJ experiments as a starting point and analyzed the function of interneuronal GJs in hippocampal ripple oscillations by simulating networks of PV+BCs. I found that interneuronal GJs increase the synchrony and the firing rates of interneurons during ripple oscillations. These effects are predominately mediated by the (fast) transmission of action potentials via GJs. In the Supplementary Material of this thesis, I also demonstrate that this increase of synchrony cannot be achieved by increasing inhibitory coupling, which is the primary generator of the oscillations. Interestingly, I found that the network frequency is not strongly altered by interneuronal GJ coupling, and it remains determined by the time scales of the inhibitory synapses and the excitatory input of the interneuronal network (see Fig. S3 & S4).

Additionally, I showed that ripple oscillations generated in INT-INT networks coupled by GJs are more robust to the size of the network, i.e., GJs reduce the minimal number of necessary interneurons to generate ripples. These findings are complemented by simulations in the Supplementary Material, in which I demonstrate that ripples are also more robust to the strength of excitation and the strength of inhibitory coupling when interneuronal GJs are present. Further, I employed multicompartmental neuron models to calculate the delay of gap junction transmission, which can be up to 3 ms depending on the morphology of the neuron and the GJ location in the neuronal tree. Feeding these delays back into the neuronal network, I showed that GJs only support ripple oscillations when the GJ delays are smaller than ≈ 0.5 ms, which requires proximal coupling.

In Chapter 4, I tested whether ripple-like oscillations can be generated by interneuronal networks that are exclusively coupled by (interneuronal) GJs. Therefore, I reanalyzed data from Nimmrich et al. (2005), who observed ripple-like oscillations in the absence of chemical synaptic coupling, whose origin is not fully understood. My analysis confirms that ripple-like steady-state oscillations are present in these recordings. Furthermore, my computational analysis shows that such exclusively GJ-coupled INT-INT networks are able to oscillate at ripple frequency, when sufficient GJ coupling and excitatory drive is present. To further validate whether such GJ-mediated network oscillations clocked the observed ripple-like oscillation, I simulated the firing rates and the network frequency in an exclusively GJ-coupled network that is excited by an elevated extracellular potassium concentration. In a next step, I could show that my theoretical predictions were qualitatively different from the experimentally recorded neuronal activity, which rendered the hypothesis that the observed ripple-like oscillations are generated by exclusively GJ-coupled INT-INT networks unlikely. Thus, further analyses are needed to test alternative hypotheses: Nimmrich et al. (2005) proposed that the oscillations could be generated by pyramidal GJs (Traub et al., 1999), however, the anatomical and electrophysiological evidence for such GJs is sparse. Another theory would be that in the experiments by Nimmrich et al. (2005) not all chemical synaptic transmission was blocked, and the residual inhibitory connectivity was still strong enough to generate ripple-like oscillations. Furthermore, Chiovini et al. (2014) suggested that ion-channels in dendrites of PV+BCs could be able to maintain ripple-like oscillations when sufficient excitatory input is present.

Throughout this thesis, I developed proposals and predictions for experiments that could reveal the functional role of interneuronal GJs in ripple oscillations. In Chapter 2, I reviewed experimental studies that investigated the impact of a putative deactivation of GJs on ripples. These studies proved difficult to interpret because their outcomes are ambiguous and hence inconclusive, possibly due to the side effects of attempts to block GJs. Based on my simulations of INT-INT networks, I predict that when interneuronal GJs are specifically deactivated in hippocampal area CA1, ripples will be less synchronous, whereas the network frequency will only change mildly. These effects could be shown by directly accessing the spike times of the CA1 (inter)neurons either by simultaneously recording multiple neuronal potentials or by spike sorting performed on extracellular field potentials. Note that these predictions do not consider any homeostatic or compensatory

effects that might be present in real neuronal networks.

Further, I simulated gap junction coupling potentials in multicompartmental models of hippocampal PV+BCs and demonstrated that the GJ transmission delay is predominantly determined by the location of the GJ in the neuronal tree. I showed that GJ coupling potentials with long delays $> 1.0\,\text{ms}$ should be present when GJs couple distal dendrites (Fukuda and Kosaka, 2000b); however, such long delays have not been shown experimentally (Galarreta and Hestrin, 2001a). Previously, I showed that GJ potentials with delays $> 0.5\,\text{ms}$ do not support ripples but they might play a role in slower oscillations, or dendritic computations. Additional to long delays, I predict short delays ($\lesssim 0.5\,\text{ms}$) between PV+BCs (Bartos et al., 2002), motivated by experimental evidence for proximal coupling between PV+ interneurons ($\lesssim 100\,\mu\text{m}$, Fukuda and Kosaka, 2000b). Such delays have been shown in neocortex (Galarreta and Hestrin, 2001a) but dual-cell recordings of fast GJ transmission in hippocampal PV+BCs, which quantify delays and shapes of GJ coupling potentials, are – to my best knowledge – still pending (Bartos et al., 2002).

Stimulated by the results of Chapter 3 and 4, I propose the following experiment to probe the function of GJs for ripple oscillations: First, CA1's extracellular field potentials are recorded during optogenetic activation of the PV+ interneurons as in Schlingloff et al. (2014) and Stark et al. (2014). Additionally, the number of active interneurons, i.e., the neurons that receive optogenetic excitation, is varied. Second, the optogenetic activation is repeated, and additionally all synaptic transmission is blocked (Nimmrich et al., 2005; Schlingloff et al., 2014). These experiments are carried out in wild-type mice and in connexin36/45 double knockout mice, which lack the respective GJs proteins (Vandecasteele et al., 2008). According to my findings, I predict: Ripple-like oscillations will only be observed above a minimal number of active interneurons. Further, this minimal number of neurons is smaller when GJs are intact. Additionally, the second part of the experiments would probe whether GJs are required for the ripple-like oscillations that have been experimentally observed in absence of chemical transmission (Chapter 4; Nimmrich et al., 2005). The use of optogenetical techniques improves the experiments carried out by Nimmrich et al. (2005) because optogenetic activation can be better controlled than potassium triggered activity.

In this thesis, I discovered that gap junctions increase the synchrony of ripple oscillation. In the light of SWRs as a cognitive biomarker, I conjecture that this increase in synchrony might improve the efficiency of memory consolidation. This effect could be mediated by facilitating the formation of associations between neurons that form a memory trace. I hypothesize that these memory traces could be formed more efficiently via synaptic plasticity, which critically depends on spike timing, when neuronal firing is more synchronous.

During my time as a PhD student, several advances have been made to understand ripple oscillations (e.g., Schlingloff et al., 2014; Stark et al., 2014; English et al., 2014; Buzsáki, 2015; Gan et al., 2017; Donoso et al., 2018). Nevertheless, many questions relevant for this thesis are still waiting to be answered. First and foremost, it still needs to be clarified how hippocampal ripples are generated. Furthermore, for a full model of

the generation of SWRs, we also need to understand how sharp waves are generated. If we do have a model for SWRs, we might gain more insights in how SWRs support the process of hippocampal memory consolidation, and whether, and how they contribute to the process of transferring memories to the neocortex.

In conclusion, I showed that interneuronal gap junctions synchronize hippocampal ripples beyond the level of synchrony that could be reached with only inhibitory coupling. Therefore, gap junctions could play an important role in memory consolidation.

Supplementary Material

Here, I present additional information that support the content of this thesis.

1 Action potentials and bipolar current pulses in single cell models

In Fig. 3.5, two different multicompartment models are used to measure postsynaptic gap junction coupling potentials that are caused by presynaptic action potentials. It was argued in Section 3.3.4 that the action potentials are broader than APs of real hippocampal PV+BCs.

In Fig. S1, APs are elicited by current injections into three different multicompartment models (for details see Section 3.2). I find that the width of the APs in the models are in a range from 0.6–1.2 ms. The modeled APs are too wide in comparison to data from hippocampal PV+BCs (≈ 0.3 ms FWHM; Buhl et al., 1996; Kohus et al., 2016). Since realistic APs are important for simulating realistic GJ potentials, I excluded the model of Saraga et al. (2006) from further analysis.

To calculate more realistic GJ coupling potentials, I replaced the APs with fast bipolar current pulses. These current pulses are shown in Fig. S1B1 and C1. They have a comparable amplitude to the APs, however, their FWHM is below 0.1 ms.

2 How do multiple gap junctions affect the postsynaptic gap junction coupling potential?

In Fig. 3.5, we calculated the GJ coupling potentials and displayed their delay and their amplitude. In contrast to chemical synaptic potentials, GJ coupling potentials are dependent on a direct current transfer from pre- to postsynaptic neuron. In this section, I analyze how the GJ coupling potential is influenced by multiple GJs between the presynaptic and several postsynaptic neurons. The multicompartment model from Lee et al. (2014) with (by default) active conductances is used (see also Section 3.2.6).

The results of this analysis are depicted in Fig. S2. In Fig. S2A, I investigate how the postsynaptic GJ potential is affected when one neuron is coupled to up to 10 neurons via GJs at the same GJ location. As expected the GJ potential in the observed neuron is decreasing. While the GJ potential has an amplitude of ≈ 0.6 mV with only one GJ-coupled neuron, this potential is halved to ≈ 0.3 mV when 10 neurons are coupled via a GJ at the same location.

Because in real neurons GJ coupling is not restricted to one location, I allowed the pre- and postsynaptic coupling location to vary randomly within one branch of the dendritic

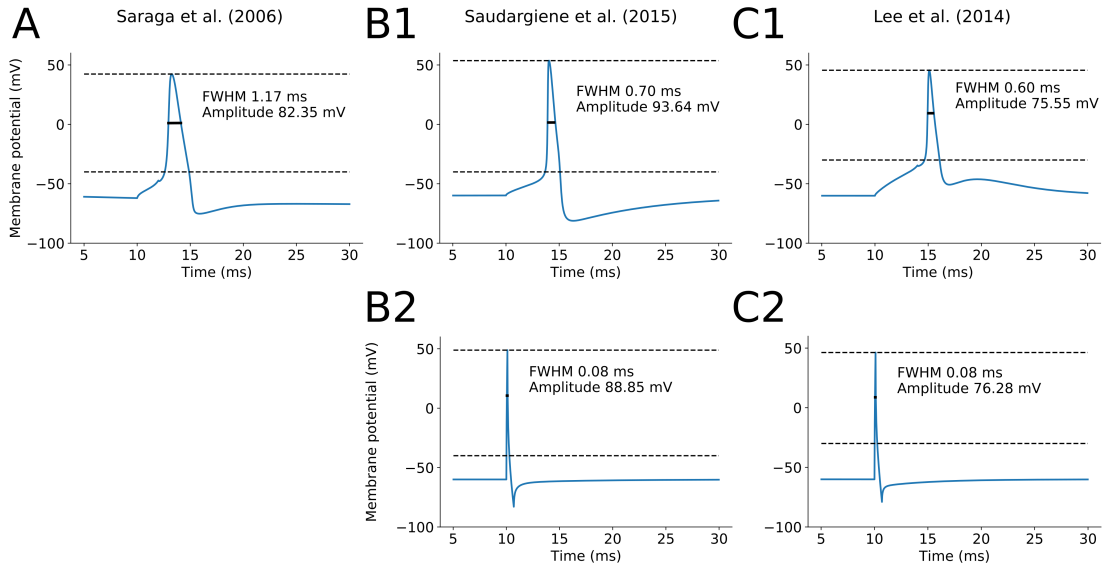

Figure S1: Action potentials and bipolar current pulses in parvalbumin-positive basket cell models. APs with their respective FWHM and amplitude from the models of Saraga et al. (2006) in **A1**, Saudargiene et al. (2015) in **B1**, Lee et al. (2014) in **C1**. **B2**, **C2**, same as B1 and C1 but for the fast bipolar current pulse. Supplementary figure for Fig. 3.5.

tree (In Fig. S2B). The location of the GJ in the postsynaptic neuron whose GJ potential is recorded is the same as in Fig. S2A to allow a direct quantitative comparison. I find that GJs at different locations in one dendritic branch influence the postsynaptic GJ potentials differentially. In total, the observed postsynaptic GJ potential is only reduced by $\approx 0.1\,\mathrm{mV}$ when 10 GJs are added at random locations in the same dendritic branch.

In Fig. S2C, the previous analysis is repeated for pre- and postsynaptic GJ locations that are chosen randomly from the entire dendritic tree, while the GJ location for the recorded neuron is the same as in Fig. S2A and B. The overall reduction of the GJ potential is of the same magnitude as I found in B, however, I observe an increase of variability of the effect of each GJ on the postsynaptic GJ potential, which is probably caused by the location of the GJs that differ more strongly. I observe that when the additional GJ is located close to the soma or in the same branch the effect on the measured GJ potential is stronger than for GJs in more distal locations.

In summary, the combined effect on the postsynaptic GJ potential is a reduction from $0.6\,\mathrm{mV}$ to $0.3\,\mathrm{mV}$, when 10 GJs are coupled at the same location to the presynaptic neuron. However, the effect of a single GJ on the postsynaptic potential is strongly dependent on the position of the GJ, in particular, on the electrotonic distance of the newly introduced GJ to the GJ of interest.

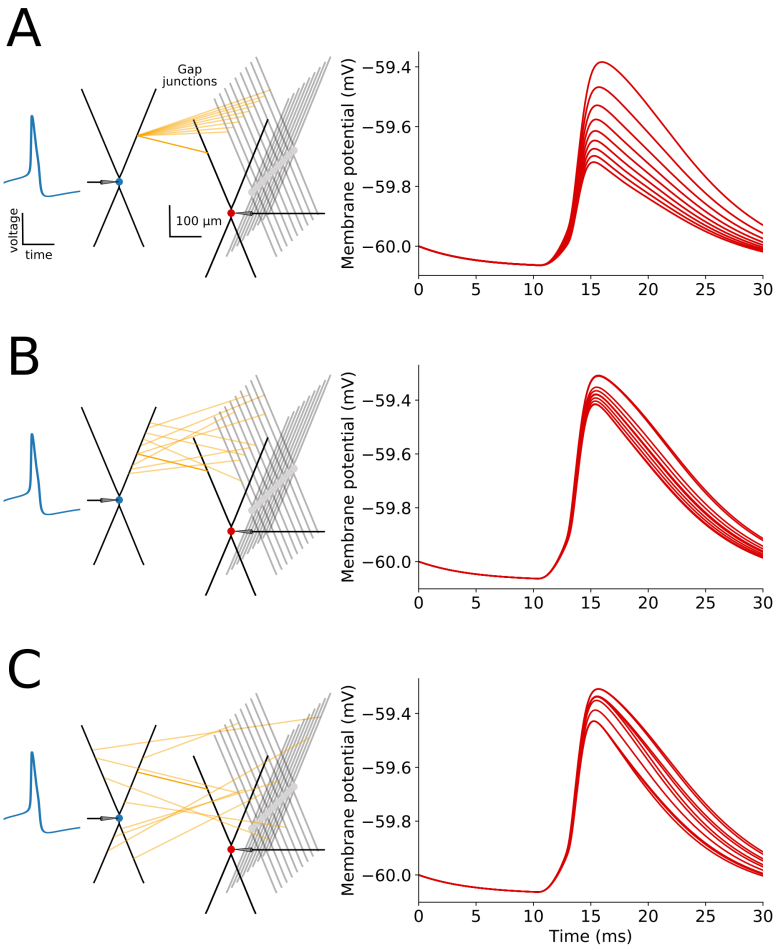

Figure S2: Effect of multiple gap junctions (GJs) on a single GJ coupling potential. **A**, GJ coupling potential for increasing number of GJs at the same location in the presynaptic and the respective postsynaptic dendritic tree. Left, Schematic of the network with multiple GJs from the presynaptic neuron to 10 postsynaptic neurons. All GJs are at the same pre- and postsynaptic location in the respective tree of the neurons. Right, GJ coupling potential of the highlighted postsynaptic neuron (left). For each plot one GJ-coupled, postsynaptic neuron is added to the network, a presynaptic AP is triggered, and the GJ coupling potential is measured in the observed neuron. **B**, Same A but for random pre- and postsynaptic GJ location in the same dendritic branch. The location of the GJ whose neuronal potential is measured is the same as in A. **C**, Same as A and B but for random pre- and postsynaptic GJ location in the whole dendritic tree. As in B the location of the GJ whose postsynaptic GJ coupling potential is measured is the location from A and B.

3 What sets the network frequency in recurrently coupled interneuron networks?

In Chapter 3, we showed that GJs only have mild effects on the network oscillation frequency. The oscillation frequency, however, is one of the main observables when ripple oscillations are characterized. In the following section, I analyze which network properties control the network frequency and other network dynamics, and compare my findings to previous results (Brunel and Wang, 2003; Donoso et al., 2018).

3.1 Time scales of the chemical inhibition

Brunel and Wang (2003) showed that the synaptic time scales can set the oscillation frequency in recurrently coupled interneuronal networks (INT-INT). Here, I calculate the dynamics of our network in dependence on these inhibitory synaptic time scales.

The inhibitory GABAergic conductances in our simulations are modeled by a biexponential function (Fig. 3.1C; also Eq. (3.2))

$$g_i^{\mathrm{inh}}(t) = g^{\mathrm{peak}} K \left(\mathrm{e}^{-(t-\tau_\mathrm{l})/\tau_\mathrm{d}} - \mathrm{e}^{-(t-\tau_\mathrm{l})/\tau_\mathrm{r}} \right) \tag{1}$$

for a spike event at $t = 0$ and $t > \tau_\mathrm{l}$, otherwise $g_i^{\mathrm{inh}}(t) = 0$. Here $\tau_\mathrm{l} = 1.0\,\mathrm{ms}$ sets the latency till the onset of the response, $\tau_\mathrm{r} = 0.45\,\mathrm{ms}$ is the rise time, and $\tau_\mathrm{d} = 1.2\,\mathrm{ms}$ is the decay time of the conductance. Further, $g^{\mathrm{peak}} = 5\,\mathrm{nS}$ is the peak conductance, and K normalizes the difference of the exponentials to 1 so that the maximum of $g_i^{\mathrm{inh}}(t)$ is g^{peak} (Bartos et al., 2002).The given values are the standard parameters used throughout this thesis (Table 3.1). Thus, in total, three time constants determine the synaptic time scales. How do they affect the dynamics of our network model?

In Fig. S3, I analyze how the network dynamics vary as a function of the different synaptic time constants. At first, let us have a look at the latency τ_l. The oscillation strength, a measure for the oscillatory power distributed around the peak of the network frequency in the power spectral density, is depicted in Fig. S3A. The emergence of oscillations critically depends on τ_l, the delay time constant. The functional relation of τ_l and the oscillation strength can be approximated as binary (Fig. S3A1): For $\tau_\mathrm{l} \lesssim 0.4\,\mathrm{ms}$ no oscillations occur in the network, and for $\tau_\mathrm{l} \gtrsim 0.6\,\mathrm{ms}$ oscillations are present, however, the oscillation strength does not depend strongly on τ_l.

The network frequency is depicted for values of the time constants at which the oscillation strength is above its threshold (Fig. S3B1). The network frequency strongly depends on τ_l and decreases from $\approx 300\,\mathrm{Hz}$ to $\approx 70\,\mathrm{Hz}$ with increasing τ_l. The firing rate of the neurons is depicted in the same plot. The firing rate increases for $\tau_\mathrm{l} \gtrsim 0.6\,\mathrm{ms}$ when oscillations are present in the network. Interestingly, the firing rates are higher than the network frequency from $\tau_\mathrm{l} \approx 2.4\,\mathrm{ms}$. The reason for this is that the inhibitory feedback is so slow that the neuronal population can spike twice before the inhibitory currents arrive at the neurons, and cause a hyperpolarization. The synchrony index (Fig. S3C1) increases at the onset of oscillatory activity, and stays relatively stable for higher values of the latency time constant.

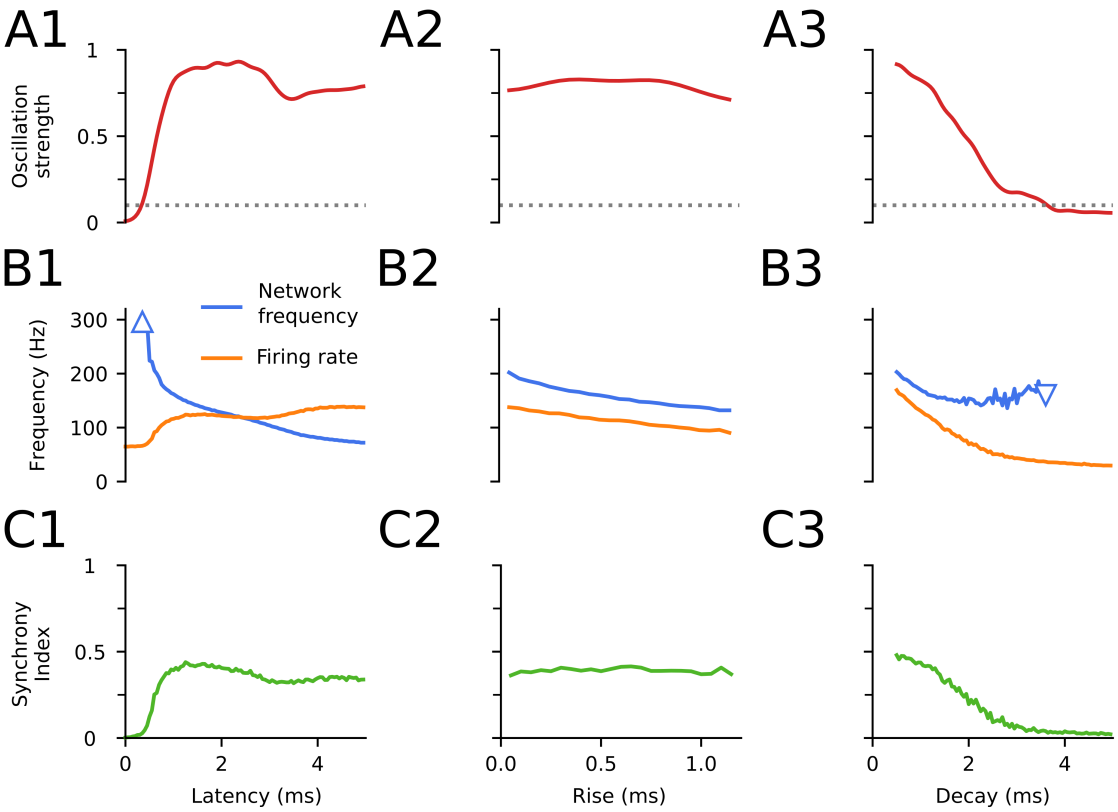

Figure S3: Influence of inhibitory synaptic time scales on the network dynamics. Oscillation strength (**A**), network frequency and firing rate (**B**), and synchrony index (**C**) are calculated for different values of the latency (**1**), rise time (**2**), and decay time (**3**) of the inhibitory synapses of the recurrently coupled interneurons (see Eq. (1)). Note the different time scales on the x-axis. Gray line in A denotes threshold (0.1) above which oscillations are observed reliably. The network frequency in B is depicted for suprathreshold oscillation strength A (Triangles). See Table 3.1 for parameters and Section 3.2 for the definitions of the network and the network measures.

Varying the rise time, $0 < \tau_\mathrm{r} < 1.2\,\mathrm{ms}$, does not have a strong effect on the network dynamics besides that the network frequency and the firing rate both decrease monotonically (Fig. S3A2–C2).

An increase of the decay time, $0.5 < \tau_\mathrm{d} < 5.0\,\mathrm{ms}$, leads to a decrease of the quality of the oscillations (Fig. S3A3). While the oscillation strength, the firing rates, and the synchrony index decay monotonically, the network frequency remains at the same average value (Fig. S3A3-C3).

The analysis of the time constants shows that the latency τ_l is the most important one of the synaptic time scales. This reproduces findings from Brunel and Wang (2003, their Fig. 4). They also provide limits for the network frequency

$$\frac{1}{4\,(\tau_\mathrm{l}+\tau_\mathrm{r})} < f < \frac{1}{2\pi}\,\sqrt{\frac{1}{\tau_\mathrm{l}\tau_\mathrm{r}}+\frac{1}{\tau_\mathrm{l}\tau_\mathrm{d}}} \quad . \tag{2}$$

For our standard parameters that leads to

$$172\,\mathrm{Hz} < f < 278\,\mathrm{Hz} \quad ,$$

which is not far from our findings for the network frequency ($\approx 160\,\mathrm{Hz}$). Note that without GJ coupling the network frequency would be $\approx 180\,\mathrm{Hz}$. Furthermore, were the given boundaries (Eq. (2)) derived in the limit of small oscillation amplitudes, which does not hold for the observed oscillatory regime.

3.2 Excitatory drive of the network

Another parameter that is important to set the network frequency is the excitatory drive of the interneuron network. In this section, I analyze how different conditions of the drive affect the network dynamics of our network model.

As pointed out in Brunel (2000), INT-INT networks can maintain oscillations in two distinct regimes: synchronous irregular and synchronous regular. The network regime depends on the balance of excitation and inhibition. If excitation dominates, the network is in a synchronous regular firing regime, and if inhibition dominates, the network is in a synchronous irregular firing regime. These regimes differ in their ratio of the firing rate to the network frequency, which is ≈ 1 for the regular, and < 1 for the irregular regime.

In Fig. S4A1–C1, the excitatory drive to the interneuron network is varied for a network with GJs and a network without GJs, and the oscillation strength, the network frequency, the firing rate, and the synchrony index are computed.

In Fig. S4A1, the oscillation strength is depicted. The oscillations increase with increasing drive and are stronger in the GJ network. Consequently, the threshold of 0.1 is reached for less excitatory drive. Note that here the oscillation strength is normalized by the same value as in Fig. 3.4.

The firing rates and the network frequency are depicted in Fig. S4B1. The firing rates increase monotonically for increasing drive. On the contrary, the network frequency, which is depicted for suprathreshold oscillation strength (Fig. S4A1), shows less variation and remains relatively stable. Furthermore, I find that increasing the excitatory input

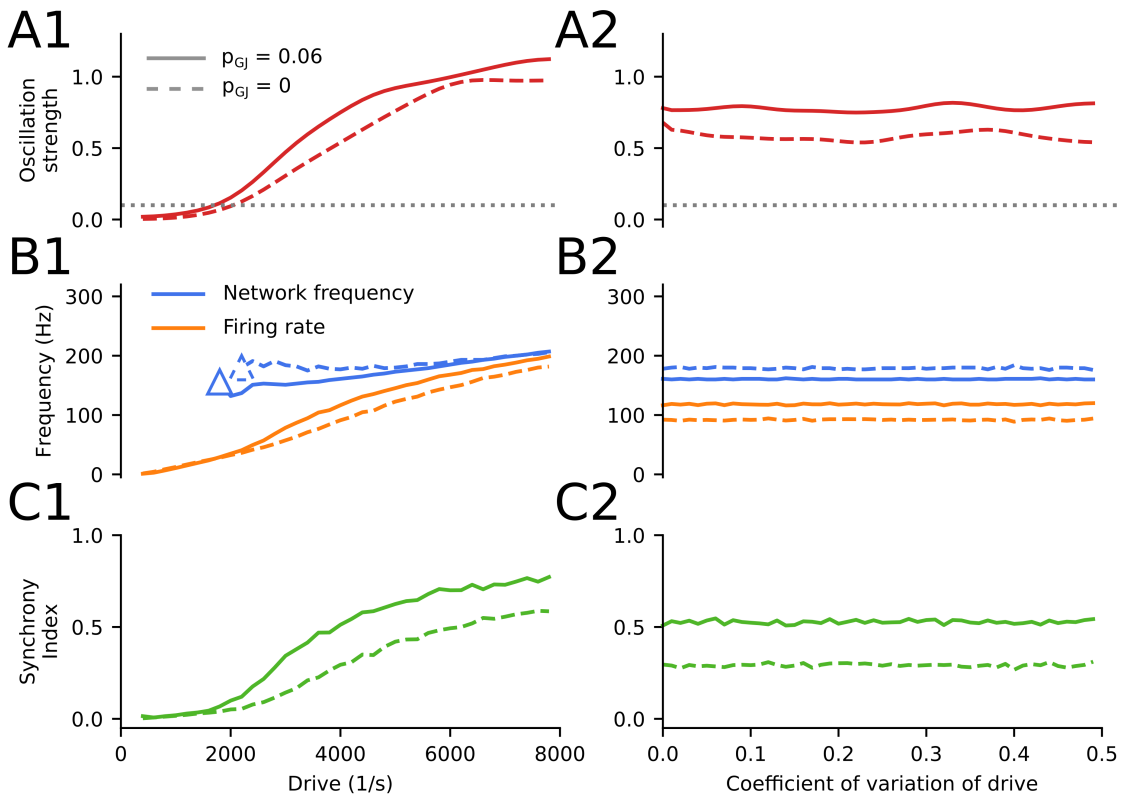

Figure S4: How do the excitatory drive (left) and heterogeneities of this drive (right) influence the network dynamics? **A1**, Oscillation strength is depicted as a function for the excitatory drive for GJ network (solid line) and GJ-free network (dashed line). **B1**, Network frequency and firing rate. Network frequency is depicted when the oscillation strength is beyond its threshold 0.1 (Triangles).**C1,** Synchrony index. **A2**–**C2**, same as A1–C2 but for increasing value of coefficient of variation of the Gaussian distribution according to which the mean of the excitatory input to each neuron is distributed. The mean of the excitatory input is kept constant at 4000 1/s. See Table 3.1 for parameters and Section 3.2 for the definitions of the network and the network measures.

.

drives the network from a synchronous irregular regime to a synchronous regular regime, in which every neuron is firing in every oscillation cycle (Brunel, 2000). In the latter regime ($\gtrsim$ 5000 1/s), the network frequency increases in parallel to the firing rates of the network.

The synchrony index also increases monotonically with increasing excitatory input (Fig. S4C1) and it is higher in the GJ network than GJ-free network.

In Fig. S4A2–C2, the drive that previously had the same constant mean for each interneuron, is here distributed across neurons according to a Gaussian distribution. The simulations are carried out for fixed drive = 4000 1/s, and increasing coefficient of variation of the Gaussian according to which the drive is distributed. Interestingly, increasing the variability of the drive does not influence the network dynamics neither in the GJ network nor in the GJ-free network.

In summary, the excitatory drive can determine the network frequency, however, only when the network dynamics are dominated by excitation and firing is synchronous regular. My results for the GJ-free networks confirm the results obtained by Donoso et al. (2018, their Fig. 1). Additionally, I observe that gap junctions reduce the excitatory drive necessary for oscillatory activity.

4 Influence of inhibition on synchrony

As pointed out in Chapter 3, GJs increase the synchrony in INT-INT networks. In this section, I show that this effect is specific to GJs and cannot be achieved by inhibitory synapses. To test this hypothesis, I use the interneuron network introduced in Section 3.2. In Fig. S5, I calculate the oscillation strength, the network frequency, the firing rate, and the synchrony index for increasing values of inhibitory coupling probability (Fig. S5A1–C1) and increasing strength of inhibitory peak conductance (Fig. S5A2–C2; Eq. (1)). The simulations are done for GJ networks and GJ-free networks.

In Fig. S3A1, the oscillation strength is calculated as a function of the connectivity of inhibition in the network. There are no oscillations in a network without inhibitory coupling because the oscillations are critically dependent on the inhibitory synapses, which holds true for GJ and GJ-free networks. When the inhibitory coupling increases ($0 <$ inh.coupling $\lesssim 0.1$) oscillations start rapidly. For inhibitory coupling $\gtrsim 0.15$, the oscillation strength remains relatively constant. For small values of the coupling (< 0.4), the GJ network shows a higher value of oscillatory activity than the GJ-free network, however, for higher connectivity (> 0.5), this effect vanishes.

The dependence of the firing rate and the network frequency on the inhibitory coupling are depicted in Fig. S5B1. The firing rates decrease for increasing inhibitory coupling. This reduction of firing rates is caused by an increasing amount of inhibitory currents that are fed back into the network. The network frequency, which is depicted for values of the inhibitory coupling at which the oscillation strength crosses its threshold, shows qualitatively the same trend as the firing rates, i.e., a decrease for increasing inhibitory coupling.

The synchrony index is shown in Fig. S5C1. At low values of inhibitory coupling the

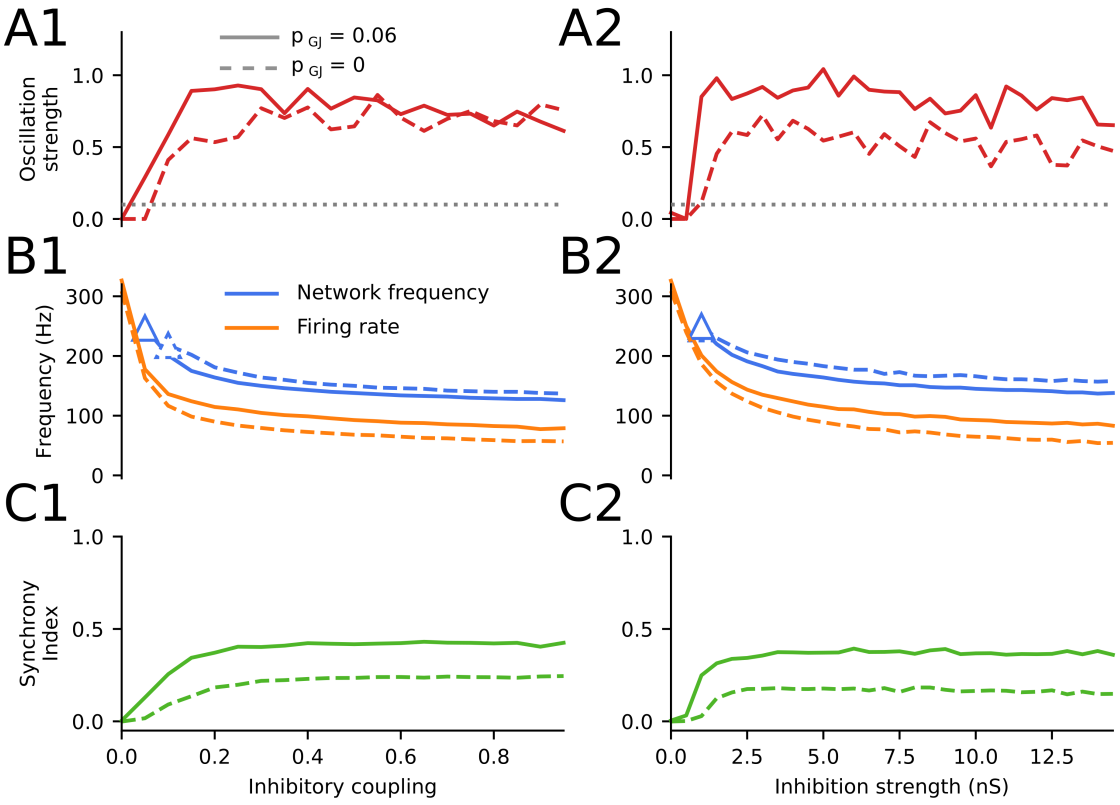

Figure S5: Influence of inhibition on the network dynamics. **A1**–**C1**, Variation of the inhibitory coupling probability. **A1**, Oscillation strength for varying values of the inhibitory coupling probability for GJ-network (solid line) and GJ-free network (dashed line). **B1**, Network frequency and firing rate. **C1**, Synchrony index. **A2**–**C2**, same as A1–C1 but for the strength of the peak inhibitory conductance (Eq. (1)). See Table 3.1 for parameters and Section 3.2 for the definitions of the network and the network measures.

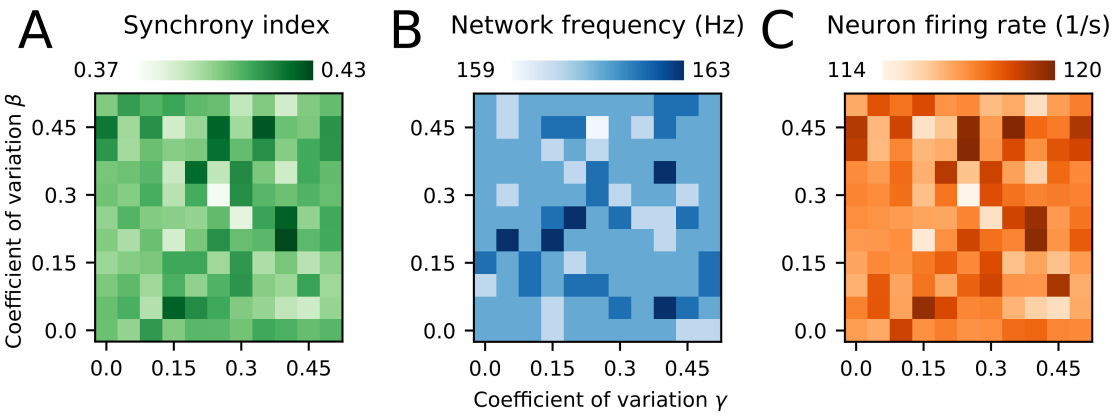

Figure S6: Heterogeneities of gap junction parameters do not influence network dynamics. Effect of heterogeneities of the two gap junction parameters, active-spike component β and passive ohmic conductance γ, on the synchrony index (**A**), network frequency (**B**), and neuron firing rate (**C**). See Table 3.1 for parameters and Section 3.2 for the definitions of the network and the network measures.

synchrony is low because the network is not in an oscillatory state. With increasing inhibitory coupling the synchrony index increases, and remains constant for a coupling $\gtrsim 0.2$. The synchrony in the GJ network is higher than in the GJ-free network.

Figure S5A2–C2 shows the same network measures as Fig. S5A1–C1 but for varying values of the inhibitory peak conductance (Eq. (1)). I find that all measures, i.e., the oscillation strength (Fig. S5A2), the firing rates and the network frequency (Fig. S5B2), and the synchrony index (Fig. S5C2) show a similar qualitative dependence on the strength of the inhibitory coupling as found for the coupling probability.

Together, this indicates that the network dynamics are not determined by the connection probability or the inhibitory conductances but by the total amount of inhibition. Moreover, I find that the synchrony index does not dependent strongly on the inhibition. Most importantly, the synchrony index is $\lesssim 0.25$, when there are no GJs in the network: gap junctions lead to an increase of neuronal synchrony in ripple oscillations generated by INT-INT networks that cannot be achieved by increasing recurrent inhibition.

5 Heterogeneities of gap junction parameters

In Chapter 3 (Fig. 3.3), we analyzed the influence of the GJ parameters on the network dynamics, i.e., the synchrony index, the network frequency and the firing rate. In these simulations all GJs in the network were modeled by identical parameters. However, in real neuronal tissue GJs are heterogeneous (Chapter 2).

In Fig. S6, I introduce heterogeneities to the GJ parameters (Eq. (3.1)). For this the GJ parameters, i.e., the active-spike component β and the passive ohmic conductance γ, are drawn from a Gaussian distribution whose coefficient of variation is varied between 0 and 0.5 of their respective standard values $\beta = 0.25\,\mathrm{mV}$ and $\gamma = 1.0\,\mathrm{nS}$ (Table 3.1).

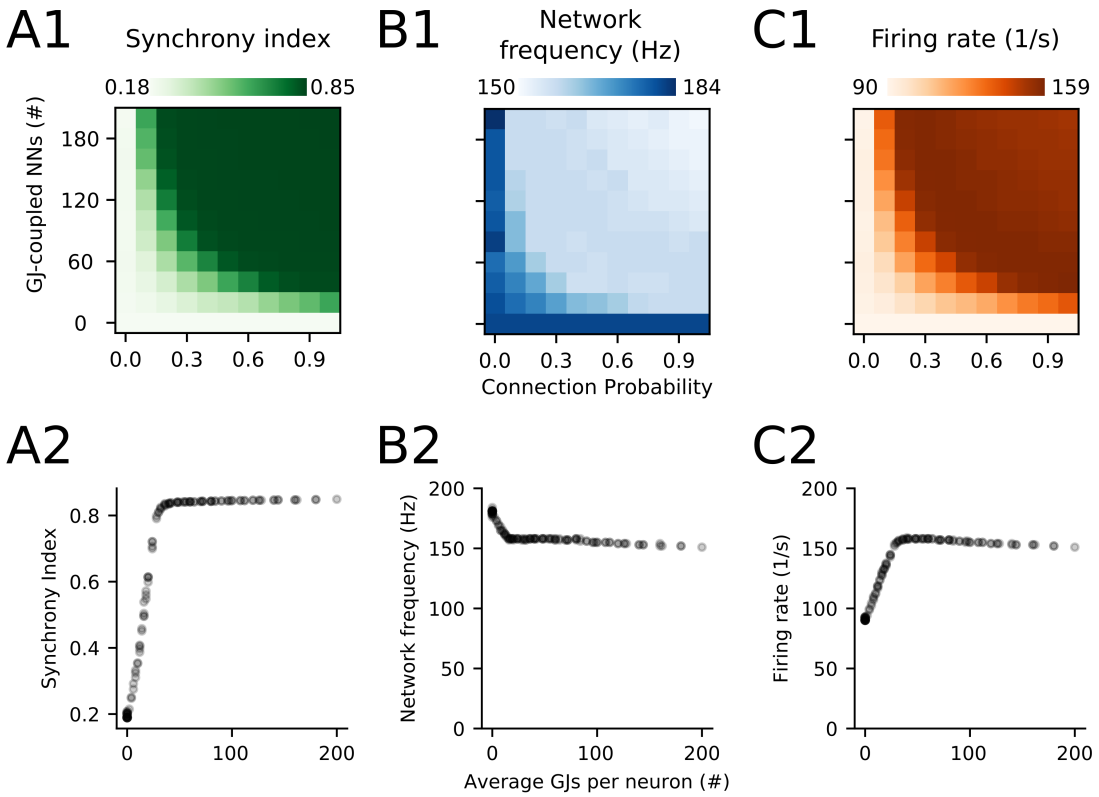

Figure S7: Influence of GJ-coupled nearest neighbors (NNs) and gap junction connectivity on the network dynamics. Synchrony index (**A1**), network frequency (**B1**), and firing rate (**C1**) as a function of GJ-coupled NNs and the GJ connection probability. **A2**–**C2**, Same as A1–C1, but for the average number of GJs per neuron, i.e., the product of the GJ-coupled NNs and the GJ-coupling probability. Each (semitransparent) point represents one square of the upper plots, respectively. See Table 3.1 for parameters and Section 3.2 for the definitions of the network and the network measures.

These simulations show that heterogeneities of β and γ do not influence the network dynamics, and hence justify the previous treatment.

6 Structure of gap junction connectivity

Only when dendritic trees overlap (dendritic) GJ coupling can only be established, and hence the coupling probability depends on the spatial proximity of neurons. This explains the experimental observation that the probability for GJ coupling is high when the somata of the neurons are within a sphere of $\approx 200\,\mu m$, and low outside of the sphere (Chapter 2.3.2, Table 2.1).

To incorporate these experimental results in our simulations, we introduced GJ coupling between 40 nearest neighbors in our network simulations (Fig. 3.1). In this section,

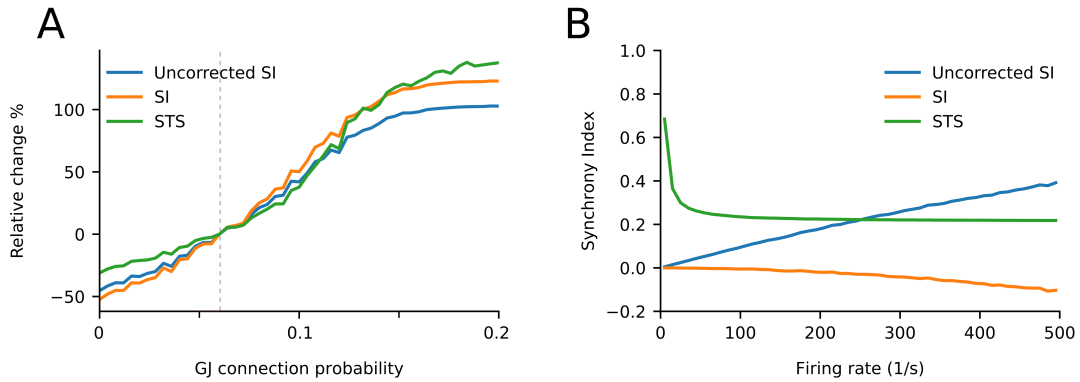

Figure S8: Different synchrony indices. **A**, Data from Fig. 3.3 for three different synchrony indices: the synchrony index (SI), the corrected synchrony index (Corr. SI), and spike train synchrony (STS) index defined by Brunel and Wang (2003). Depicted the relative change of the synchrony indices. **B**, Same as left but for random generated spike trains.

I analyze how a changing number of nearest neighbors that are coupled with GJs affects the network dynamics.

In Fig. S7A1-C1, I compute the synchrony index, oscillation frequency, and firing rate as a function of potentially GJ-coupled nearest neighbors (NNs) and gap junction coupling probability in the interneuronal network: I observe that these two parameters have the same effect on the network dynamics.

Consequently, I plot the same quantities over the average number of GJ-coupled neurons, i.e., the product of the GJ-coupled NNs and the GJ coupling probability (Fig. S72–C2). Since the resulting plots are seemingly surjective functions I conclude that all measures of the network dynamics are predominantly determined by the average number of coupled neurons, and not by the amount of GJ-coupled NN or the GJ-connection probability. Furthermore, these plots show that our previous analysis covers a lot of the variability observed in the network dynamics, by considering the range of 1–40 GJs per neuron (Chapter 3).

In conclusion, I find that the average number of coupled neurons is the relevant parameter that affects the observed global network measures. This justifies our previous analysis, in which we only varied the GJ connection probably and left the GJ nearest neighbor coupling constant (Fig. 3.3).

7 Comparison of different measures of synchrony

There have been many different measures proposed to measure synchrony of spike trains (for review see Kreuz et al., 2007). Here, I compare three of them:

1. The SPIKE-synchronization measure from Kreuz et al. (2007, 2015) with a fixed coincidence window $\tau = 0.5\,\text{ms}$ (for details see Section 3.2.5). In the latter, I refer to it as the (uncorrected) synchrony index (Uncorrected SI).

2. SPIKE-synchronization corrected by the current firing rate of the network to exclude firing that is synchronous by chance (for details see Section 3.2.5, Eq. (3.3)). In the latter, referred to as the synchrony index (SI). This is the synchrony measure that is used throughout this thesis.

3. The spike train synchrony (STS) index introduced by Brunel and Wang (2003). It is defined as the value at zero of the autocorrelation of the firing rates that is computed in 0.5 ms bins (originally 1 ms bins were used) and normalized by the square of the mean firing rate.

In Fig. S8, these three synchrony indices are compared for two different firing regimes: realistic oscillatory activity from the simulations depicted in Fig. 3.3 (Fig. S8A), and randomly generated spike trains (Fig. S8B).

In Fig. S8A, I find that the three different measures are behaving qualitatively similar for the oscillatory activity. To allow a direct comparison to Fig. 3.3, the synchrony indices are normalized by their respective value at GJ connection probability = 0.06 and their relative change is depicted.

In Fig. S8B, the synchrony indices are evaluated for randomly generated spike trains with increasing firing rates. Here, I depict the explicit values of the synchrony indices and not their relative changes. Note that the STS is normalized by the maximal value it takes in Fig. S8A (before the relative values are computed). In contrast to Fig. S8A, strong differences between the synchrony measures are evident. While the uncorrected SI is increasing with increasing firing rates from 0 to ≈ 0.4, the (corrected) SI stays relatively stable and slightly decreases from 0 to ≈ -0.1. The measure from Brunel and Wang (2003) remains relatively stable for increasing values of the firing rate except for a firing rate $\lesssim 30\,1/\mathrm{s}$.

To sum up, I find that the corrected synchrony index (SI) motivated by Kreuz et al. (2007) remains close to zero for random spike trains, does not depend strongly on the firing rate, and hence is a good measure to compute synchrony over a wide range of firing rates.

List of abbreviations

ACSF	Artificial cerebrospinal fluid
AP	Action potential
CA	Cornu ammonis (part of the hippocampus)
Cx36	Connexin36
Cx36KO mice	Cx36 knockout mice
DG	Denate gyrus
EC	Entorhinal cortex
EFP	Extracellular field potential
FWHM	Full width at half maximum
GJ	Gap junction
HC	Hippocampus
INT-INT	Interneuron-interneuron, which are recurrently coupled
KCl	Potassium chloride
LIF	Leaky integrate-and-fire (neuron)
PC	Pyramidal cell
PV+BC	Parvalbumin-positive basket cell
PV+	Parvalbumin-positive
SWR	Sharp wave-ripple

Bibliography

L. F. Abbott. Theoretical Neuroscience Rising. *Neuron*, 60:489–495, 2008.

P. Aivar, M. Valero, E. Bellistri, and L. Menendez de la Prida. Extracellular calcium controls the expression of two different forms of ripple-like hippocampal oscillations. *J. Neurosci.*, 34:2989–3004, 2014.

Y. Amitai, J. R. Gibson, M. Beierlein, S. L. Patrick, A. M. Ho, B. W. Connors, and D. Golomb. The spatial dimensions of electrically coupled networks of interneurons in the neocortex. *J. Neurosci.*, 22:4142–4152, 2002.

P. Andersen, R. Morris, D. Amaral, T. Bliss, and J. O'Keefe, editors. *The Hippocampus Book*. Oxford University Press, 2006.

F. Bahner, E. K. Weiss, G. Birke, N. Maier, D. Schmitz, U. Rudolph, M. Frotscher, R. D. Traub, M. Both, and A. Draguhn. Cellular correlate of assembly formation in oscillating hippocampal networks in vitro. *Proc. Natl. Acad. Sci. U.S.A.*, 108:E607–E616, 2011.

M. Bartos, I. Vida, M. Frotscher, J. R. Geiger, and P. Jonas. Rapid signaling at inhibitory synapses in a dentate gyrus interneuron network. *J. Neurosci.*, 21:2687–2698, 2001.

M. Bartos, I. Vida, M. Frotscher, A. Meyer, H. Monyer, J. R. P. Geiger, and P. Jonas. Fast synaptic inhibition promotes synchronized gamma oscillations in hippocampal interneuron networks. *Proc. Natl. Acad. Sci. U.S.A.*, 99:13222–13227, 2002.

M. Bartos, I. Vida, and P. Jonas. Synaptic mechanisms of synchronized gamma oscillations in inhibitory interneuron networks. *Nat. Rev. Neurosci.*, 8:45–56, 2007.

M. Bear, B. Connors, and M. Paradiso. *Neuroscience: Exploring the Brain*. Lippincott Williams & Wilkins, 2007.

C. J. Behrens, R. Ul Haq, A. Liotta, M. L. Anderson, and U. Heinemann. Nonspecific effects of the gap junction blocker mefloquine on fast hippocampal network oscillations in the adult rat in vitro. *Neuroscience*, 192:11–19, 2011.

A. B. Belousov and J. D. Fontes. Neuronal gap junctions: Making and breaking connections during development and injury. *Trends Neurosci.*, 36:227–236, 2013.

T. Bem and J. Rinzel. Short duty cycle destabilizes a half-center oscillator, but gap junctions can restabilize the anti-phase pattern. *J. Neurophysiol.*, 91:693–703, 2004.

M. V. L. Bennett. Gap junctions and electrical synapses. *Encyclopedia of Neuroscience*, 366:529–548, 1997.

M. V. L. Bennett and R. S. Zukin. Electrical coupling and neuronal synchronization in the mammalian brain. *Neuron*, 41:495–511, 2004.

M. J. Bezaire and I. Soltesz. Quantitative assessment of CA1 local circuits: Knowledge base for interneuron-pyramidal cell connectivity. *Hippocampus*, 23:751–785, 2013.

N. Brunel. Dynamics of sparsely connected networks of excitatory and inhibitory spiking neurons. *J. Comput. Neurosci.*, 8:183–208, 2000.

N. Brunel and X. J. Wang. What determines the frequency of fast network oscillations with irregular neural discharges? I. Synaptic dynamics and excitation-inhibition balance. *J. Neurophysiol.*, 90:415–430, 2003.

L. Buñuel. *My Last Breath.* Fontana Paperbacks, 1987.

D. L. Buhl, K. D. Harris, S. G. Hormuzdi, H. Monyer, and G. Buzsáki. Selective impairment of hippocampal gamma oscillations in connexin-36 knock-out mouse in vivo. *J. Neurosci.*, 23:1013–1018, 2003.

E. H. Buhl, S. R. Cobb, K. Halasy, and P. Somogyi. Properties of unitary IPSPs evoked by anatomically identified basket cells in the rat hippocampus. *Eur. J. Neurosci.*, 7: 1989–2004, 1995.

E. H. Buhl, T. Szilágyi, K. Halasy, and P. Somogyi. Physiological properties of anatomically identified basket and bistratified cells in the CA1 area of the rat hippocampus in vitro. *Hippocampus*, 6:294–305, 1996.

G. Buzsáki. Hippocampal sharp waves: Their origin and significance. *Brain Res.*, 398: 242–252, 1986.

G. Buzsáki. Two-stage model of memory trace formation: a role for "noisy" brain states. *Neuroscience*, 31:551–570, 1989.

G. Buzsáki. Hippocampal sharp wave-ripple: A cognitive biomarker for episodic memory and planning. *Hippocampus*, 1188, 2015.

G. Buzsáki and X.-J. Wang. Mechanisms of gamma oscillations. *Annu. Rev. Neurosci.*, 35:203–25, 2012.

G. Buzsáki, Z. Horvath, R. Urioste, J. Hetke, and K. Wise. High-frequency network oscillation in the hippocampus. *Science*, 256:1025–1027, 1992.

G. Buzsáki, C. A. Anastassiou, and C. Koch. The origin of extracellular fields and currents – EEG, ECoG, LFP and spikes. *Nat. Rev. Neurosci.*, 13:407–420, 2012.

G. Buzsáki, N. Logothetis, and W. Singer. Scaling brain size, keeping timing: Evolutionary preservation of brain rhythms. *Neuron*, 80:751–764, 2013.

P. L. Carlen, F. Skinner, L. Zhang, C. Naus, M. Kushnir, and J. L. Perez Velazquez. The role of gap junctions in seizures. *Brain Res. Rev.*, 32:235–241, 2000.

M. S. Cembrowski, J. L. Bachman, L. Wang, K. Sugino, B. C. Shields, and N. Spruston. Spatial Gene-Expression Gradients Underlie Prominent Heterogeneity of CA1 Pyramidal Neurons. *Neuron*, 89:351–368, 2016.

S. Chamberland and L. Topolnik. Inhibitory control of hippocampal inhibitory neurons. *Frontiers in Neuroscience*, 6:1–13, 2012.

B. Chiovini, G. F. Turi, G. Katona, A. Kaszás, D. Pálfi, P. Maák, G. Szalay, M. F. Szabó, G. Szabó, Z. Szadai, S. Káli, and B. Rózsa. Dendritic spikes induce ripples in parvalbumin interneurons during hippocampal sharp waves. *Neuron*, 82:908–924, 2014.

L. L. Colgin. Rhythms of the hippocampal network. *Nat. Rev. Neurosci.*, 17:239–249, 2016.

D. F. Condorelli, N. Belluardo, A. Trovato-Salinaro, and G. Mudò. Expression of Cx36 in mammalian neurons. *Brain Res. Rev.*, 32:72–85, 2000.

B. W. Connors and M. A. Long. Electrical synapses in the mammalian brain. *Annu. Rev. Neurosci.*, 27:393–418, 2004.

P. Coulon and C. E. Landisman. The potential role of gap junctional plasticity in the regulation of state. *Neuron*, 93:1275–1295, 2017.

S. J. Cruikshank, M. Hopperstad, M. Younger, B. W. Connors, D. C. Spray, and M. Srinivas. Potent block of Cx36 and Cx50 gap junction channels by mefloquine. *Proc. Natl. Acad. Sci. U.S.A.*, 101:12364–12369, 2004.

J. Csicsvari, H. Hirase, a. Czurkó, a. Mamiya, and G. Buzsáki. Fast network oscillations in the hippocampal CA1 region of the behaving rat. *J. Neurosci.*, 19:RC20, 1999a.

J. Csicsvari, H. Hirase, a. Czurkó, a. Mamiya, and G. Buzsáki. Oscillatory coupling of hippocampal pyramidal cells and interneurons in the behaving Rat. *J. Neurosci.*, 19: 274–287, 1999b.

J. Csicsvari, H. Hirase, A. Mamiya, and G. Buzsáki. Ensemble patterns of hippocampal CA3-CA1 neurons during sharp wave–associated population events. *Neuron*, 28:585–594, 2000.

H. Dale. The occurrence in ergot and action of acetylcholine. *J. Physiol. (Lond.)*, 48:3, 1914.

H. Dale and O. Loewi. The Nobel Prize in Physiology or Medicine 1936. Nobelprize.org, 1936.

M. D'Antuono, P. De Guzman, T. Kano, and M. Avoli. Ripple activity in the dentate gyrus of dishinibited hippocampus-entorhinal cortex slices. *J. Neurosci. Res.*, 80:92–103, 2005.

P. Dayan and L. Abbott. *Theoretical Neuroscience: Computational And Mathematical Modeling of Neural Systems*. Computational Neuroscience. Massachusetts Institute of Technology Press, 2005.

J. Defelipe, P. L. López-Cruz, R. Benavides-Piccione, C. Bielza, P. Larrañaga, S. Anderson, A. Burkhalter, B. Cauli, A. Fairén, D. Feldmeyer, G. Fishell, D. Fitzpatrick, T. F. Freund, G. González-Burgos, S. Hestrin, S. Hill, P. R. Hof, J. Huang, E. G. Jones, Y. Kawaguchi, Z. Kisvárday, Y. Kubota, D. A. Lewis, O. Marín, H. Markram, C. J. McBain, H. S. Meyer, H. Monyer, S. B. Nelson, K. Rockland, J. Rossier, J. L. Rubenstein, B. Rudy, M. Scanziani, G. M. Shepherd, C. C. Sherwood, J. F. Staiger, G. Tamás, A. Thomson, Y. Weng, R. Yuste, and G. A. Ascoli. New insights into the classification and nomenclature of cortical GABAergic interneurons. *Nat. Rev. Neurosci.*, 14:202–216, 2013.

R. Dermietzel and D. C. Spray. Gap junctions in the brain: where, what type, how many and why? *Trends Neurosci.*, 16:186–192, 1993.

K. Diba and G. Buzsáki. Forward and reverse hippocampal place-cell sequences during ripples. *Nat. Neurosci.*, 10:1241–2, 2007.

S. Diekelmann and J. Born. The memory function of sleep. *Nat. Rev. Neurosci.*, 11: 114–126, 2010.

J. R. Donoso, D. Schmitz, N. Maier, and R. Kempter. Hippocampal ripple oscillations and inhibition-first network models: Frequency dynamics and response to GABA modulators. *J. Neurosci.*, 12:0188–17, 2018.

K. A. Dougherty, T. Islam, and D. Johnston. Intrinsic excitability of CA1 pyramidal neurones from the rat dorsal and ventral hippocampus. *J. Physiol. (Lond.)*, 590:5707–5722, 2012.

A. Draguhn, R. D. Traub, D. Schmitz, and J. G. Jefferys. Electrical coupling underlies high-frequency oscillations in the hippocampus in vitro. *Nature*, 394:189–192, 1998.

Y. Dudai, A. Karni, and J. Born. The consolidation and transformation of memory. *Neuron*, 88:20–32, 2015.

V. Ego-Stengel and M. A. Wilson. Disruption of ripple-associated hippocampal activity during rest impairs spatial learning in the rat. *Hippocampus*, 20:1–10, 2010.

H. Eichenbaum. Time cells in the hippocampus: A new dimension for mapping memories. *Nat. Rev. Neurosci.*, 15:732–744, 2014.

D. F. English, A. Peyrache, E. Stark, L. Roux, D. Vallentin, M. A. Long, and G. Buzsáki. Excitation and inhibition compete to control spiking during hippocampal ripples: intracellular study in behaving mice. *J. Neurosci.*, 34:16509–16517, 2014.

C. G. Fink, S. Gliske, N. Catoni, and W. C. Stacey. Network mechanisms generating abnormal and normal hippocampal High Frequency Oscillations: A computational analysis. *eNeuro*, 2:0024–15.2015, 2015.

D. J. Foster and M. A. Wilson. Reverse replay of behavioural sequences in hippocampal place cells during the awake state. *Nature*, 440:680–683, 2006.

F. Fröhlich, M. Bazhenov, V. Iragui-Madoz, and T. J. Sejnowski. Potassium dynamics in the epileptic cortex: new insights on an old topic. *Neuroscientist*, 14:422–433, 2008.

T. Fukuda and T. Kosaka. The dual network of GABAergic interneurons linked by both chemical and electrical synapses: A possible infrastructure of the cerebral cortex. *Neurosci. Res.*, 38:123–130, 2000a.

T. Fukuda and T. Kosaka. Gap junctions linking the dendritic network of GABAergic interneurons in the hippocampus. *J. Neurosci.*, 20:1519–1528, 2000b.

T. Fukuda and T. Kosaka. Ultrastructural study of gap junctions between dendrites of parvalbumin-containing GABAergic neurons in various neocortical areas of the adult rat. *Neuroscience*, 120:5–20, 2003.

T. Fukuda, T. Kosaka, W. Singer, and R. A. W. Galuske. Gap junctions among dendrites of cortical GABAergic neurons establish a dense and widespread intercolumnar network. *J. Neurosci.*, 26:3434–43, 2006.

E. Furshpan and D. Potter. Transmission at the giant motor synapses of the crayfish. *J. Physiol. (Lond.)*, 145:289–325, 1959.

M. Galarreta and S. Hestrin. A network of fast-spiking cells in the neocortex connected by electrical synapses. *Nature*, 402:72–75, 1999.

M. Galarreta and S. Hestrin. Electrical synapses between GABA-releasing interneurons. *Nat. Rev. Neurosci.*, 2:425–433, 2001a.

M. Galarreta and S. Hestrin. Spike transmission and synchrony detection in networks of GABAergic interneurons. *Science*, 292:2295–2299, 2001b.

J. Gan, S.-m. Weng, A. J. Pernía-Andrade, J. Csicsvari, and P. Jonas. Phase-locked inhibition, but not excitation, underlies hippocampal ripple oscillations in awake mice in vivo. *Neuron*, 93:308–314, 2017.

J. R. Gibson, M. Beierlein, and B. W. Connors. Two networks of electrically coupled inhibitory neurons in neocortex. *Nature*, 402:75–79, 1999.

G. Girardeau, K. Benchenane, S. I. Wiener, G. Buzsáki, and M. Zugaro. Selective suppression of hippocampal ripples impairs spatial memory. *Nat. Neurosci.*, 12:1222–1223, 2009.

C. Golgi. Nobel Lecture: The neuron doctrine – theory and facts. Nobel Lecture, 1906.

D. Goodman and R. Brette. Brian: a simulator for spiking neural networks in python. *Front. Neuroinf.*, 2:5, 2008.

F. M. Gribble, T. M. E. Davis, C. E. Higham, A. Clark, and F. M. Ashcroft. The antimalarial agent mefloquine inhibits ATP-sensitive K-channels. *Br. J. Pharmacol.*, 131:756–760, 2000.

M. Güldenagel, J. Ammermüller, A. Feigenspan, B. Teubner, J. Degen, G. Söhl, K. Willecke, and R. Weiler. Visual transmission deficits in mice with targeted disruption of the gap junction gene connexin36. *J. Neurosci.*, 21:6036–44, 2001.

D. Guo, Q. Wang, and M. Perc. Complex synchronous behavior in interneuronal networks with delayed inhibitory and fast electrical synapses. *Phys. Rev. E*, 85:1–8, 2012.

A. S. Gupta, M. A. van der Meer, D. S. Touretzky, and A. D. Redish. Hippocampal replay is not a simple function of experience. *Neuron*, 65:695–705, 2010.

J. S. Haas, B. Zavala, and C. E. Landisman. Activity-dependent long-term depression of electrical synapses. *Science*, 334:389–393, 2011.

T. Hafting, M. Fyhn, S. Molden, M. B. Moser, and E. I. Moser. Microstructure of a spatial map in the entorhinal cortex. *Nature*, 436:801–806, 2005.

F. Hamzei-Sichani, N. Kamasawa, W. G. M. Janssen, T. Yasumura, K. G. V. Davidson, P. R. Hof, S. L. Wearne, M. G. Stewart, S. R. Young, M. A. Whittington, J. E. Rash, and R. D. Traub. Gap junctions on hippocampal mossy fiber axons demonstrated by thin-section electron microscopy and freeze fracture replica immunogold labeling. *Proc. Natl. Acad. Sci. U.S.A.*, 104:12548–12553, 2007.

R. J. Hatch, G. D. C. Mendis, K. Kaila, C. A. Reid, and S. Petrou. Gap junctions rink regular-spiking and fast-spiking interneurons in layer 5 somatosensory cortex. *Front. Cell. Neurosci.*, 11:204, jul 2017.

U. Heinemann and H. Lux. Ceiling of stimulus induced rises in extracellular potassium concentration in the cerebral cortex of cat. *Brain Res.*, 120:231–249, 1977.

C. Hinrichsen. Coupling between cells of the trigeminal mesencephalic nucleus. *J. Dent. Res.*, 49:1369–1373, 1970.

A. Holzbecher and R. Kempter. Interneuronal gap junctions increase synchrony and robustness of hippocampal ripple oscillations. *bioRxiv, https://doi.org/10.1101/311662*, 2018.

S. G. Hormuzdi, I. Pais, F. E. N. LeBeau, S. K. Towers, A. Rozov, E. H. Buhl, M. A. Whittington, and H. Monyer. Impaired electrical signaling disrupts gamma frequency oscillations in connexin 36-deficient mice. *Neuron*, 31:487–495, 2001.

B. K. Hulse, L. C. Moreaux, E. V. Lubenov, A. G. Siapas Correspondence, and A. G. Siapas. Membrane potential dynamics of CA1 pyramidal neurons during hippocampal ripples in awake mice. *Neuron*, 89:800–813, 2016.

S. P. Jadhav, C. Kemere, P. W. German, and L. M. Frank. Awake hippocampal sharp-wave ripples support spatial memory. *Science*, 336:1454–1458, 2012.

S. Jahnke, M. Timme, and R.-M. Memmesheimer. A unified dynamic model for learning, replay, and sharp-wave/ripples. *J. Neurosci.*, 35(49):16236–16258, 2015.

J. Johnston, I. D. Forsythe, and C. Kopp-Scheinpflug. Going native: Voltage-gated potassium channels controlling neuronal excitability. *J. Physiol. (Lond.)*, 588:3187–3200, 2010.

E. Jones, T. Oliphant, P. Peterson, et al. SciPy: Open source scientific tools for Python, 2001–. [Online; accessed 22.03.2018].

M. Jouvet, F. Michel, and J. Courjon. Láctivite electrique du rhinencephale au cours du sommeil chez le chat. *C.R. Soc. Biol. (Paris)*, 153:101–105, 1959.

G. R. Juszczak and A. H. Swiergiel. Properties of gap junction blockers and their behavioural, cognitive and electrophysiological effects: Animal and human studies. *Prog. Neuropsychopharmacol. Biol. Psychiatry*, 33:181–198, 2009.

H. Katsumaru, T. Kosaka, C. Heizmann, and K. Hama. Gap junctions on GABAergic neurons containing the calcium-binding protein parvalbumin in the rat hippocampus (CA1 region). *Exp. Brain Res.*, 72:363–370, 1988a.

H. Katsumaru, T. Kosaka, C. W. Heizmann, and K. Hama. Immunocytochemical study of GABAergic neurons containing the calcium-binding protein parvalbumin in the rat hippocampus. *Exp. Brain Res.*, 72:347–362, 1988b.

T. B. Kepler, E. Marder, and L. F. Abbott. The effect of electrical coupling. *Science*, 248:83–85, 1990.

D. Khodagholy, J. N. Gelinas, and G. Buzsáki. Learning-enhanced coupling between ripple oscillations in association cortices and hippocampus. *Science*, 358:369–372, oct 2017.

T. Klausberger and P. Somogyi. Neuronal diversity and temporal dynamics: the unity of hippocampal circuit operations. *Science*, 321:53–7, 2008.

T. Klausberger, P. J. Magill, L. F. Márton, J. D. B. Roberts, P. M. Cobden, G. Buzsáki, and P. Somogyi. Brain-state-and cell-type-specific firing of hippocampal interneurons in vivo. *Nature*, 421:844–848, 2003.

T. Klausberger, L. F. Márton, A. Baude, J. D. B. Roberts, P. J. Magill, and P. Somogyi. Spike timing of dendrite-targeting bistratified cells during hippocampal network oscillations in vivo. *Nat. Neurosci.*, 7:41–47, 2004.

T. Klausberger, L. F. Marton, J. O'Neill, J. H. J. Huck, Y. Dalezios, P. Fuentealba, W. Y. Suen, E. Papp, T. Kaneko, M. Watanabe, J. Csicsvari, and P. Somogyi. Complementary roles of cholecystokinin- and parvalbumin-expressing GABAergic neurons in hippocampal network oscillations. *J. Neurosci.*, 25:9782–9793, 2005.

Z. Kohus, S. Káli, L. Rovira, D. Schlingloff, O. Papp, T. F. Freund, N. Hájos, and A. I. Gulyás. Properties and dynamics of inhibitory synaptic communication within the CA3 microcircuits of pyramidal cells and interneurons expressing parvalbumin or cholecystokinin. *J. Physiol. (Lond.)*, 82:1496–1514, 2016.

J. Konopacki, R. Bocian, T. Kowalczyk, and P. Kazmierska. Chapter 7 - Involvement of gap junctions in the generation of the hippocampal formation theta rhythm in rats. In E. Dere, editor, *Gap Junctions in the Brain*, pages 101 – 125. Academic Press, San Diego, 2013.

N. Kopell and B. Ermentrout. Chemical and electrical synapses perform complementary roles in the synchronization of interneuronal networks. *Proc. Natl. Acad. Sci. U.S.A.*, 101:15482–15487, 2004.

T. Kosaka. Gap junctions between non-pyramidal cell dendrites in the rat hippocampus (CA1 and CA3 regions). *Brain Res.*, 271:157–161, 1983.

T. Kosaka and K. Hama. Gap junctions betwen non-pyramidal cell dendrites in the rat hippocampus (CA1 and CA3 regions): A combined Golgi- electron microscopy study. *J. Comp. Neurol.*, 231:150–161, 1985.

T. Kreuz, J. S. Haas, A. Morelli, H. D. I. Abarbanel, and A. Politi. Measuring spike train synchrony. *J. Neurosci. Methods*, 165:151–161, 2007.

T. Kreuz, M. Mulansky, and N. Bozanic. SPIKY: a graphical user interface for monitoring spike train synchrony. *J. Neurophysiol.*, 113:3432–3445, 2015.

A. Kumar. Long-term potentiation at CA3-CA1 hippocampal synapses with special emphasis on aging, disease, and stress. *Front. Aging Neurosci.*, 3:1–20, 2011.

F. E. LeBeau, R. D. Traub, H. Monyer, M. A. Whittington, and E. H. Buhl. The role of electrical signaling via gap junctions in the generation of fast network oscillations. *Brain Res. Bull.*, 62:3–13, 2003.

A. K. Lee and M. A. Wilson. Memory of sequential experience in the hippocampus during slow wave sleep. *Neuron*, 36:1183–1194, 2002.

S. H. Lee, I. Marchionni, M. Bezaire, C. Varga, N. Danielson, M. Lovett-Barron, A. Losonczy, and I. Soltesz. Parvalbumin-positive basket cells differentiate among hippocampal pyramidal cells. *Neuron*, 82:1129–1144, 2014.

B. Leuner and E. Gould. Structural Plasticity and Hippocampal Function. *Annu. Rev. Psychol.*, 61:111–140, 2010.

T. J. Lewis and J. Rinzel. Dynamics of spiking neurons connected by both inhibitory and electrical coupling. *J. Comput. Neurosci.*, 14:283–309, 2003.

O. Loewi. Über humorale Übertragbarkeit der Herznervenwirkung. *Pflüger's Archiv für die gesamte Physiologie des Menschen und der Tiere*, 189:239–242, 1921.

R. Maex and E. De Schutter. Resonant synchronization in heterogeneous networks of inhibitory neurons. *J. Neurosci.*, 23:10503–10514, 2003.

N. Maier and R. Kempter. *Cognitive neuroscience of memory consolidation*, chapter Hippocampal sharp wave/ripple complexes–physiology and mechanisms, pages 227–249. Studies in Neuroscience, Psychology and Behavioral Economics. Springer International Publishing, Cham, 2017.

N. Maier, M. Güldenagel, G. Söhl, H. Siegmund, K. Willecke, and A. Draguhn. Reduction of high-frequency network oscillations (ripples) and pathological network discharges in hippocampal slices from connexin 36-deficient mice. *J. Physiol. (Lond.)*, 541:521–528, 2002.

N. Maier, V. Nimmrich, and A. Draguhn. Cellular and network mechanisms underlying spontaneous sharp wave–ripple complexes in mouse hippocampal slices. *J. Physiol. (Lond.)*, 550:873–887, 2003.

N. Maier, Á. Tejero-Cantero, A. L. Dorrn, J. Winterer, P. S. Beed, G. Morris, R. Kempter, J. F. A. Poulet, C. Leibold, and D. Schmitz. Coherent phasic excitation during hippocampal ripples. *Neuron*, 72:137–152, 2011.

N. Maier, G. Morris, S. Schuchmann, T. Korotkova, A. Ponomarenko, C. Böhm, C. Wozny, and D. Schmitz. Cannabinoids disrupt hippocampal sharp wave-ripples via inhibition of glutamate release. *Hippocampus*, 22:1350–1362, 2012.

N. Maier, A. Draguhn, D. Schmitz, and M. Both. Fast network oscillations in the hippocampus. *e-Neuroforum*, 4:1–10, 2013.

N. Maingret, G. Girardeau, R. Todorova, M. Goutierre, and M. Zugaro. Hippocampo-cortical coupling mediates memory consolidation during sleep. *Nat. Neurosci.*, 19: 959–964, 2016.

C. J. McBain and A. Fisahn. Interneurons unbound. *Nat. Rev. Neurosci.*, 2:11–23, 2001.

R. A. McDougal, T. M. Morse, T. Carnevale, L. Marenco, R. Wang, M. Migliore, P. L. Miller, G. M. Shepherd, and M. L. Hines. Twenty years of ModelDB and beyond: building essential modeling tools for the future of neuroscience. *J. Comput. Neurosci.*, 42:1–10, 2017.

E. C. McKiernan and D. F. Marrone. CA1 pyramidal cells have diverse biophysical properties, affected by development, experience, and aging. *PeerJ*, 5:e3836, 2017.

R. M. Memmesheimer. Quantitative prediction of intermittent high-frequency oscillations in neural networks with supralinear dendritic interactions. *Proc. Natl. Acad. Sci. U.S.A.*, 107:11092–11097, 2010.

A. Mercer, A. P. Bannister, and A. M. Thomson. Electrical coupling between pyramidal cells in adult cortical regions. *Brain Cell Biol.*, 35:13–27, 2006.

A. H. Meyer, I. Katona, M. Blatow, A. Rozov, and H. Monyer. In vivo labeling of parvalbumin-positive interneurons and analysis of electrical coupling in identified neurons. *J. Neurosci.*, 22:7055–7064, 2002.

R. Meyer and K. Obermayer. pypet: A python toolkit for data management of parameter explorations. *Frontiers in Neuroinformatics*, 10:38, 2016.

S. Mikula, I. Trotts, J. M. Stone, and E. G. Jones. Internet-enabled high-resolution brain mapping and virtual microscopy. *Neuroimage*, 35:9–15, 2007.

B. Milner, L. R. Squire, and E. R. Kandel. Cognitive neuroscience review and the study of memory. *Neuron*, 20:445–468, 1998.

R. J. Montoro and R. Yuste. Gap junctions in developing neocortex: A review. *Brain Res. Rev.*, 47:216–226, 2004.

M. Moscovitch, R. Cabeza, G. Winocur, and L. Nadel. Episodic memory and beyond: the hippocampus and neocortex in transformation. *Annu. Rev. Psychol.*, 67:105–134, 2016.

J. I. Nagy. Evidence for connexin36 localization at hippocampal mossy fiber terminals suggesting mixed chemical/electrical transmission by granule cells. *Brain Res.*, 1487: 107–122, 2012.

V. Nimmrich, N. Maier, D. Schmitz, and A. Draguhn. Induced sharp wave-ripple complexes in the absence of synaptic inhibition in mouse hippocampal slices. *J. Physiol. (Lond.)*, 563:663–70, 2005.

J. O'Keefe. Place units in the hippocampus of the freely moving rat. *Exp. Neurol.*, 51: 78–109, 1976.

J. O'Keefe and J. Dostrovsky. The hippocampus as a spatial map. Preliminary evidence from unit activity in the freely-moving rat. *Brain Res.*, 34:171–175, 1971.

J. O'Keefe and L. Nadel. *The hippocampus as a cognitive map*. Clarendon Press Oxford, 1978.

J. O'Keefe, M.-B. Moser, and E. I. Moser. The Nobel Prize in Physiology or Medicine 2014. Nobelprize.org, 2014.

S. Ostojic, N. Brunel, and V. Hakim. Synchronization properties of networks of electrically coupled neurons in the presence of noise and heterogeneities. *J. Comput. Neurosci.*, 26:369–392, 2009.

I. Pais, S. G. Hormuzdi, H. Monyer, R. D. Traub, I. C. Wood, E. H. Buhl, M. A. Whittington, and F. E. N. LeBeau. Sharp wave-like activity in the hippocampus in vitro in mice lacking the gap junction protein connexin 36. *J. Neurophysiol.*, 89:2046–2054, 2003.

G. Palade and S. Palay. Electron microscope observations of interneuronal and neuromuscular synapses. *Anatomical Record*, 118:335–336, 1954.

A. E. Pereda. Electrical synapses and their functional interactions with chemical synapses. *Nat. Rev. Neurosci.*, 15:250–263, 2014.

J. L. Perez-Velazquez, T. A. Valiante, and P. L. Carlen. Modulation of gap junctional mechanisms during calcium-free induced field burst activity: a possible role for electrotonic coupling in epileptogenesis. *J. Neurosci.*, 14:4308–4317, 1994.

B. Pfeuty, G. Mato, D. Golomb, and D. Hansel. The combined effects of inhibitory and electrical synapses in synchrony. *Neural Comput.*, 17:633–670, 2005.

A. A. Ponomarenko, T. M. Korotkova, O. A. Sergeeva, and H. L. Haas. Multiple GABAA receptor subtypes regulate hippocampal ripple oscillations. *Eur. J. Neurosci.*, 20:2141–2148, 2004.

A. Posłuszny. The contribution of electrical synapses to field potential oscillations in the hippocampal formation. *Front. Neural Circuits*, 8:32, 2014.

R. Quian Quiroga. Declarative Memory Functions. *Nature*, 13:587–597, 2012.

R. Quian Quiroga, T. Kreuz, and P. Grassberger. Event synchronization: A simple and fast method to measure synchronicity and time delay patterns. *Phys. Rev. E*, 66: 041904, Oct 2002.

R. Quian Quiroga, L. Reddy, G. Kreiman, C. Koch, and I. Fried. Invariant visual representation by single neurons in the human brain. *Nature*, 435:1102–1107, 2005.

S. Ramón y Cajal. *Histologie du systeme nerveux de lh́omme & des vertebres*, volume Vols. 1 and 2. 1911.

B. Rasch and J. Born. About sleep's role in memory. *Physiol. Rev.*, 93:681–766, 2013.

J. E. Rash, H. S. Duffy, F. E. Dudek, B. L. Bilhartz, L. R. Whalen, and T. Yasumura. Grid-mapped freeze-fracture analysis of gap junctions in gray and white matter of adult rat central nervous system, with evidence for a panglial syncytium that is not coupled to neurons. *J. Comp. Neurol.*, 388:265–292, 1997.

H. G. Rey, C. Pedreira, and R. Quian Quiroga. Past, present and future of spike sorting techniques. *Brain Res. Bull.*, 119:106–117, 2015.

E. Rolls. *The handbook of multisensory processes*, chapter Multimodal neuronal convergence of taste, somatosensory, visual, olfactory and auditory inputs. Ch. 19. The MIT Press, 2004.

F. Saraga, L. Ng, and F. K. Skinner. Distal gap junctions and active dendrites can tune network dynamics. *J. Neurophysiol.*, 95:1669–1682, 2006.

A. Saudargiene, S. Cobb, and B. P. Graham. A computational study on plasticity during theta cycles at Schaffer collateral synapses on CA1 pyramidal cells in the hippocampus. *Hippocampus*, 25:208–218, 2015.

D. Schlingloff, S. Káli, T. F. Freund, N. Hájos, and A. I. Gulyás. Mechanisms of sharp wave initiation and ripple generation. *J. Neurosci.*, 34:11385–11398, 2014.

H. Schmalbruch and H. Jahnsen. Gap junctions on CA3 pyramidal cells of guinea pig hippocampus shown by freeze-fracture. *Brain Res.*, 217:175–8, 1981.

W. B. Scoville. The limbic lobe in man. *J. Neurosurg.*, 11:64–66, 1954.

W. B. Scoville and B. Milner. Loss of recent memory after bilateral hippocampal lesions. *J. Neurol. Neurosurg. Psychiatry*, 20:11, 1957.

J. Sevetson and J. S. Haas. Asymmetry and modulation of spike timing in electrically coupled neurons. *J. Neurophysiol.*, 113:1743–1751, 2014.

K. Shimizu and M. Stopfer. Gap junctions. *Curr. Biol.*, 23:R1026–31, dec 2013.

A. Sik, M. Penttonen, A. Ylinen, and G. Buzsáki. Hippocampal CA1 interneurons: an in vivo intracellular labeling study. *J. Neurosci.*, 15:6651–6665, 1995.

T. A. Simeone, K. A. Simeone, K. K. Samson, D. Y. Kim, and J. M. Rho. Loss of the Kv1.1 potassium channel promotes pathologic sharp waves and high frequency oscillations in in vitro hippocampal slices. *Neurobiol. Dis.*, 54:68–81, 2013.

M. Snipas, L. Rimkute, T. Kraujalis, K. Maciunas, F. F. Bukauskas, and M. Hayward. Functional asymmetry and plasticity of electrical synapses interconnecting neurons through a 36-state model of gap junction channel gating. *PLoS Comput. Biol.*, 13: e1005464, 2017.

I. Soltesz and A. Losonczy. CA1 pyramidal cell diversity enabling parallel information processing in the hippocampus. *Nat. Neurosci.*, 21:484, 2018.

G. Somjen. Extracellular potassium in the mammalian central nervous system. *Ann. Rev. Physiol.*, 41:159–177, 1979.

G. G. Somjen. Ion regulation in the brain: implications for pathophysiology. *Neuroscientist*, 8:254–267, 2002.

C. Sotelo and H. Korn. Morphological correlates of electrical and other interactions through low-resistance pathways between neurons of the vertebrate central nervous system. *Int. Rev. Cytol.*, 55:67–107, 1978.

L. Squire and S. Zola-Morgan. The medial temporal lobe memory system. *Science*, 253: 1380–1386, 1991.

M. Srinivas, R. Rozental, T. Kojima, R. Dermietzel, M. Mehler, D. F. Condorelli, J. A. Kessler, and D. C. Spray. Functional properties of channels formed by the neuronal gap junction protein connexin36. *J. Neurosci.*, 19:9848–55, 1999.

E. Stark, L. Roux, R. Eichler, Y. Senzai, S. Royer, and G. Buzsáki. Pyramidal cell-interneuron interactions underlie hippocampal ripple oscillations. *Neuron*, 83:467–480, 2014.

D. Sullivan, J. Csicsvari, K. Mizuseki, S. Montgomery, K. Diba, and G. Buzsáki. Relationships between hippocampal sharp waves, ripples, and fast gamma oscillation: influence of dentate and entorhinal cortical activity. *J. Neurosci.*, 31:8605–8616, 2011.

Y. Sun, H. Norimoto, X.-P. Pu, N. Matsuki, and Y. Ikegaya. Cannabinoid receptor activation disrupts the internal structure of hippocampal sharp wave-ripple complexes. *J. Pharmacol. Sci.*, 118:288–294, 2012.

L. Swanson, E. Newman, A. Araque, and J. Dubinsky. *The Beautiful Brain: The Drawings of Santiago Ramon y Cajal*. ABRAMS, 2017.

G. Tamás, E. H. Buhl, a. Lörincz, and P. Somogyi. Proximally targeted GABAergic synapses and gap junctions synchronize cortical interneurons. *Nat. Neurosci.*, 3:366–371, 2000.

J. Taxidis, S. Coombes, R. Mason, and M. R. Owen. Modeling sharp wave-ripple complexes through a CA3-CA1 network model with chemical synapses. *Hippocampus*, 22: 995–1017, 2012.

T. Tchumatchenko and C. Clopath. Oscillations emerging from noise-driven steady state in networks with electrical synapses and subthreshold resonance. *Nat. Commun.*, 5: 1–9, 2014.

The Nobel Prize. The Nobel Prize in Physiology or Medicine 1906. Nobelprize.org. Nobel Media AB 2014. `http://www.nobelprize.org/nobel_prizes/medicine/laureates/1906/`, 1906. Web. 20 Apr 2018.

The Nobel Prize. The Nobel Prize in Physiology or Medicine 1936. Nobelprize.org. Nobel Media AB 2014. `http://www.nobelprize.org/nobel_prizes/medicine/laureates/1936/`, 1936. Web. 20 Apr 2018.

The Nobel Prize. The Nobel Prize in Physiology or Medicine 2014. Nobelprize.org. Nobel Media AB 2014. `http://www.nobelprize.org/nobel_prizes/medicine/laureates/2014/`, 2014. Web. 20 Apr 2018.

K. R. Tovar, B. J. Maher, and G. L. Westbrook. Direct actions of carbenoxolone on synaptic transmission and neuronal membrane properties. *J. Neurophysiol.*, 102:974–978, 2009.

R. D. Traub, D. Schmitz, J. G. R. Jefferys, and A. Draguhn. High-frequency population oscillations are predicted to occur in hippocampal pyramidal neuronal networks interconnected by axoaxonal gap junctions. *Neuroscience*, 92:407–426, 1999.

R. D. Traub, A. Bibbig, A. Fisahn, F. E. LeBeau, M. A. Whittington, and E. H. Buhl. A model of gamma-frequency network oscillations induced in the rat CA3 region by carbachol in vitro. *Eur. J. Neurosci.*, 12:4093–4106, 2000.

R. D. Traub, N. Kopell, A. Bibbig, E. H. Buhl, F. E. LeBeau, and M. A. Whittington. Gap junctions between interneuron dendrites can enhance synchrony of gamma oscillations in distributed networks. *J. Neurosci.*, 21:9478–9486, 2001.

R. D. Traub, M. O. Cunningham, T. Gloveli, F. E. N. LeBeau, A. Bibbig, E. H. Buhl, and M. A. Whittington. GABA-enhanced collective behavior in neuronal axons underlies persistent gamma-frequency oscillations. *Proc. Natl. Acad. Sci. U.S.A.*, 100:11047–11052, 2003.

R. D. Traub, D. Schmitz, N. Maier, M. A. Whittington, and A. Draguhn. Axonal properties determine somatic firing in a model of in vitro CA1 hippocampal sharp wave/ripples and persistent gamma oscillations. *Eur. J. Neurosci.*, 36:2650–2660, 2012.

E. Valenstein. *The War of the Soups and the Sparks: The Discovery of Neurotransmitters and the Dispute Over How Nerves Communicate*. Columbia University Press, 2012.

M. Vandecasteele, A. Menzies, I. Creese, D. Paul, and G. Buzsáki. Persistence of hippocampal oscillations in connexin 36, 45 double knock-out mice. Number 435.4/H9. Society for Neuroscience Abstracts., 2008.

C. H. Vanderwolf. Hippocampal electrical activity and voluntary movement in the rat. *Electroencephalogr. Clin. Neurophysiol.*, 26:407–18, 1969.

L. Venance, A. Rozov, M. Blatow, N. Burnashev, D. Feldmeyer, and H. Monyer. Connexin expression in electrically coupled postnatal rat brain neurons. *Proc. Natl. Acad. Sci. U.S.A.*, 97:10260–10265, 2000.

K. Vervaeke, A. Lörincz, P. Gleeson, M. Farinella, Z. Nusser, and R. A. Silver. Rapid desynchronization of an electrically coupled interneuron network with sparse excitatory synaptic input. *Neuron*, 67:435–451, 2010.

X. J. Wang and G. Buzsáki. Gamma oscillation by synaptic inhibition in a hippocampal interneuronal network model. *J. Neurosci.*, 16:6402–6413, 1996.

Y. Wang, A. Barakat, and H. Zhou. Electrotonic coupling between pyramidal neurons in the neocortex. *PLoS One*, 5:e10253, 2010.

A. Watanabe. The interaction of electrical activity among neurons of lobster cardiac ganglion. *Jpn. J. Physiol.*, 8:305–318, 1958.

K. Wentlandt, M. Samoilova, P. L. Carlen, and H. El Beheiry. General anesthetics inhibit gap junction communication in cultured organotypic hippocampal slices. *Anesth. Analg.*, 102:1692–1698, 2006.

M. A. Whittington, R. D. Traub, N. Kopell, B. Ermentrout, and E. H. Buhl. Inhibition-based rhythms: Experimental and mathematical observations on network dynamics. *Int. J. Psychophysiol.*, 38:315–336, 2000.

M. A. Wilson and B. L. McNaughton. Reactivation of hippocampal ensemble memories during sleep. *Science*, 265:676–9, 1994.

B. J. Wiltgen, R. A. M. Brown, L. E. Talton, and A. J. Silva. New circuits for old memories: The role of the neocortex in consolidation. *Neuron*, 44:101–108, 2004.

L. Wittner, D. A. Henze, L. Záborszky, and G. Buzsáki. Three-dimensional reconstruction of the axon arbor of a CA3 pyramidal cell recorded and filled in vivo. *Brain Struct. Funct.*, 212:75–83, 2007.

Q. Yang and H. B. Michelson. Gap junctions synchronize the firing of inhibitory interneurons in guinea pig hippocampus. *Brain Res.*, 907:139–143, 2001.

A. Ylinen, A. Bragin, Z. Nádasdy, G. Jandó, I. Szabo, A. Sik, and G. Buzsaki. Sharp wave-associated high-frequency oscillation (200 Hz) in the intact hippocampus: network and intracellular mechanisms. *J. Neurosci.*, 15:30–46, 1995.

R. Yuste, A. Peinado, and L. C. Katz. Neuronal domains in developing neocortex. *Science*, 257:665–9, 1992.

L. I. Zhang and M.-m. Poo. Electrical activity and development of neural circuits. *Nat. Neurosci.*, 4:1207–1214, 2001.

Acknowledgments

Science would be impossible without collaboration. Here, I would like to acknowledge the people that contributed to this work – in one way or another.

First and foremost, I would like to express my gratitude to Richard Kempter. Richard gave the lecture that initially got me interested in computational neuroscience and supplied continuous support and advice during the time of my thesis. Personally, I am grateful to him for sharing his enthusiasm for discussing neuroscience and my research, and also for giving me the freedom to follow my scientific curiosity.

I also want to thank Nikolaus Maier and Prof. Andreas Draguhn for giving me access to their experimental data, and for fruitful discussions. Moreover, I want to thank Constance Holman, Jan Johan Tukker, and Dietmar Schmitz for the experimental collaboration, which I enjoyed a lot.

Furthermore, I am grateful to the members of my PhD Committee from the GRK, i.e., Richard Kempter, Benjamin Lindner, Susanne Schreiber, and Dietmar Schmitz, for guiding me along the way and supplying me with valuable feedback.

I also want explicitly thank my office mates for making the time here (scientifically) entertaining and delightful: Thomas McColgan, Janina Hesse, Jan-Hendrik Schleimer, Paula Kuokkanen, José Donoso, Nikolay Chenkov, Martina Michalikova, and Tizia Kaplan. José also supplied me with python code that was very useful for my network simulations. I further want to express my gratitude to Richard and Susanne, and the whole ITB for creating a friendly and scientifically stimulating environment. Especially, I thank Rike-Benjamin Schuppner and Andreas Hantschmann for keeping the IT running; and Elvira Lauterbach and Karin Winklhöfer for keeping the ITB running.

My work place would be insufficiently described without mentioning the BCCN Berlin and its associated graduate school. Here, I would like to thank Margret Franke and Robert Martin, and everyone else who is part of this wonderful institute.

Many thanks to everyone, who provided valuable feedback for this thesis: Tiziano D'Albis, Natalie Schieferstein, Roberta Evangelista, Martina Michalikova, Susanna Susana, Paul Pfeiffer, Tizia Kaplan, Nikolaus Maier, Jan Behrends, and Anton Bruch.

I would also like to thank my friends and family for making this part of my life so enjoyable: Andre, Felix, Philipp, Raphael, Torben, Anton, Jan, Tom, Dominika, Hannes, Julius, Pia, Jane, Zahra, Philipp, Katinka, Mieke, Nele, Stefanie, and Hilda.

I would like to specially thank my parents for their trust and support, and I would like to thank Anouk for simply everything.

Selbständigkeitserklärung

Ich erkläre, dass ich die vorliegende Arbeit selbständig und nur unter Verwendung der angegebenen Literatur und Hilfsmittel angefertigt habe.

Berlin, den 02.05.2018 André Jörg Holzbecher